

AMERICAN UNIVERSITY OF BEIRUT

INTELLIGENT SYSTEMS FOR DETECTION AND  
CLASSIFICATION OF SLEEP APNEA

by  
JOE MANSOUR RAHME

A thesis  
submitted in partial fulfillment of the requirements  
for the degree of Master of Science  
to the Biomedical Engineering Program  
of the Maroun Semaan Faculty of Engineering and Architecture  
and the Faculty of Medicine  
at the American University of Beirut

Beirut, Lebanon  
May 2025

AMERICAN UNIVERSITY OF BEIRUT

INTELLIGENT SYSTEMS FOR DETECTION AND  
CLASSIFICATION OF SLEEP APNEA

by  
JOE MANSOUR RAHME

Approved by:

---

Dr. Massoud Khraiche, Associate Professor  
Biomedical Engineering Program

Advisor

---

Dr. Fouad Zouein, Associate Professor  
Department of Pharmacology and Toxicology

Co-Advisor

---

Dr. Jason Amatoury, Assistant Professor  
Biomedical Engineering Program

Member of Committee

---

Dr. Youssef Tawk, Associate Professor  
Department of Electrical and Computer Engineering

Member of Committee

Date of thesis defense: May 5, 2025

## ACKNOWLEDGEMENTS

First, I would like to thank my adviser, Professor Massoud Khraiche for his guidance and belief in me even throughout the work complications.

I would also like to thank my co-adviser, Professor Jason Amatory for his guidance and mentorship. His knowledge was essential for me to navigate through the field of sleep and upper airway studies.

I will also take the opportunity to thank Professor Ibrahim Bou Faysal for his guidance in the field of signals and systems.

I would also like to thank my colleagues Miss Sahira Saleh, Miss Tamara Sadek and Mister Jad Daorah for helping me publish in the IEEE EMBC (Orlando, Florida, USA) during spring of 2024 as well as in Elsevier journal of Pharmaceutical and Biomedical analysis open, hoping that this work will also be published one day.

I also extend my gratitude to my colleagues in my laboratories NENB and SUARG. I would like to thank my colleague Mister Charbel Al Hajj for giving me the opportunity to work outside of AUB during the 2024 fall semester where I got to learn and advance in the field of deep computing, and other advanced topics in signal processing in one of the biggest labs of the middle east.

My little brother Mister Anthony Rahme, my aunts Miss Lucile Khalil, Miss Marie Khalil Namet (Toulouse, France), Miss Houda Rahme (NSW, Australia) and Miss Therese Rahme as well as my uncle Mister Youssef Khalil (Virginia Beach, Virginia, USA) for helping me fund my studies.

My dear brother and mentor Mister Carlos Rahme and his wife Miss Jessica D'Arcangelo Rahme (Bowral, NSW, Australia), hoping that their 2 beautiful kids Sebastian and Adelina reach even higher than I did.

I also honor the memory of my late uncles and aunt, Mister Fayez Rahme, Mister Tanios Rahme and Miss Jeanette Rahme as well as my grandparents Miss Almaza Khalil and Mister Elias Khalil whose lives continue to inspire me.

My dear parents Mansour Rahme and Habca Khalil Rahme who have helped me financially and morally go through everything and to whom I owe everything. Finally, my dear sister Miss Marianne Rahme to whom I dedicate this work for everything she did for me.

# ABSTRACT OF THE THESIS OF

Joe Mansour Rahme

for

Master of Science

Major: Biomedical Engineering

Title: Intelligent Systems for Detection and Classification of Sleep Apnea

Classical machine learning has extensively been used to treat bio-signals to detect and classify multiple diseases, and this approach has also extended to deep learning, offering more sophisticated and accurate methods for analyzing complex physiological data.

Photoplethysmography (PPG) offers a non-invasive method to study blood volume changes in the vascular system. It transmits light through the skin into the vascular beds and measures the changes in the intensity of the transmitted or reflected light caused by blood volume changes, providing insights into cardiovascular functions. This method has been shown to return a high-fidelity signal regarding heart rate and blood pressure, making it a reliable and convenient way to study cardiovascular function and potentially monitor diseases such as sleep apnea.

However, PPG measurement suffers from variability based on the location of measurement, skin tone, and motion artifacts, which can lead to inaccurate readings.

This study investigates the impact of sensor location on photoplethysmography (PPG) signal quality for sleep apnea detection.

Firstly, we plan to demonstrate how the signal varies depending on the properties of different recording sites based on other factors such as skin thickness and vascular density.

The feasibility of classifying apneic events as obstructive or central using only PPG signals is examined PPG by designing intelligent systems to do so. We will then design a flowchart that will utilize a combination of PPG signals, deep learning models and algorithms, to differentiate between the two types of apneas based on the distinct physiological markers.

Our approach seeks to enhance the accuracy and reliability of sleep apnea diagnosis and classification, for a better diagnosis of sleep apnea while using minimal commonly used wearable devices.

# TABLE OF CONTENTS

ACKNOWLEDGEMENTS .....	1
ABSTRACT.....	2
ILLUSTRATIONS.....	7
TABLES .....	11
INTRODUCTION.....	14
1.1 Sleep Apnea .....	15
1.2 Polysomnography .....	16
1.3 Photoplethysmography .....	18
1.4 Pulse Amplitude Modulation: .....	21
1.5 Respiratory Sinus Arrhythmia (RSA):.....	21
1.6 PPG as a Portable Monitor.....	23
1.7.PPG for Sleep Apnea .....	24
1.8. Aims of the work and deliverables .....	28
1.8.1. Aim 1: Analysis of Anatomical Sites and PPG Features for High-Fidelity Signal Acquisition to Enhance Sleep Apnea Detection and Classification .....	28
1.8.2. Aim 2: Contribution of Multi-Site PPG Signals in Sleep Apnea Detection and Classification .....	30
PHOTOPLETHYSMOGRAPHY FOR SLEEP APNEA .....	31
2.1. Methodology of the Aims .....	31

2.1.1 Aim 1.1 Characterization of PPG Signal Variation Across Body Sites and During Apneic Events.....	31
2.1.2 Aim: Extraction of Diagnostic PPG Features for Machine Learning-Based Apnea Classification .....	32
2.1.3. Aim: Derivation of PPG-Based Respiratory Signals to Differentiate OSA and CSA .....	32
2.2 Protocol of Experiment .....	34
2.2.1 Participants .....	34
2.2.2 Data Acquisition and Instrumentation .....	34
2.2.3. Protocol .....	35
2.2.4. Signal Preprocessing .....	36
2.3 Results and Discussion .....	37
2.3.1 Data Analysis.....	37
2.4. Conclusion: .....	40
2.4.1 OSA vs. CSA on Finger PPG .....	41
<b>FEATURE EXTRACTION AND EFFORT QUANTIFICATION</b> .....	<b>43</b>
3.1 Recording from the Wrist Ventral Side .....	46
3.1.1 PPG Derived Respiration signal (PPGDR): .....	46
3.2 Vernier Belt.....	53
3.3 The Flowchart .....	59
3.5. Cases of Rejection .....	68
3.6. Recruitment Process .....	70
3.6.1 Finger PPG extraction .....	70
<b>CLASSIFICATION MODELS .....</b>	<b>75</b>

4.1. Distribution of the Data .....	75
4.2. Classification at the level of the Finger (PPG).....	75
4.3. Classification models .....	75
4.4. Logistic Regression .....	76
4.4.1 Hyperparameters .....	76
4.5. XG-Boost .....	77
4.5.1. Hyperparameters .....	77
4.6. Gaussian Naive Bayes .....	77
4.6.1. Hyperparameters .....	78
4.7. Gradient boost .....	78
4.7.1. Hyperparameters .....	78
4.8. Random Forest .....	79
4.8.1 Hyperparameters .....	79
4.9. Evaluation Metrics.....	79
4.10 Classification at the level of the Wrist (PPGDR).....	84
4.10.1 Deep Learning using Multilayer Perceptron Neural Networks: .....	86
4.10.1. K-Nearest Neighbors:.....	88
4.10.2. Naive Bayes .....	89
4.10.3. Ensemble Method: .....	89
4.11. Results.....	91
4.11.1. K-Nearest Neighbors.....	95
4.11.2 . Ensemble .....	95
4.11.3. MLPNN .....	95
4.11.4. Gaussian Naïve Bayes.....	95

4.12. Logic Synthesis of the System .....	96
4.12.1 For PPG: .....	96
4.12.2. For PPGDR: .....	96
4.12.3. K-mapping .....	99
4.12.4. CSA Logic Output .....	101
4.12.5. OSA Logic Output .....	101
4.12.6. REJECTION Logic Output .....	102
<b>EXPERIMENTAL RESULTS: .....</b>	<b>103</b>
5.1. Optimized Karnaugh Map .....	105
5.2. Main results .....	107
<b>CONCLUSION .....</b>	<b>109</b>
6.1. Significance and Future Recommendations .....	109
6.2. Limitations of the Work .....	110
6.3. Detection of Sleep Apnea Using SPO <sub>2</sub> Signal .....	113
<b>APPENDIX 1 .....</b>	<b>119</b>
<b>REFERENCES .....</b>	<b>129</b>

# ILLUSTRATIONS

## Figure

1. The multiple signals recorded in a PSG, adapted from [1].....	17
2. Transmissive Reflective PPG sensor, figure adapted from [12] .....	18
3. The AC and DC Components of PPG .....	19
4. Baseline Modulation affected by respiration figure adapted from [14]. .....	20
5. Amplitude modulation of respiration, figure adapted from [14].....	21
6. RSA Components of Respiration, figure adapted from [14]. .....	22
7. The factors modulating the PPG, figure adapted from [14].....	22
8. Types of Portable Monitors, Figure adapted from [1].....	24
9. Superposition of Normal (BLUE) and Apneic PPG signal (RED) Recoded from the tip of the Finger .....	25
10. Schematic illustration of the 6 measurement sites for PPG:Forehead, neck , wrist under , wrist upper, tip of the finger , ring location.....	38
11. A single waveform from one subject measured from the thumb at high intensity and features considered .....	38
12. second segments of PPG signal measured from different locations at low and high intensities under different conditions .....	39

13. Time to peak taken from 6 measurement sites for normal and apneic conditions in (a) High LED intensity and (b) Low LED intensity .....	39
14. (a)The drop in amplitude at different locations during normal and apneic events for Led Intensity =37 mA (b) The drop in amplitude at different locations during normal and apneic events for LED intensity = 493 mA. ....	40
15. Statistical Features Extracted from the PPG .....	43
16. PPG VPG and APG plots and the decrease of the peak-to-peak amplitude after a simulated apnea at time $t = 15$ seconds .....	46
17. Raw PPG Recorded From the Wrist.....	50
18. High Passed Filtered PPG (0.18 Hz) .....	50
19. FFT of the PPG after High Pass Filter at 0.18 Hz.....	51
20. PPGDR extracted from PPG Signal from the Wrist Under (CSA) .....	51
21. Unfiltered PPG Signal from the Wrist Under (OSA) .....	52
22. PPGDR extracted from PPG (OSA).....	53
23. The Vernier Respiration Belt .....	54
24. Comparing the PPGDR to Control Signal for the case of Central Apnea. ....	55
25. Comparing the PPGDR to Control Signal for the case of Obstructive Apnea .....	56
26. Comparing the 2 methods of extraction of PPGDR .....	57

27. Comparing the 2 methods of extraction of PPGDR. ....	58
28. Fast Fourier Transform of the PPGDR methodologies compared to the Control Signal. ....	58
29. Strategy of Detection and Classification of Apneic Events.....	59
30. Decision Tree of the full system .....	60
31. Wrist and Finger PPG with the extracted PPGDR.....	64
32. Cross-Correlation between Wrist and Finger PPG based on the Peak to Peak Intervals (of 7 peaks).....	64
33. Comparing Control Signal to PPGDR before Alignment.....	65
34. Detection of Peaks (Breaths) in both the PPGDR and the Control Signal .....	66
35. Cross-Correlation between the PPGDR and the Control Signal.....	66
36. PPGDR and Control Signal after Alignment .....	67
37. Example of a Case of Rejection .....	69
38. ROC of Gradient BOOST and Random Forest.....	81
39. ROC curves of Random Forest and XG-BOOST .....	81
40. Confusion Matrices of (a) the Random Forest and (b) the XG-Boost models for finger PPG.....	82

41. Confusion matrices of the Gradient Boost and the Ensemble model for finger PPG. .....	83
42. Permutation test of the features in PPGDR.....	85
43. Optimal MLP Neural Network Model.....	88
44. Area Under the Curve of K-NN and Ensemble method .....	92
45. Area Under the Curve of the MLP and Gaussian Naïve bayesian models. ....	93
46. Precision-Recall curves for Gaussian Naive Bayesian and K-NN models.....	93
47. Confusion Matrices of K-NN and Ensemble Methods.....	94
48. Confusion Matrices of the 4 Models – PPGDR. ....	94
49. Confusion Matrix of the whole System on the validation set .....	103
50. Correct Predictions for Central Apnea (PPGDR vs Combined) .....	104
51. The AC and DC components of PPG at different wavelengths .....	114
52. The usage of different PPG wavelength to extract SPO2 extracted from [29] .....	115
53. Filtered SPO2 signal with Apneic Threshold .....	116
54. Filtered Apneic Spo2 Signal Highlighted in Red.....	117

## TABLES

### Table

55. Features Extraction from the PPG Signal .....	44
56. Significance Test of the Extracted Features.....	71
57. Performance of the Different Algorithms Used - PPG.....	80
58. Different Hidden Layers Possibilities for Deep Learning .....	86
59. Performance of the Different Algorithms Used - PPGDR .....	91
60. Logic Table of the system.....	96
61. Logic Table of the System taking into consideration the Delay of Vasoconstriction for CSA .....	97
62. K-Map template.....	99
63. CSA Logic Output page.....	101
64. OSA Logic Output.....	101
65. REJECTION Logic Output.....	102
66. Optimized K-Map.....	105
67. Optimized K-Map OSA .....	106
68. Optimized K-Map CSA .....	106
69. Optimized K-Map Rejection .....	107

To my parents...

إلى أمي وأبي وأحبائي ...

# CHAPTER 1

## INTRODUCTION

Sleep apnea is a term that refers to intermittent, repeated cessations or reductions of airflow, with or without upper airway obstruction. During sleep, the muscles that keep the upper airway (or throat) open lose their usual support from the nervous system. If the upper airway is already weak or prone to collapse, it results in a narrow airway, which can cause it to close, leading to breathing interruptions. The severity of obstructive sleep apnea is characterized by the apnea-hypopnea index (AHI), which is defined as the number of apneic events per hour of sleep [1].

Although sleep apnea is classified as a cessation of breathing by at least 10 seconds during sleep (AASM) [2], a large amount of these events can last up to 2 minutes.

This work aims to enhance the specificity of the detection of sleep apnea and the classification of each type of sleep apnea by using only the characteristics of the PPG signals obtained from different locations of the human body therefore leading to a more accurate diagnostic.

Also, more hardware will be able to identify sleep apnea outside of the finger (which is considered as gold standard location of PPG) location by investigating new body sites that are not frequently used for sleep apnea diagnosis.

## 1.1 Sleep Apnea

Sleep apnea, a prevalent sleep disorder, affects a significant portion of the global population and poses substantial health risks if left untreated [3]. The disorder is primarily categorized into two types: obstructive sleep apnea (OSA) and central sleep apnea (CSA).

OSA, the more common form, occurs when the muscles and nerves supporting the upper airway soft tissues, such as the tongue and soft palate, temporarily relax, causing a physical blockage of the airflow.

In contrast, CSA arises due to a lack of respiratory effort resulting from neurological issues where the brain fails to signal the muscles involved in breathing [4, 5]

Treatment approaches for CSA and OSA differ significantly due to their distinct underlying causes and mechanisms. Obstructive sleep apnea typically responds well to continuous positive airway pressure (CPAP) therapy [6], which involves wearing a mask during sleep that delivers a continuous flow of air to keep the airway open. Additionally, lifestyle modifications such as weight loss, positional therapy, and avoiding alcohol and sedatives before bedtime can also be effective in reducing the severity of OSA.

In contrast, CSA often requires more complex interventions. While CPAP may be beneficial for some patients with CSA, it may exacerbate symptoms in others by interfering with the natural respiratory drive [7]. Treatment options for CSA may include

adaptive servo-ventilation (ASV), which adjusts the airflow based on the patient's breathing patterns or underlying medical conditions such as heart failure or neurological disorders.

Furthermore, the distinction between central and obstructive sleep apnea can be influenced by various factors, including anatomical abnormalities, obesity, age, and comorbidities such as heart disease or stroke [8]. Understanding these differences is crucial for tailoring treatment strategies to individual patients and optimizing outcomes in the management of sleep apnea.

## **1.2 Polysomnography**

Diagnosis and management of sleep apnea typically involves polysomnography (PSG), considered the gold standard diagnostic tool. PSG is a comprehensive sleep study used to diagnose sleep disorders by recording multiple physiological signals as shown in Figure 1. The physiological markers are oxygen saturation, respiratory effort, airflow, brain waves (Electroencephalogram), heart rate (Electrocardiogram), breathing, as well as eye and leg movements (Electrooculogram and Electromyogram) during sleep [9]

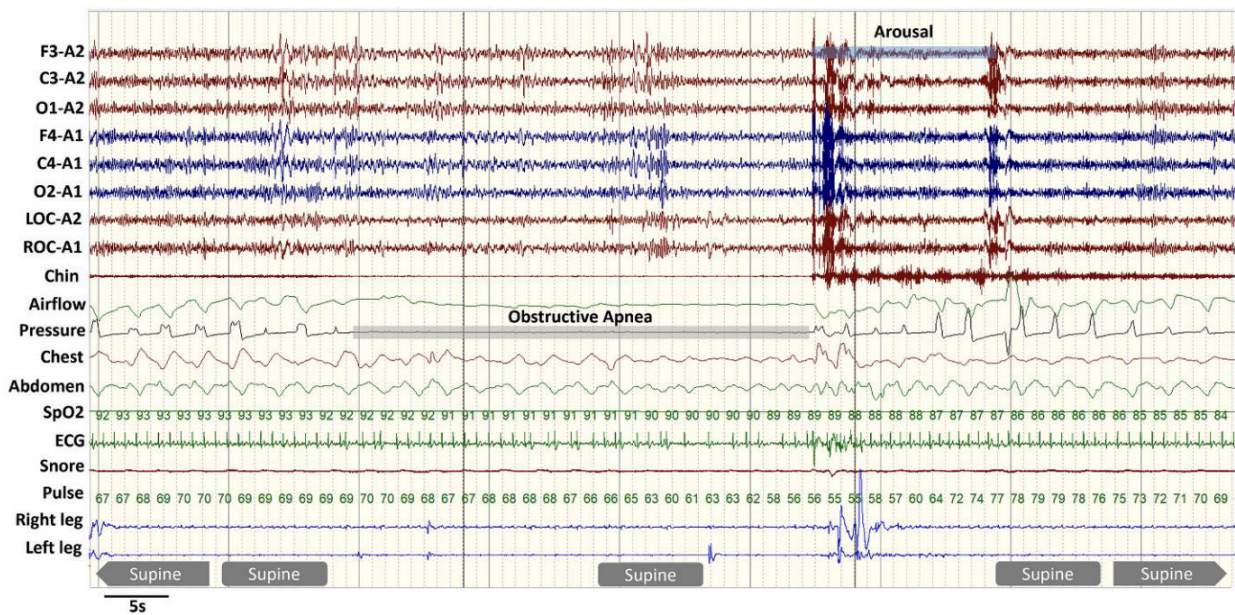


Figure 1. The multiple signals recorded in a PSG, adapted from [10]

The signals acquired in PSG are used to calculate the Apnea Hypopnea Index widely used as the standard metric for the quantification of the severity of Sleep Apnea [11]. The AHI is the sum of the hypopnea and apnea events per hour of sleep with each event lasting at least 10 seconds. Hypopnea is the reduction in airflow by  $\geq 30\%$  of the baseline and apnea is the decrease  $\geq 90\%$  of the baseline. AHI less than five signifies normalcy, whereas an AHI score more than five indicates pathophysiology, and the higher the AHI, the higher the severity of sleep apnea.

Despite its effectiveness, PSG is costly, resource-intensive, and requires an overnight stay in a specialized sleep laboratory, which can be inconvenient for patients. PPG can be a non-complicated alternative to PSG for the detection of sleep apnea in symptomatic patients with no cardiovascular comorbidities.

### 1.3 Photoplethysmography

The wearable technology market has experienced a remarkable surge in popularity over the past few years, revolutionizing how we monitor and manage our health and lifestyle. One of the most popular wearables is the smartwatch. Smartwatches have been commonly studied as an alternative to multiple classical medical check-ups, for example, in the form of PPG in place of Electrocardiography (ECG), to predict heart diseases [12, 13]. Wearables tend to rely on surface technology given the complexity of penetrating electrode in protentional or optical measurement[14].

Photoplethysmography (PPG) is a non-invasive methodology for measuring blood vessel dynamics. It is composed of a photodiode emitting green ( $\lambda = 530$  nm) or red light ( $\lambda = 660$  nm) and is composed of an LED and a photodetector. It is based on the optical property of reflectance or transmission [15]. Reflectance mode has the photodiode and the LED on the same side of the device, with the photodetector detecting light reflected from the tissue. On the other hand, transmission mode is when the photodiode and the LED are on opposite sides of each other. The light that passes through the tissue is detected by the photodiode (Figure 2).



Figure 2. Transmissive Reflective PPG sensor, figure adapted from [12]

PPG signal is modulated by 2 waveforms: the direct current (DC) and the alternating current (AC). The direct current component corresponds to the signal from the density and volume of the tissue. The DC component is known to shift in amplitude due to respiration and other types of movement. On the other hand, the AC component of the signal changes depending on the amount of blood flowing through the tissue and according to the heart rate. It goes up in amplitude during the systolic phase and down during the diastolic phase of the cardiac cycle (refer to Figure 3 for visuals) [16, 17].

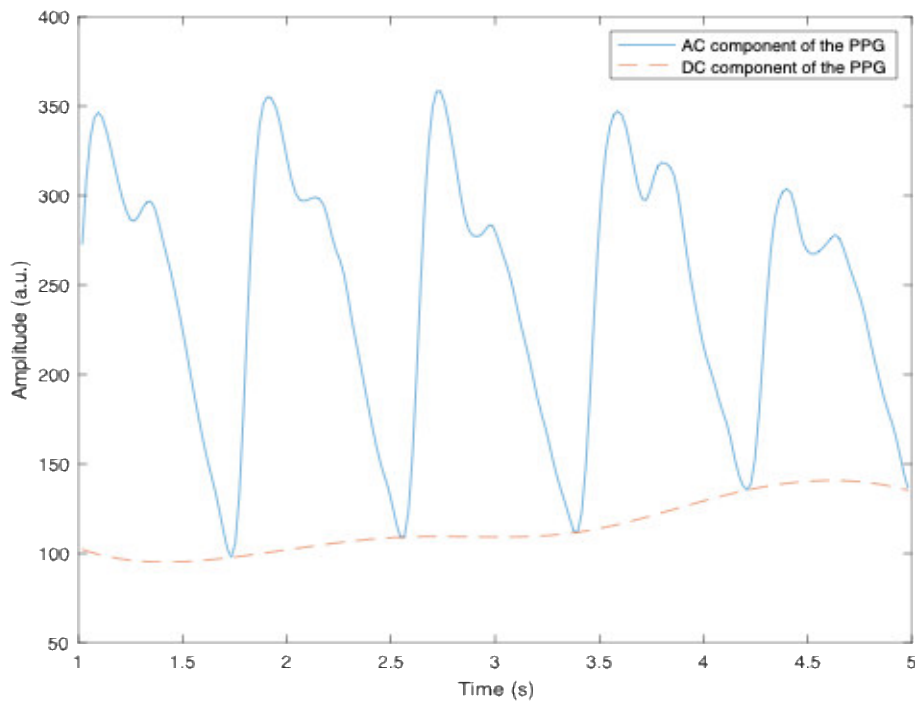


Figure 3. The AC and DC Components of PPG

The PPG is commonly known to be also modulated by respiration, [18] described the PPG signal as a sine wave modulated by both heart rate ( $A_k$ ) and respiration (B) and added a noise  $v(n)$ .

$$X(n) = \sum_{k=1}^M \left( \left[ A_k \sin \left( w_0 kn + \phi_k \right) \right] + B \sin(w_1 n + \sin \phi_0) \right) + v(n)$$

It is believed that respiration affects PPG in three ways [19]:

**Baseline Modulation:**

- Description: Baseline modulation is characterized by a low-frequency fluctuation superimposed on the PPG signal baseline, which corresponds to the respiratory cycle.
- Mechanism: The baseline of the PPG waveform shifts up and down in sync with the respiration. This modulation occurs due to the changes in intrathoracic pressure during breathing, which affects venous return and thus the volume of blood in peripheral vessels.
- Identification: A dashed line is added to the non-modulated PPG waveform to highlight these baseline shifts. Figure 4.

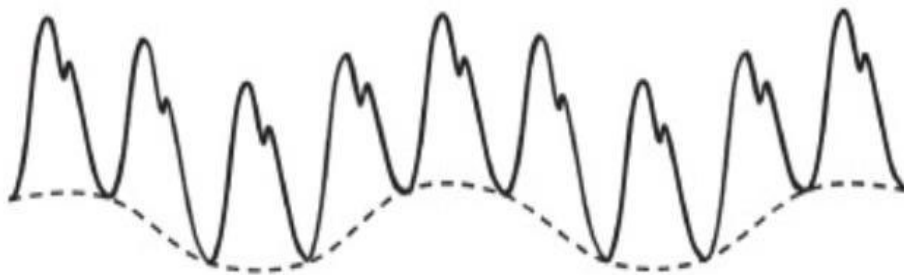


Figure 4. Baseline Modulation affected by respiration figure adapted from [14].

#### 1.4 Pulse Amplitude Modulation:

- Description: Pulse amplitude modulation involves changes in the amplitude of the individual PPG pulses in response to the respiratory cycle.
- Mechanism: During inspiration, the amplitude of the PPG pulses decreases due to the reduced stroke volume and venous return caused by the negative intrathoracic pressure. Conversely, during expiration, the amplitude increases.
- Identification: This is visualized by measuring the peak-to-trough amplitudes of the cardiac pulses in the PPG signal. Figure 5.

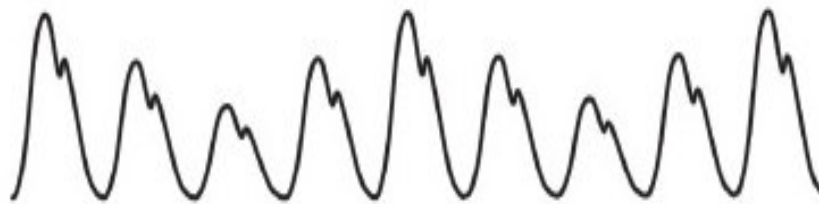


Figure 5. Amplitude modulation of respiration, figure adapted from [14].

#### 1.5 Respiratory Sinus Arrhythmia (RSA):

- Description: Respiratory sinus arrhythmia refers to the variability in heart rate that occurs at the respiratory frequency.
- Mechanism: Heart rate increases during inspiration and decreases during expiration due to autonomic nervous system modulation.
- Identification: RSA is extracted by measuring the peak-to-peak time periods of the PPG signal, reflecting the heart rate variability in relation to the respiratory cycle Figure 6.



Figure 6. RSA Components of Respiration, figure adapted from [14].

These three variations—baseline modulation are shown in Figure 7.

Understanding these phenomena is crucial for accurately analyzing PPG data and extracting breathing states and frequencies, especially in medical settings where breathing patterns might affect how we assess sleep apnea.

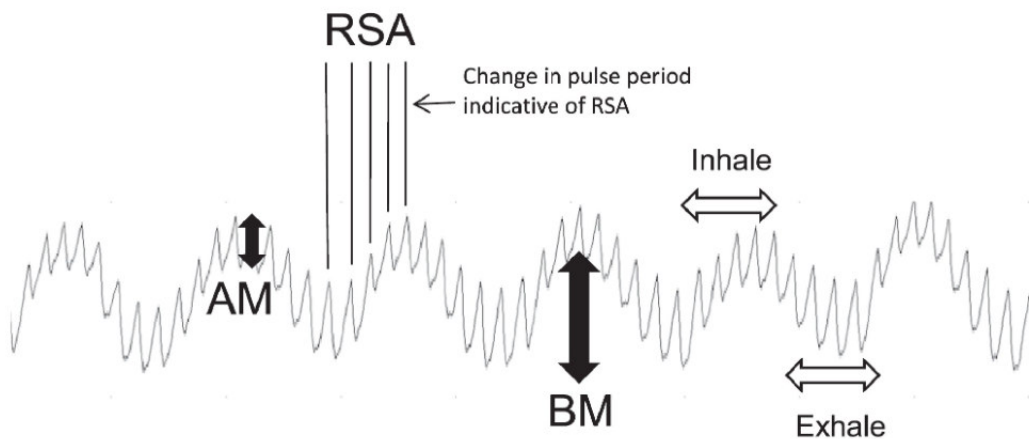


Figure 7. The factors modulating the PPG, figure adapted from [14].

## 1.6 PPG as a Portable Monitor

Portable monitors (PM) have emerged as an alternative to PSG for the diagnosis of sleep apnea.

PM is classified as PM 1,2,3,4 depending on the number of channels they use. Like PSG, PM 1 uses seven channels or more and is rarely utilized outside of clinical settings. PM 2 is a seven-channel device intended for usage at home by unsupervised individuals. PM 3 includes at least four channels, including respiratory, cardiac, and oxygen saturation measurements. PM 4 only employs one or two channels—usually heart rate and oxygen saturation or airflow. PPG offers a simple method that concentrates on vital indicators such as heart rate and oxygen saturation, which makes it perfect for usage at home [8] *Figure 8*.

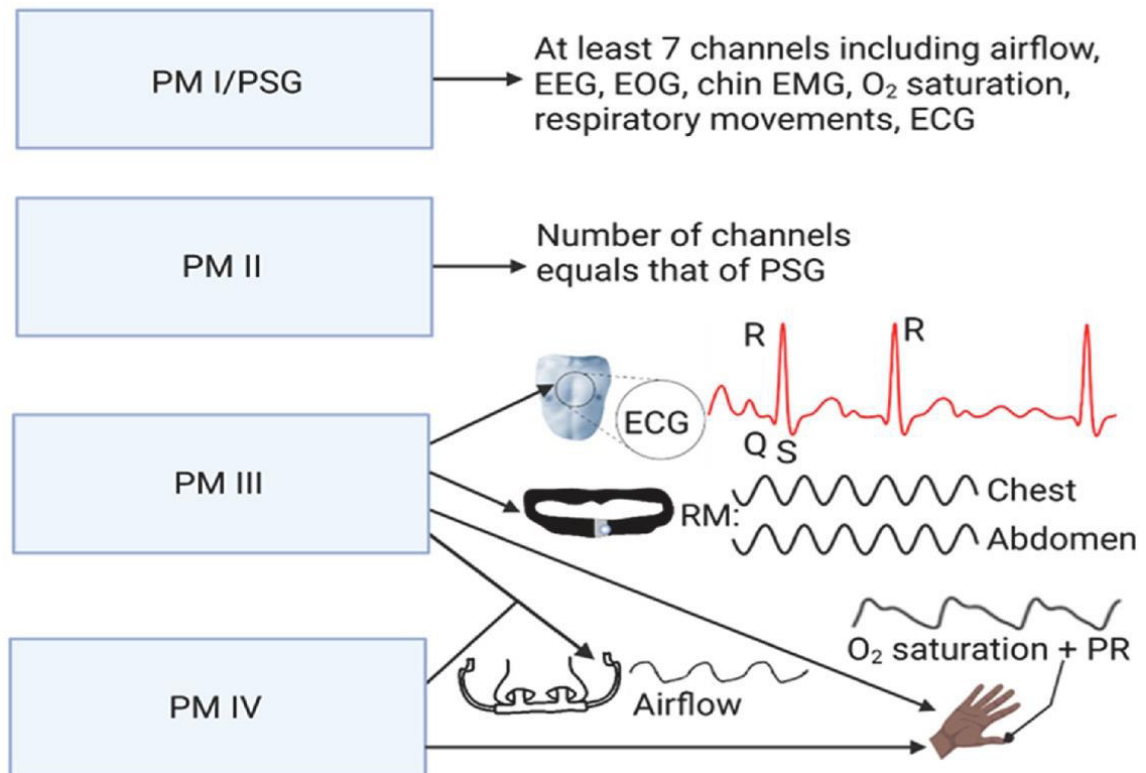


Figure 8.Types of Portable Monitors, Figure adapted from [1]

### 1.7.PPG for Sleep Apnea

Due to the drawbacks of PSG such as its cost, discomfort, and logistical challenges, multiple alternatives using wearable devices have been developed to monitor sleep apnea during the night. This movement toward minimal, accessible diagnostic technologies aligns with the broader trend of point-of-care systems designed for real-time neuromonitoring and physiological assessment, including in domains such as traumatic brain injury [20].

These PMs use various signals like respiratory, electrocardiography (ECG), **photoplethysmography (PPG)**, EEG, snoring loudness, and SpO<sub>2</sub>, either individually or in combination [8]. PPG detects changes in the blood volume caused by sympathetic

nervous system activation associated with Sleep Apnea. Sleep apnea is usually characterized by a decrease in PPG-signal amplitude due to vasoconstriction from muscle contraction around the vessels and the activation of the sympathetic nervous system (fight or flight).

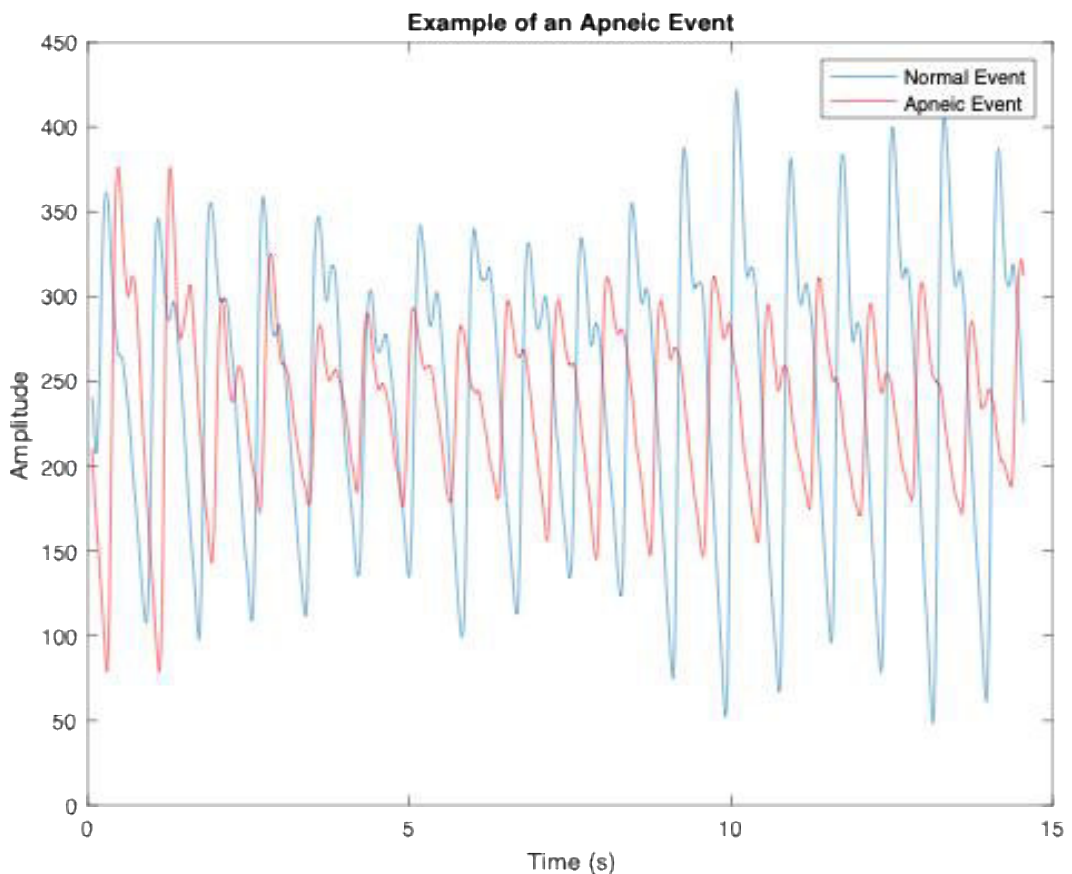


Figure 9 Superposition of Normal (BLUE) and Apneic PPG signal (RED) Recorded from the tip of the Finger

It has been demonstrated that finger PPG is a valid technique for assessing sympathetic activity since the finger's cutaneous vascular walls are highly innervated by  $\alpha$ -adrenoceptors [8], making them more sensitive to changes in blood volume (such as vasoconstriction and vasodilation) than other body locations. For that reason, the tip of

the finger and most specifically the tip of the index has always been the go-to when it comes to recording PPG.

Extensive research has been undertaken on the classification of photoplethysmography signals acquired from the fingertips of patients, which has led to the development of several algorithms [16, 21-24]. These algorithms discriminate between features characteristic of apneic episodes and those of normal respiratory patterns during sleep. The fingertip is recognized as the benchmark location for acquiring PPG signals. From the fingertip, PPG-derived respiration (PPGDR) was extracted from 236 patients using the fingertip [21]. PPGDR extraction facilitates the understanding of respiration states of patients in which a flat signal means no effort of breathing. During that process, if that cessation of breathing lasted at least 10 seconds, it would have been considered as central apneic event.

Nevertheless, the study did not go over Obstructive apnea which is known to be the most common type of apnea with only 10% of apneic events being central on average. Additionally, this study was limited by the exclusion of substantial data segments due to low signal-to-noise ratio episodes affected by strong vasoconstrictions [21] which led to a low signal-to-noise ratio PPGDR (will be discussed further in Aim 1.3).

Research efforts have been directed towards refining rejection techniques [22]. An episode is identified as apneic if a Drop in Amplitude of the Pulse (DAP) occurs simultaneously with a decrease in SpO<sub>2</sub> levels by a minimum of 3%, amid a reduction in airflow lasting no less than 10 seconds [22]. Another investigation introduced a methodology for detecting and categorizing respiratory events by distinguishing between apneas and hypopneas and further identifying their origins—whether central or obstructive—utilizing PPG alongside SpO<sub>2</sub> signals. This methodology integrates diverse

features, including those derived from PPG, SpO<sub>2</sub>, and the pulse rate analyzed in both time and frequency domains. However, this study did not conduct a patient-wise performance evaluation and fell short in providing details on the accuracy of estimating the central Apnea-Hypopnea Index (cAHI), which leaves the readiness of their approach for clinical application as ambiguous.

Other studies have concentrated on deriving respiration signals from PPG measurements taken at various body locations using assorted transfer functions and signal processing techniques[25, 26]. PPG was used to study breathing effort in mixed sleep apnea by extracting features from PPG and correlating them with esophageal pressure signals from 8 PSG recordings[27]. All these algorithms were used to replace large amount of hardware of the PSG only using a minimal amount of wearable devices.

Previous studies have not explored the feasibility of classifying apnea types directly from PPG signals without the use of SPO<sub>2</sub>, wearable chest inductance bands or other devices. Due to differences in physiological implications in OSA and CSA, it is believed that classifying sleep apneas is just as important as its detection to give patients an accurate treatment. In subsequent work, we intend to use all the acquired knowledge to develop a cohesive unit diagram that utilizes signal processing and machine learning techniques to detect apneic episodes and accurately classify them into central and obstructive types.

## **1.8. Aims of the work and deliverables**

### *1.8.1. Aim 1: Analysis of Anatomical Sites and PPG Features for High-Fidelity Signal Acquisition to Enhance Sleep Apnea Detection and Classification*

Hypothesis 1.1: The accuracy of PPG signals for sleep apnea detection and classification varies by anatomical location due to differences in responses to vasoconstriction and vasodilation. Key locations include:

- Tip of the finger
- Ring location on the finger
- Underside of the wrist
- Upper side of the wrist
- Head
- Neck

Rationale: Different anatomical sites have unique physiological properties and varying densities of blood vessels, impacting PPG signal quality and reliability. For example, a ring-like PPG sensor on the ring finger may provide more comfort compared to a tight-fitting sensor on the fingertip, potentially improving sleep data acquisition.

Significance: Identifying the optimal location for high-fidelity PPG recording for sleep apnea monitoring.

Impact: By classifying anatomical sites based on the severity of vasoconstriction during sleep apneic events, this research will guide the selection of optimal PPG measurement locations, enhancing the reliability of respiratory signals. Identifying regions less prone to significant vasoconstriction will improve the signal-to-noise ratio (SNR), ensuring consistent and accurate respiratory data even during apneic events.

Hypothesis 1.2: Additional PPG features, which will later be used in machine learning, can be extracted to effectively differentiate between normal and apneic PPG signals.

Rationale: Identifying and extracting a broader set of PPG features is crucial for accurately distinguishing between normal breathing and apneic events. Analyzing signal characteristics in both time and frequency domains will help capture subtle variations in waveform morphology indicative of apnea.

Significance: Establishing features that will optimize machine learning models for the classification of PPG signals into apneic and normal.

Impact: A detailed feature set will enhance the performance of machine learning models, leading to more reliable and precise detection of apneic events, ultimately improving diagnostic outcomes in sleep apnea monitoring.

Hypothesis 1.3: The PPGDR signal can be extracted and will reflect the breathing frequency and effort.

Rationale: The PPGDR signal could serve as a reliable surrogate for assessing respiratory effort, especially when obtained from wrist PPG, as it is less affected by vasoconstriction, ensuring a high SNR.

Significance: Providing a clear understanding of breathing effort and frequency without the need for a respiratory inductance plethysmography belt.

Impact: This method offers a clearer, more reliable assessment of the patient's breathing effort and frequency, enhancing patient comfort and ensuring more precise and dependable monitoring by eliminating the need for additional equipment.

### *1.8.2. Aim 2: Contribution of Multi-Site PPG Signals in Sleep Apnea Detection and Classification*

Hypothesis 2.1: Using multi-site PPG signals will significantly improve sleep apnea detection and classification in wearable devices.

Rationale: By analyzing both PPG and PPGDR signals from the finger and the wrist, respectively, we can better understand apneic events related to vasoconstriction and breathing patterns. Advanced signal processing can leverage the synchrony between vasoconstriction and respiratory events to discriminate between central and obstructive sleep apnea.

Significance: Enhancing sleep apnea classification in PPG-based wearables.

Impact: This approach allows for more precise discrimination between central and obstructive sleep apnea, leading to better-targeted treatments and more effective management, ultimately improving patient outcomes.

Hypothesis 2.2: A study involving 15 or more volunteers recording wrist and finger PPG data will confirm that meaningful real-time data, sensitive to changes in breathing rate and vasoconstriction/vasodilation, can be derived, leading to the development of an alternative to polysomnography (PSG).

Rationale: Testing the algorithm on a large population will validate previous hypotheses.

Significance: Improving sleep apnea detection and classification using wearable devices accessible to large populations.

Impact: Successful validation could revolutionize sleep apnea diagnosis by providing a cost-effective, accessible alternative to PSG, making detection and classification more widely available through wearable devices.

## CHAPTER 2

# PHOTOPLETHYSMOGRAPHY FOR SLEEP APNEA

### **2.1. Methodology of the Aims**

Aim 1: Analysis of Anatomical Sites and PPG Features for High-Fidelity Signal Acquisition to Enhance Sleep Apnea Detection and Classification

#### *2.1.1 Aim 1.1 Characterization of PPG Signal Variation Across Body Sites and During Apneic Events*

This aim investigates how PPG signals vary across multiple anatomical sites and how these variations reflect physiological changes during simulated apneic episodes. Signals will be acquired using a reflectance-mode PPG sensor (Eval-ADPD1081Z, Analog Devices) placed at the fingertip, finger base, dorsal and ventral wrist, neck, and forehead.

Signal features such as amplitude, systolic duration, and diastolic duration will be extracted to quantify inter-site variability and detect alterations associated with apneic events. To examine the influence of tissue penetration depth, recordings will be conducted at two LED intensities: 37 mA and 493 mA.

Participants will be healthy adults who abstain from stimulants for at least 12 hours prior. Each will perform a protocol including baseline breathing (20 seconds) and apneic maneuvers (20 seconds), simulating both central (complete breath cessation) and obstructive apnea (breath-holding with airway occlusion).

Data will be processed in MATLAB 2020, and statistical analysis will be conducted using ANOVA in SPSS. This aim also explores PPG's potential to provide surrogate insights into stroke volume and cardiovascular dynamics in the context of apnea.

### *2.1.2 Aim: Extraction of Diagnostic PPG Features for Machine Learning-Based Apnea Classification*

This aim focuses on identifying and extracting time- and frequency-domain features from PPG signals that differentiate normal from apneic states, to inform machine learning classification models.

Features of interest include geometric mean, standard deviation, kurtosis, area under the curve (AUC), and the low-frequency to high-frequency (LF/HF) ratio[28]. These features will serve as input variables for Support Vector Machines (SVMs) and other supervised learning models trained to distinguish between normal and apneic PPG segments.

### *2.1.3. Aim: Derivation of PPG-Based Respiratory Signals to Differentiate OSA and CSA*

This aim evaluates the feasibility of extracting a PPG-derived respiration (PPGDR) signal capable of distinguishing obstructive from central sleep apnea based on respiratory effort.

Given that CSA is characterized by absent respiratory effort and OSA by preserved effort with obstruction, accurate extraction of respiration-related modulation from the PPG signal is critical. PPGDR will be derived using narrowband filters centered

on the respiratory frequency range. Signal quality will be enhanced by targeting body sites less prone to vasoconstriction, aiming for high signal-to-noise ratios.

## Aim 2: Contribution of Multi-Site PPG Signals in Sleep Apnea Detection and Classification

### Aim 2.1: Use of Finger and Wrist PPG/PPGDR Signals for Sleep Apnea Type Classification

This aim evaluates the utility of PPG and PPG-derived respiration (PPGDR) signals from the finger and wrist for detecting and classifying sleep apnea subtypes—specifically, central sleep apnea (CSA) and obstructive sleep apnea (OSA).

PPG signals from the finger are sensitive to vasoconstrictive responses, commonly seen during apneic events, while wrist-derived PPGDR may provide insight into respiratory effort. By analyzing the temporal relationship between vasoconstriction at the finger and changes in PPGDR amplitude at the wrist, it is possible to infer the underlying mechanism—absent effort (CSA) or exaggerated effort (OSA).

Signal features such as Hjorth parameters, Hurst exponent, standard deviation, and mean will be used to quantify the complexity of the PPGDR signal, helping to distinguish between normal and apneic respiratory patterns. This feature-based classification aims to identify OSA more accurately while minimizing false positives caused by non-apneic vasoconstrictions (e.g., due to arousals, anxiety, or stress responses).

The ultimate goal is to develop a signal processing framework capable of non-invasively classifying sleep apnea types without the need for full polysomnography (PSG), thus improving accessibility and treatment precision.

## Aim 2.2: Validation of the Proposed Classification Framework Across Multiple Subjects

This aim assesses the generalizability and robustness of the classification flowchart developed in Aim 2.1 by testing it on a broader subject population.

Data will be collected from multiple participants at MSFEA under controlled conditions. Subjects will lie supine and perform standardized apneic maneuvers using a mouthpiece and nose clip to simulate airflow obstruction. The same signal acquisition and processing protocols will be applied to evaluate the reproducibility of the results across individuals.

Validation metrics will include classification accuracy, sensitivity, specificity, and false-positive rates. Successful validation would demonstrate the applicability of the multi-site PPG framework for real-world screening of sleep apnea subtypes.

## **2.2 Protocol of Experiment**

### *2.2.1 Participants*

Five healthy volunteers participated in the study (all male, mean age  $\pm$  standard deviation:  $23 \pm 1.2$  years, mean weight  $\pm$  standard deviation:  $74 \pm 6.4$  kg) that had no previous record of cardiovascular or cardiological issues.

### *2.2.2 Data Acquisition and Instrumentation*

Analog Devices, USA's EVAL-ADPD1081ZPPG Evaluation Board (at a sampling frequency of 50 Hz) was used to collect all PPG measurements.

### 2.2.3. Protocol

The locations were the following and are depicted in Figure 10:

- Forehead.
- Neck.
- Wrist dorsal (upper).
- Wrist ventral (under).
- Finger, positioned where a ring would typically sit
- The tip of the finger.

PPG signals were recorded under both simulated normal and apneic conditions, using two different LED light intensities, low (37mA) and high (493mA), to assess the impact of light penetration on signal quality (Figure 12). In our first part of the work, we decided to check on features related to the stroke volume,  $T_p$  being the time to end the systolic period of the heartbeat, amplitude of the pulse which is the volume of blood ejected per heartbeat, and the time to end the diastolic phase of the heartbeat and how these features differ under apneic events (Figure 11).

We used epochs of 20 seconds for studies [29]

The subjects were forbidden from alcohol, tobacco, caffeine, or any type of drug that could impact the function cardiovascular or cardiological system. Each trial was recorded while the subjects were seated and relaxed for ten minutes. To lessen motion artifacts, individuals were instructed not to speak or move while recordings were being made.

After positioning the PPG board on the measurement site, it was secured in place with a Velcro closure.

For the two simulated conditions, CSA and OSA, 24 measurements were taken from each subject at six different body locations: the head, neck, wrist under (anatomically volar), wrist upper (anatomically dorsal), thumb, and ring finger.

For every measurement, records lasting 40 seconds were acquired.

To replicate CSA, participants were told to breathe normally for 20 seconds, then shut their mouth and nose fully for the subsequent 20 seconds. Participants were instructed to carry out a similar motion to simulate OSA, but they also had to try to inhale for 20 seconds [29, 30] against an obstruction while keeping their lips and nose shut.

For the recordings, they were asked to simulate obstructive sleep apnea by having 1 epoch of normal breathing followed by a Mueller Maneuver (an epoch of 20 seconds where the participants breathed through an occlusion which in our case was done using their hands).

Used the Mueller maneuver [29, 30] for 20 seconds to study the effect of obstructive sleep apnea on heart arrhythmia and concluded that negative intrathoracic pressure changes may be a contributory mechanism linking OSA to cardiac dysrhythmias. For the Central Apnea, participants were asked not to breathe for 20 seconds, after an epoch of normal breathing (20 seconds).

#### *2.2.4. Signal Preprocessing*

The measurements were taken at two different LED light intensities: low (37mA) and high (493mA). And filtered using a Chebyshev2 type 2 filter order 4 bandpass filter (0.45 -20 Hz) followed by a moving average filter.

## **2.3 Results and Discussion**

### *2.3.1 Data Analysis*

Our study revealed that the finger and ring locations demonstrated good fidelity in detecting apnea, consistent with existing literature, showing significant changes in waveform features under apneic conditions.

At low LED intensity, the head and thumb locations exhibited the highest signal amplitudes, while the wrist dorsal consistently showed the lowest amplitudes at both LED intensities. This suggests that the wrist dorsal location is less effective for PPG measurements due to poorer light penetration and lower signal quality even when this location is the most popular one among smart devices.

Notably, no vasoconstriction was observed in the wrist ventral location, which might have influenced the signal characteristics, making it less reliable for detecting apnea.

Additionally, the neck seemed to be a bad place to localize obstructive and central apnea due to the noise generated by muscle contraction from breathing and swallowing. For the forehead, at high intensity, we seemed to detect the drop in amplitude in the PPG signal in central apnea only but not at lower intensity. This might be due to the higher intensity resulting in higher penetration.

The wrist's lower side showed no significant change in shape during both central and obstructive apnea at both LED intensities.

The ring and finger sites, however, were sensitive to changes in LED intensity, particularly in the detection of time to peak ( $T_p$ ) changes, with higher LED intensity providing more distinct waveform features.

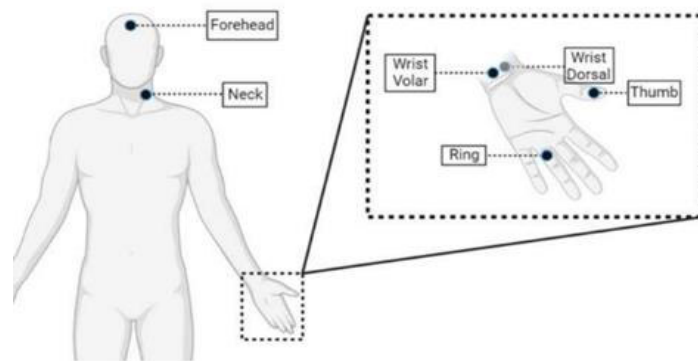


Figure 10 Schematic illustration of the 6 measurement sites for PPG:Forehead, neck , wrist under , wrist upper, tip of the finger , ring location.

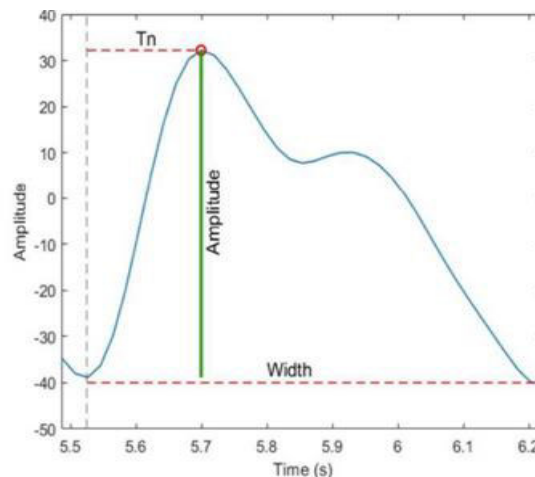


Figure 11 A single waveform from one subject measured from the thumb at high intensity and features considered

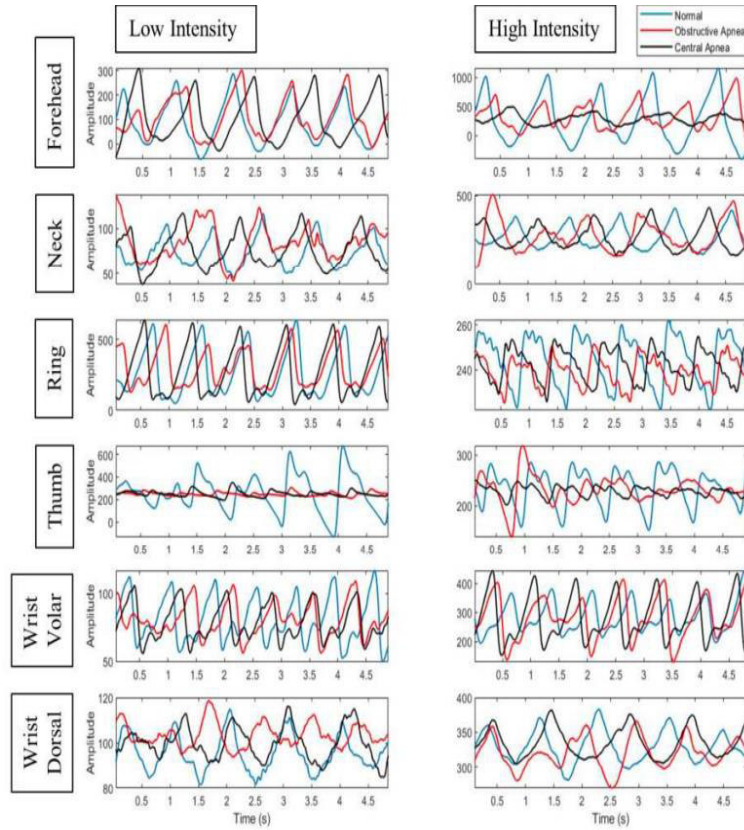


Figure 12 second segments of PPG signal measured from different locations at low and high intensities under different conditions

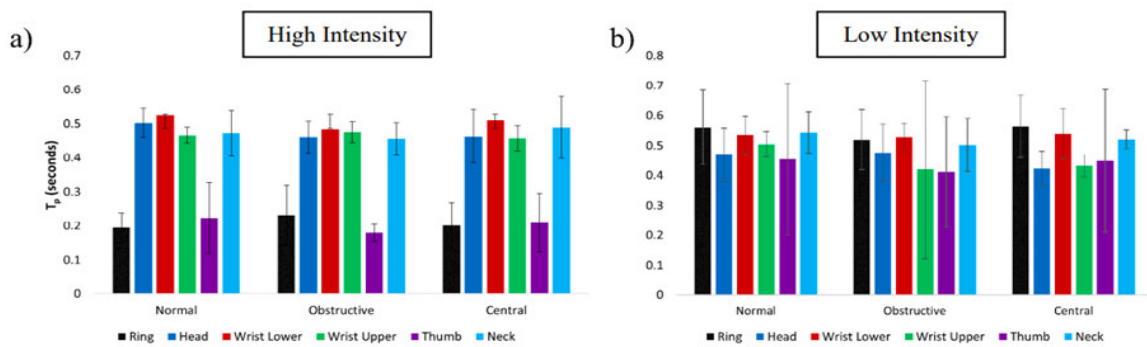


Figure 13 Time to peak taken from 6 measurement sites for normal and apneic conditions in (a) High LED intensity and (b) Low LED intensity

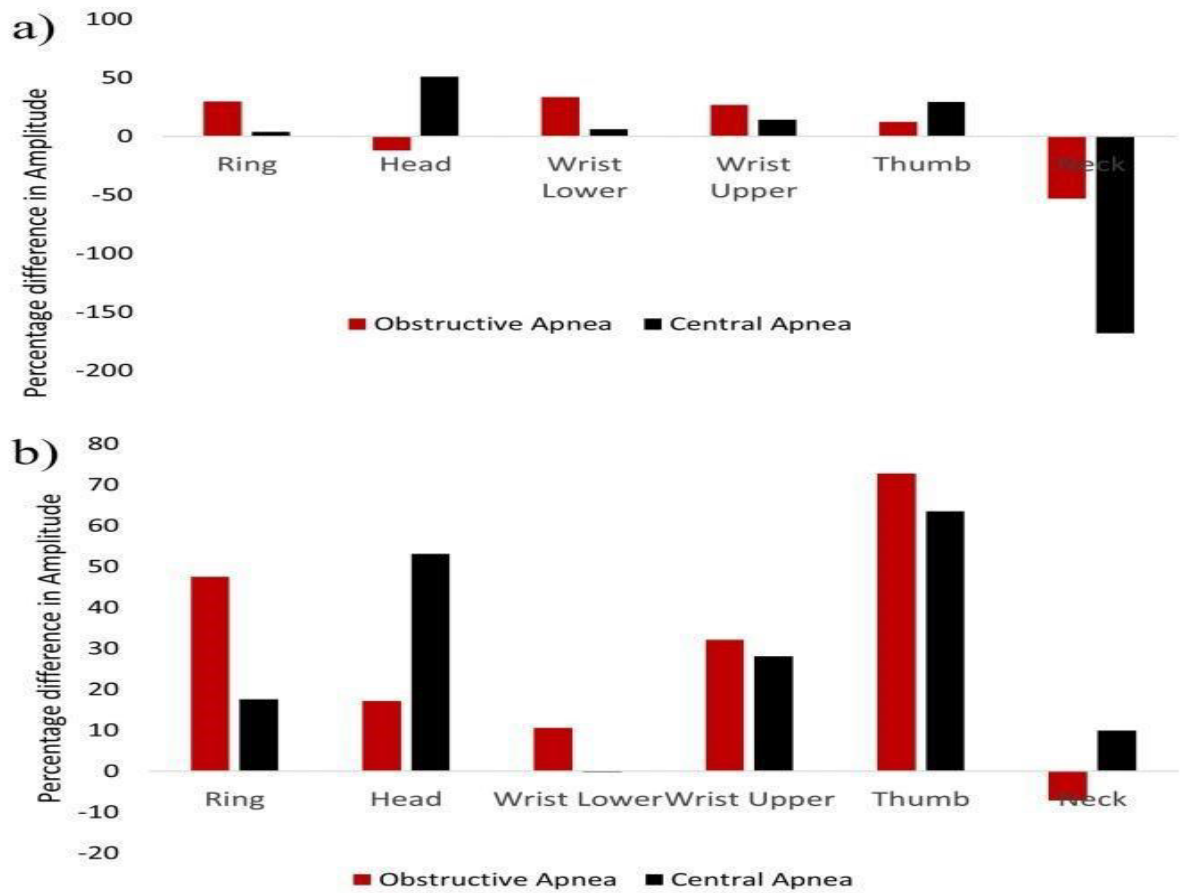


Figure 14 (a) The drop in amplitude at different locations during normal and apneic events for Led Intensity = 37 mA (b) The drop in amplitude at different locations during normal and apneic events for LED intensity = 493 mA.

## 2.4. Conclusion:

These findings emphasize the importance of selecting optimal measurement sites and appropriate LED intensities to enhance the accuracy and reliability of sleep apnea detection using wearable devices. This research provides a foundation for the future development of PPG hardware, aiming to improve the fidelity of sleep apnea monitoring

in non-clinical settings by understanding the variations in PPG waveform characteristics across different body locations and LED light intensities.

We concluded from our work that the ring finger at the location of the ring was just as accurate as the gold standard (the tip of the finger) ( $p < 0.05$ ) in detecting the decrease of amplitude to the similarity of the tissue. This leads to the fact that smart rings could be indeed a good alternative for the tip of the finger clips.

We couldn't conclude if the stroke volume durations (Time to end a Systolic phase and time to end a diastolic phase) were affected by the apneic events which may be the difference between a real and a simulated apnea). (Figure 13).

We also could conclude that OSA generates a much bigger vasoconstriction compared to CSA which is due to the hemodynamic changes it causes and therefore might be easier to detect. Also, we noticed that multiple times CSA generated a vasoconstriction only after the procedure of breath holding was done, whereas during the procedure of cessation of breathing, it sometimes generated a vasodilation.

#### *2.4.1 OSA vs. CSA on Finger PPG*

##### 2.4.1.1 Obstructive Sleep Apnea (OSA):

In OSA, the physical blockage of the airway leads to a rapid drop in blood oxygen levels, triggering an immediate vasoconstrictive response.

This is seen in the PPG signal as a decrease in amplitude (DAP) due to reduced blood flow immediately. Vasoconstriction happens because the body is trying to maintain blood pressure and ensure oxygen reaches vital organs despite the obstruction. The

hemodynamic changes are large and consistent, making vasoconstriction a clear and reliable marker in OSA.

#### 2.4.1.2 Central Sleep Apnea (CSA):

In CSA, the absence of breathing effort doesn't always cause immediate vasoconstriction. Instead, the body may first respond with vasodilation to increase blood flow and oxygen delivery during the apnea. Once breathing resumes, vasoconstriction often follows as the body works to restore oxygen levels. This pattern of vasodilation followed by vasoconstriction, along with changes in heart rate, makes the hemodynamic response in CSA more variable and harder to predict compared to OSA.

This work has been defended and published in the journal Institute of Electrical and Electronics Engineers – Engineers in Medicine and Biology Society (IEEE-EMBC) and displayed publicly in Orlando City, Florida, USA for its 46<sup>th</sup> conference.

## CHAPTER 3

### FEATURE EXTRACTION AND EFFORT QUANTIFICATION

In this part of our work, we aim to expand on these efforts by attempting to classify apneic signals across both time and frequency domains [24, 31, 32].

Figure 15 shows some of the statistical features used, the Area Under the Curve (1) the Mean of the signal and the trimmed mean at 50% as well as the Amplitude of the AC signal which was computed as the difference between the maximum (peak) of the PPG subtracted by the previous minima(4).

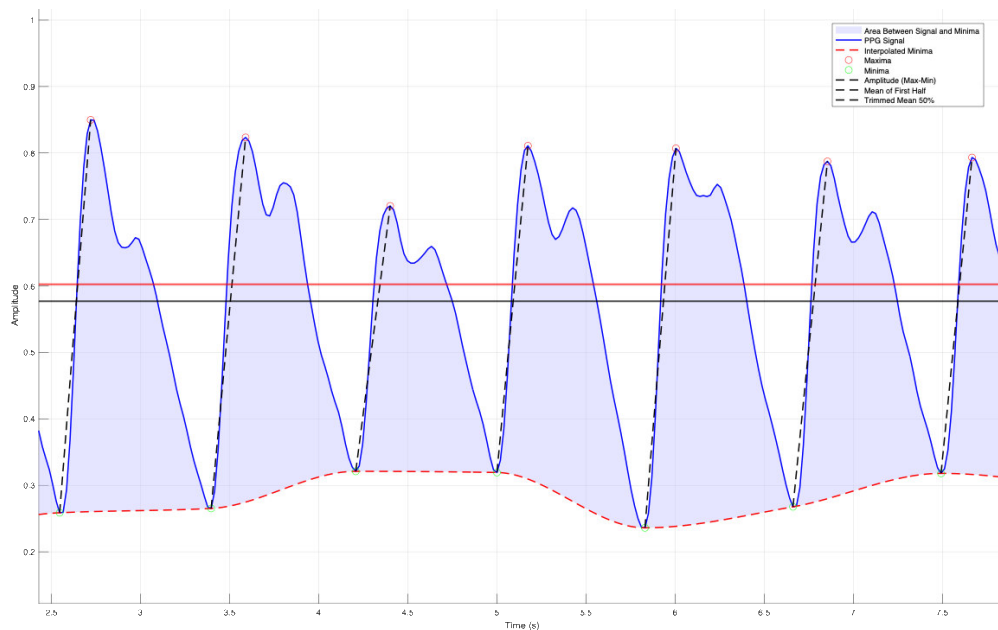


Figure 15 Statistical Features Extracted from the PPG

The rest of the features will be depicted in the table below.

Table 1 Features Extraction from the PPG Signal

No.	Feature	
1	AUC (Area Under the Curve)	
2	Mean	
3	Median	
4	Trimmed Mean 25%	
5	Trimmed Mean 50%	
6	MAD (Median Absolute Deviation)	
7	Mean Amplitude	
8	RMS (Root Mean Square)	
9	IQR (Interquartile Range)	
10	STD (Standard Deviation)	
11	Standard Error	
12	Teager Energy	
13	Average Low/High Frequency Energy Ratio	
14	Shape Factor	
15	Central Moment (10th order)	
16	Skewness	
17	Kurtosis	
18	Mean Tp	
19	Geometric Mean	
20	Mean Time Differences	

21	DK (Dispersion Coefficient)	
22	Xmin (Minimum Value)	
23	Xmax (Maximum Value)	
24	Mean Width	
25	Activity	
26	Mobility	
27	Complexity	
28	p-value (from Sign Test) h-value (from Sign Test)	
29	Mode	
30	Velocity PG(VPG) and Acceleration PG (APG) (Figure 16)	
31	Td	

Some of these features included are the Velocity of the PPG (VPG) which shows the velocity of the blood in the vessels and Acceleration of the PPG(APG).

In Figure 16 an apnea was simulated at time  $t = 15$  seconds which resulted in a decrease in amplitude of the PPG and a decrease in both the velocity and acceleration of the blood in the blood vessels which is the result of stiffer blood vessels.

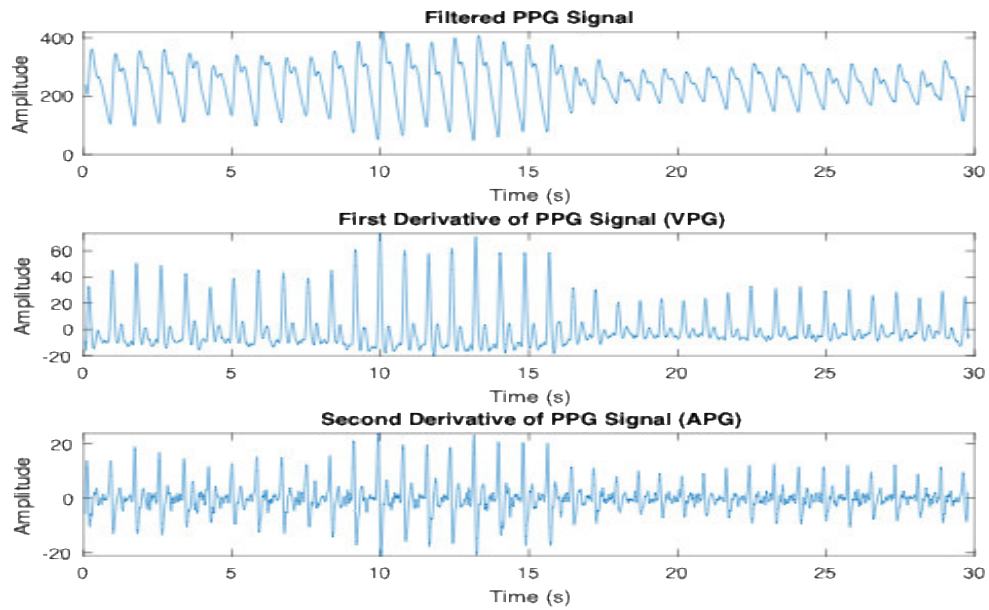


Figure 16 PPG VPG and APG plots and the decrease of the peak-to-peak amplitude after a simulated apnea at time  $t = 15$  seconds

### 3.1 Recording from the Wrist Ventral Side

#### 3.1.1 PPG Derived Respiration signal (PPGDR):

It is quite known that Respiratory signals could be derived from PPG since the DC drift of the PPG is affected by the breathing modulation. Multiple methods have been used to determine breathing rates from PPG.

Analytical methods such as Principal Component Analysis and Deep Learning have been used to compute PPGDR but seem to need a large amount of time to converge towards an accurate breathing rate. Advances in ultra-sensitive photonic devices have demonstrated the feasibility of high-fidelity physiological signal acquisition, which

supports the rationale for exploring novel PPG-based respiratory monitoring approaches, especially in wearable systems [33].

Adaptive estimations such as Empirical Mode Decomposition and Adaptive respiration rate estimators are very sensitive to noise resulting in a low fidelity PPGDR and are easily disrupted [34].

Both these methods also require large time and space complexity. Hartmann et al., used multiple Digital Filtering methods to deduce the respiration rate from multiple locations on the body and concluded in that the best PPG-derived Respiratory Frequency could be obtained from the forehead and finger, respectively, for normal and deep breathing patterns and that the wrist under resulted in a higher amplitude signal than the wrist upper[25].

Massie et al. [21] evaluated Digital filtering to classify CSA by high pass filtering the PPG signal of over 200 patients at a cutoff frequency of 0.15 Hz claiming that the respiration rate of the patients during sleep is around 0.2 to 0.33 Hz and therefore will remain unaffected by the filtering. He showed that the surface (Hilbert Transformation) of the signal would reflect the patient's effort to breathe. The PPG signal measured at the fingertip inherently contains respiratory information because the blood flow to the body's extremities gets affected by alterations in thoracic pressure throughout the respiratory cycle. Therefore, the PPG signal amplitude oscillates in synchrony with the respiratory cycle. This amplitude modulation can be isolated to retain a signal representing respiratory effort.

This method resulted in a sensitivity of 81%, a specificity of 99% a positive predictive value of 90%, and a negative predictive value of 98%. However, in this work, a large amount of data had to be rejected due to strong vasoconstriction which follows

most sleep apneas resulting in a low Signal to Noise ratio making it impossible to derive a PPGDR. This is due to the vasoconstrictive property of the finger that were already discussed earlier in this work resulting in a high Signal to Noise Ratio (SNR).

In our work, we chose the wrist ventral side since that location would never be affected by vasoconstriction therefore always returning a high-fidelity PPG and therefore a high-fidelity PPG-Derived Respiration (PPGDR) under any circumstance and would have a higher amplitude than the wrist upper.

To derive the PPGDR we tested the following:

To isolate the respiratory signal from the PPG data, we first apply a high-pass filter using a Butter order 4 filter with a cutoff frequency to remove low-frequency components unrelated to respiration (Under 0.18 Hz), such as baseline wander and motion artifacts. This choice of cutoff frequency effectively separates the respiratory and cardiac components from slower physiological variations.

Following the high-pass filtering, we apply a band-pass filter with cutoff frequencies set between 0.2 Hz and 0.4 Hz. This range was selected because typical human respiratory rates fall within this frequency band (A cutoff of 0.2 Hz corresponds to a breathing rate of about 12 breaths per minute, while 0.4 Hz corresponds to 24 breaths per minute (which is higher than normal but may occur under certain conditions)).

This frequency range effectively isolates the respiratory signal from the PPG data. The filtering is performed using a 2nd-order Butterworth filter to ensure a smooth response with minimal phase distortion.

For us to test our filters we decided to record PPG from the wrist under in an attempt to extract a respiration signal. The participant was asked to breathe at a frequency of 0.2 Hz (12 breaths per minute) using a metronome. And around the times  $t=40$  seconds

and time  $t = 60$  seconds, cessation of breathing of 20 seconds would be simulated to resemble a central apnea for a whole cycle (leaving around 40 seconds between each attempt for the patient to restore his/her physiological stability) for that maneuver, the patient wore a nose clip to make sure no air was flowing through their noses.

Figure 17 shows an unfiltered PPG signal which was later on filtered as previously explained to derive the PPGDR. Figure 18 shows the fluctuation of the PPG after being high-passed filtered at 0.18 Hz which resembles what Massie et al. published in his work to derive respiration signal out of PPG.

Figure 19 shows the Fast Fourier Transform (FFT) of the raw signal from time 0 to 40 seconds. A clear peak coming from the respiration frequency enforced on the patient could be seen (at 0.2001 Hz), the heartbeat (1.295 Hz which stands for 77 heartbeats per minute), the first and second harmonics of the heartbeat ( $2f, 3f$ ) of the heartbeats could also be seen at 2.451 and 3.685 Hz.

Figure 20 shows a clear drop in amplitude in the signal could be shown in the timelapse where the Central Apnea was simulated (40 to 60 seconds and 100 to 120 seconds) meaning that the energy of the signal at the respiratory frequencies decreased during these periods.

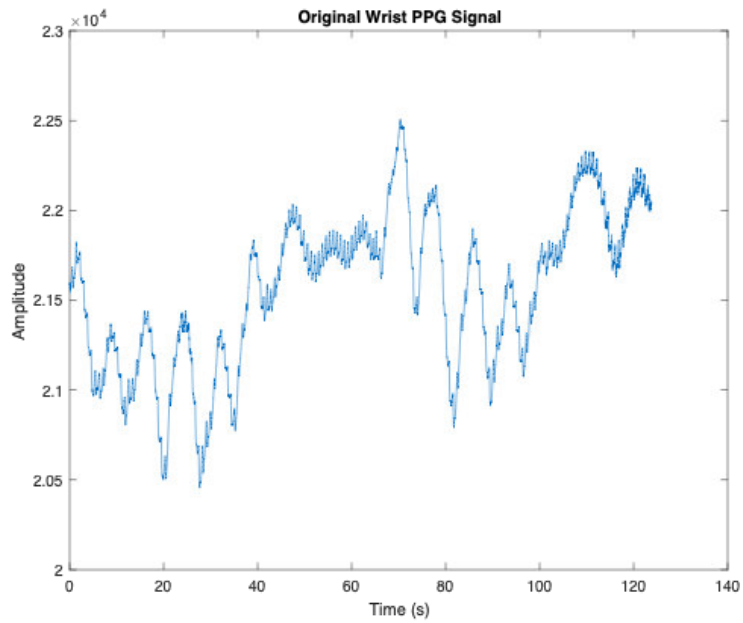


Figure 17 Raw PPG Recorded From the Wrist

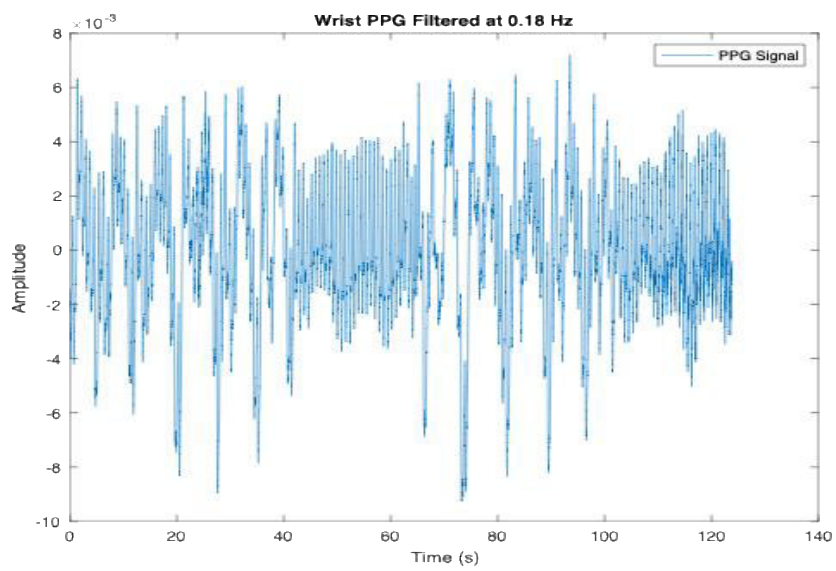


Figure 18 High Passed Filtered PPG (0.18 Hz)

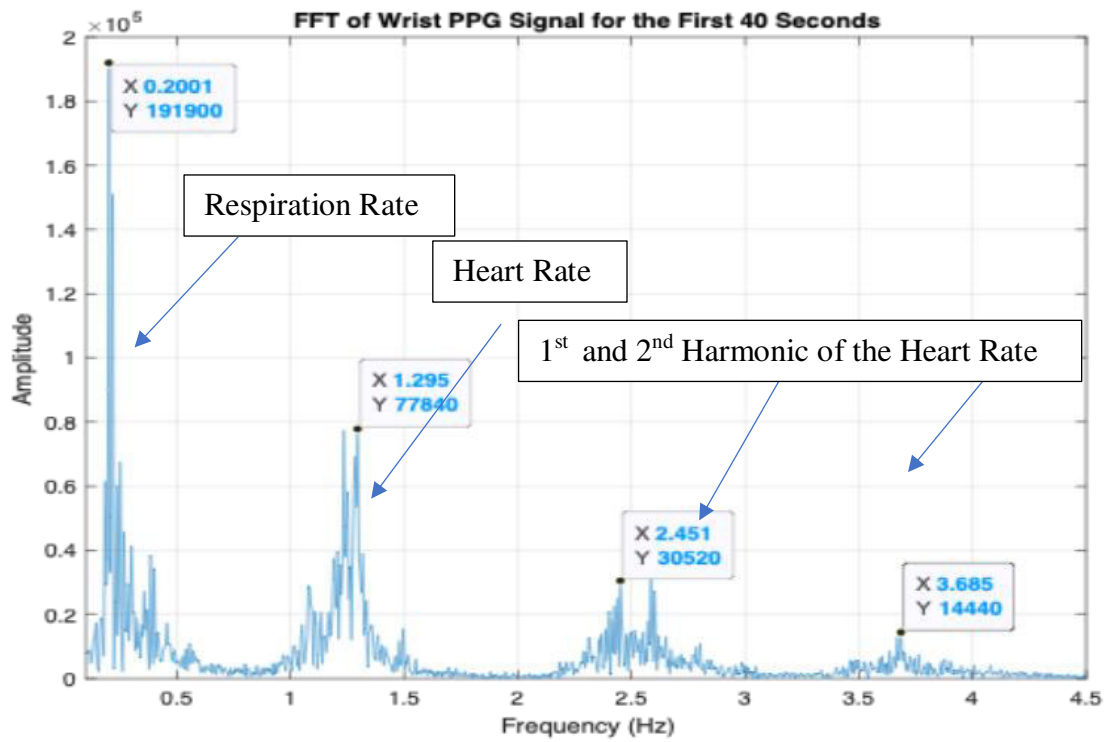


Figure 19 FFT of the PPG after High Pass Filter at 0.18 Hz

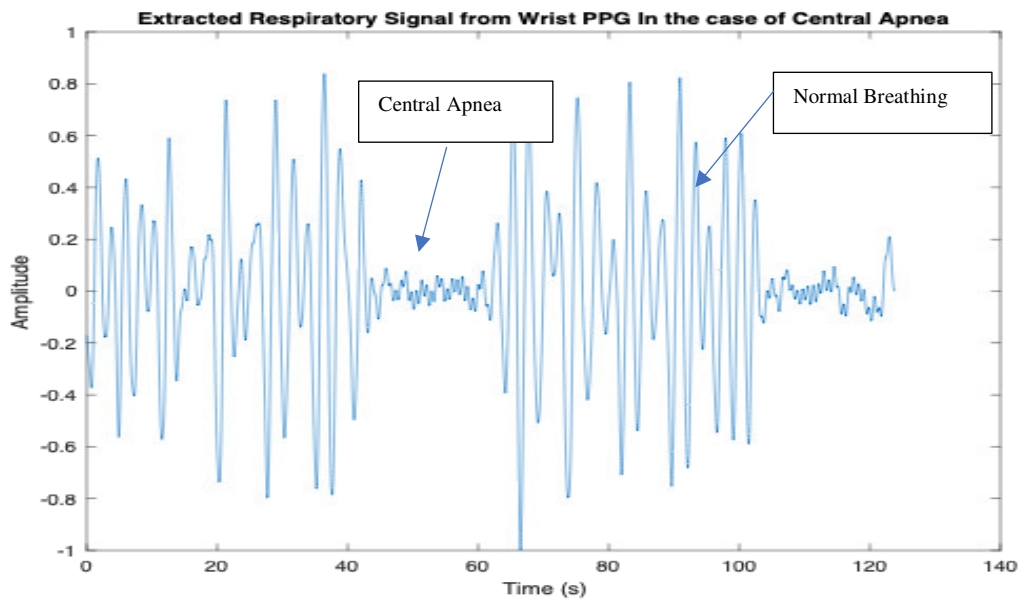


Figure 20 PPGDR extracted from PPG Signal from the Wrist Under (CSA)

To simulate OSA, the Mueller Maneuver was performed using a nose clip and a mouthpiece wide enough to let the participant breathe comfortably during normal episodes of time.

The mouthpiece was then occluded during the apneic episodes (40 to 60 seconds and 100 to 120 seconds).

Figure 21 shows the unfiltered PPG signal recorded for that experiment. After filtering (Figure 22), an increase in the amplitude of the PPGDR signal during apneic episodes is due to the increase in the effort of breathing.

A pattern classification methodology will be trained and tested to classify the PPGDR in Aim 2.3.

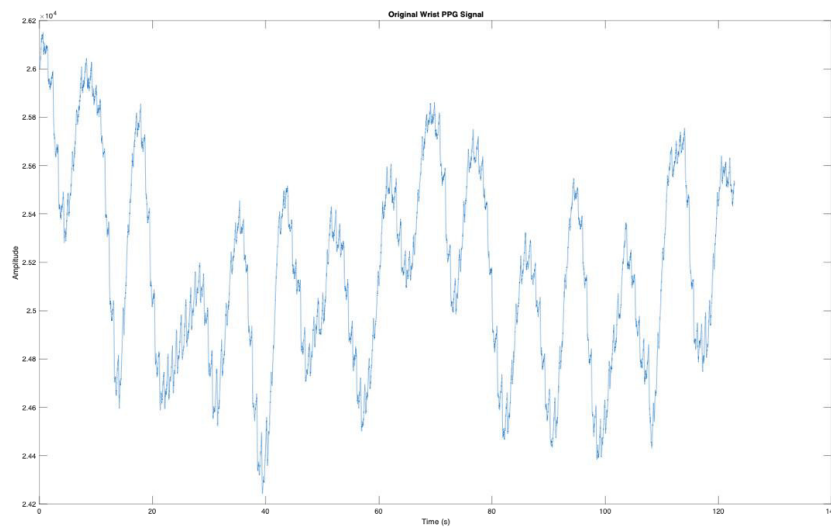


Figure 21 Unfiltered PPG Signal from the Wrist Under (OSA)

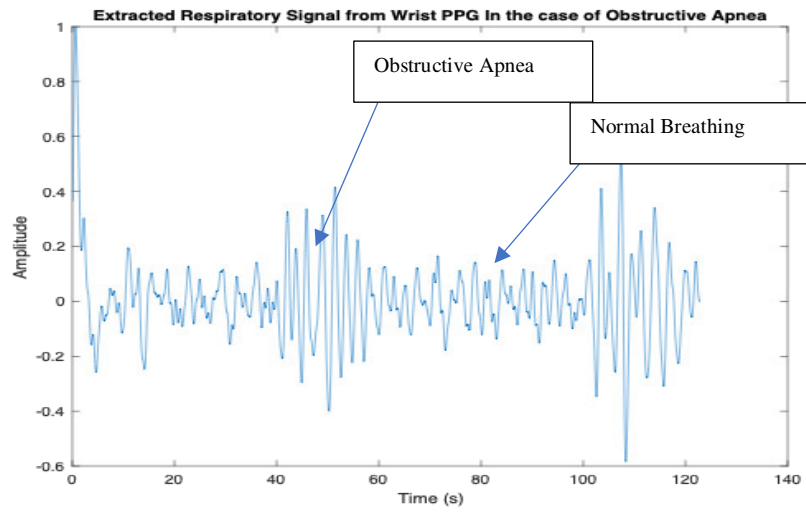


Figure 22 PPGDR extracted from PPG (OSA)

### 3.2 Vernier Belt

To ensure our method for extracting PPG-derived respiration (PPGDR) was accurate, we used a Vernier belt (Figure 23) as a reference. The Vernier belt is a trusted tool for measuring respiratory patterns, such as breathing rate and depth.



Figure 23 The Vernier Respiration Belt

The Vernier belt was positioned on the abdomen, since in OSA, upper airway obstruction often leads individuals to rely more on diaphragmatic or abdominal breathing aiming to maintain adequate ventilation during apneic events, this placement allows for effective monitoring of this diaphragmatic activity, capturing the increased effort exerted by the diaphragm during OSA episodes. [28] discusses how the lack of air reaching the lungs at high amplitudes necessitates increased diaphragmatic effort to maintain airflow, potentially leading to diaphragmatic fatigue over time.

By placing the belt on the abdomen, we can accurately assess the heightened diaphragmatic effort characteristic of OSA, providing valuable insights into the patient's respiratory patterns and the physiological demands placed on the diaphragm during obstructive events with the PPGDR extracted from the wrist's PPG.

Upon comparing the PPG-derived respiratory (PPGDR) signal with the data from the abdominal belt, we observed a high degree of similarity in both frequency and amplitude, indicating that both methods effectively captured the same breathing patterns. This correlation was consistent across various breathing scenarios, including central and obstructive apneas. The strong agreement between the PPGDR signal and the abdominal belt data reinforces the reliability of PPGDR as a tool for accurately detecting respiratory activity such as Central Apneas due to very low Energy of the signal at the band [0.2 – 0.4 Hz] (figure 25) and Obstructive Apneas due to increased energy of the signal at the band [0.2 – 0.4 Hz] (figure 26).

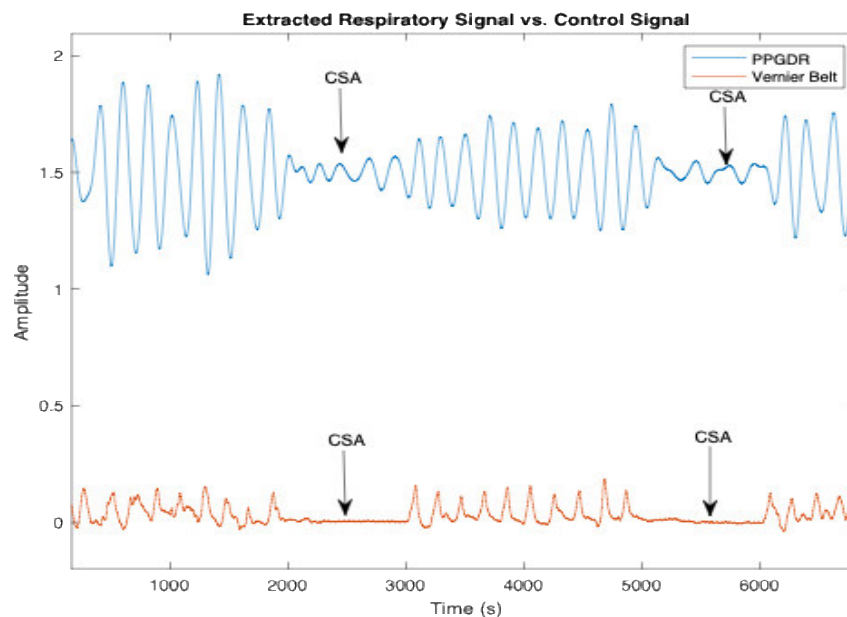


Figure 24 Comparing the PPGDR to Control Signal for the case of Central Apnea.

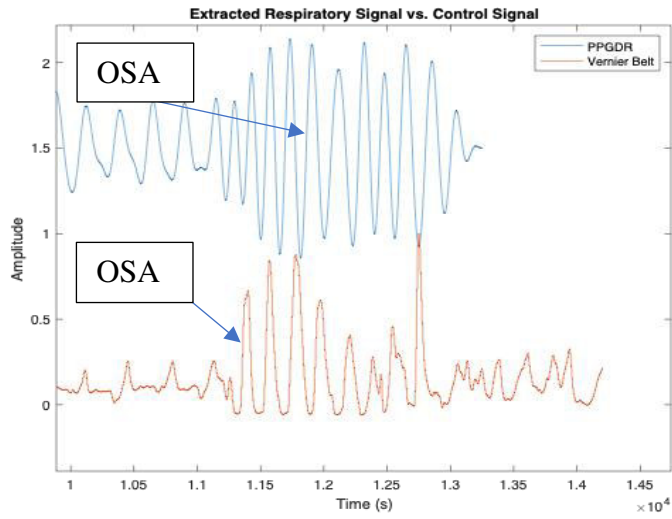


Figure 25 Comparing the PPGDR to Control Signal for the case of Obstructive Apnea

Figure 27 shows the comparison of the PPGDR extracted from filtering the respiration to the one extracted from high-pass filtering the PPG to a control signal.

We therefore show that the method we used (Method 1) results in similar results as the one of Massie et al. (Method 2) Where we seem to have close results in both methods while comparing the frequencies of the fluctuations of each signal as seen from the FFT algorithm (Figure 29).

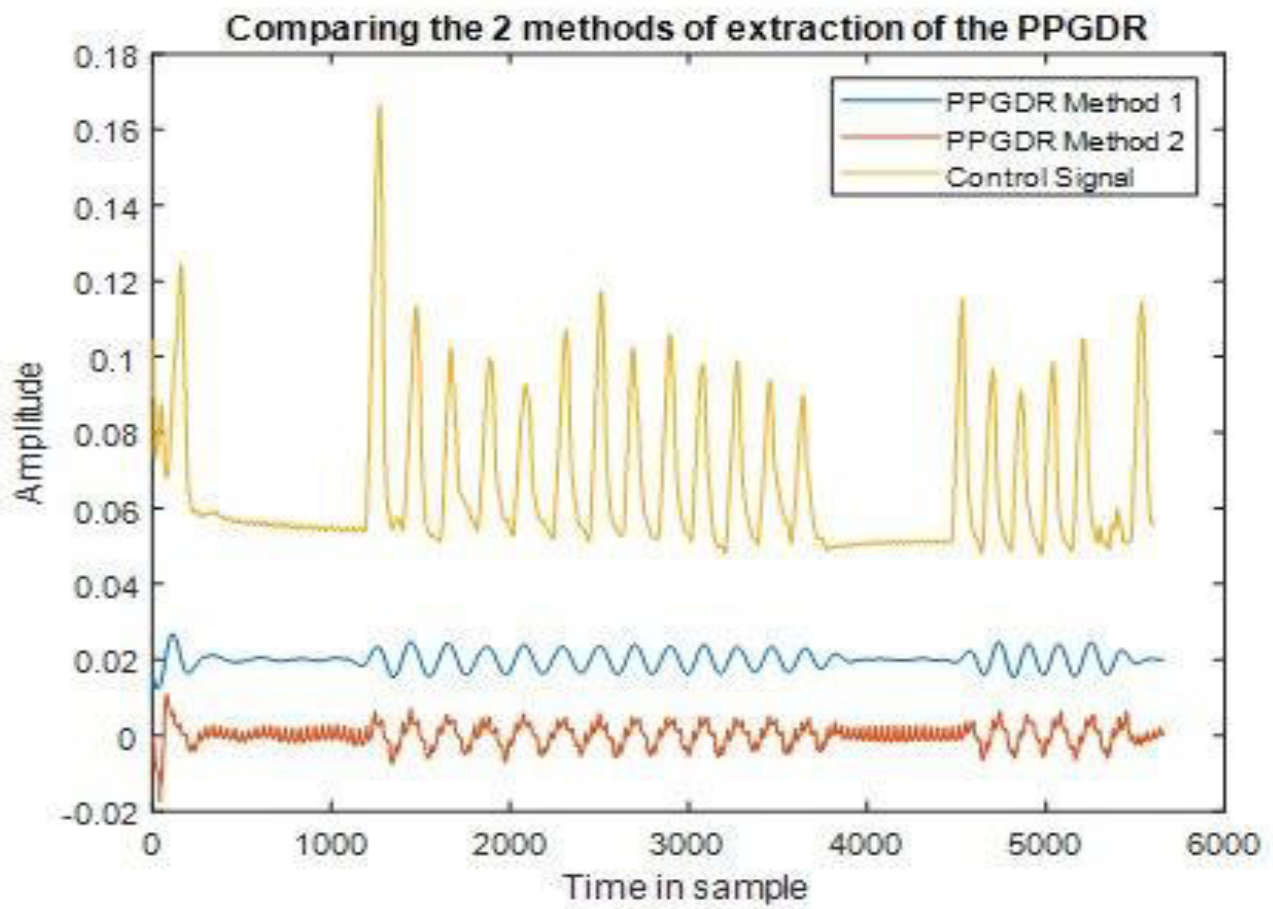


Figure 26 Comparing the 2 methods of extraction of PPGDR

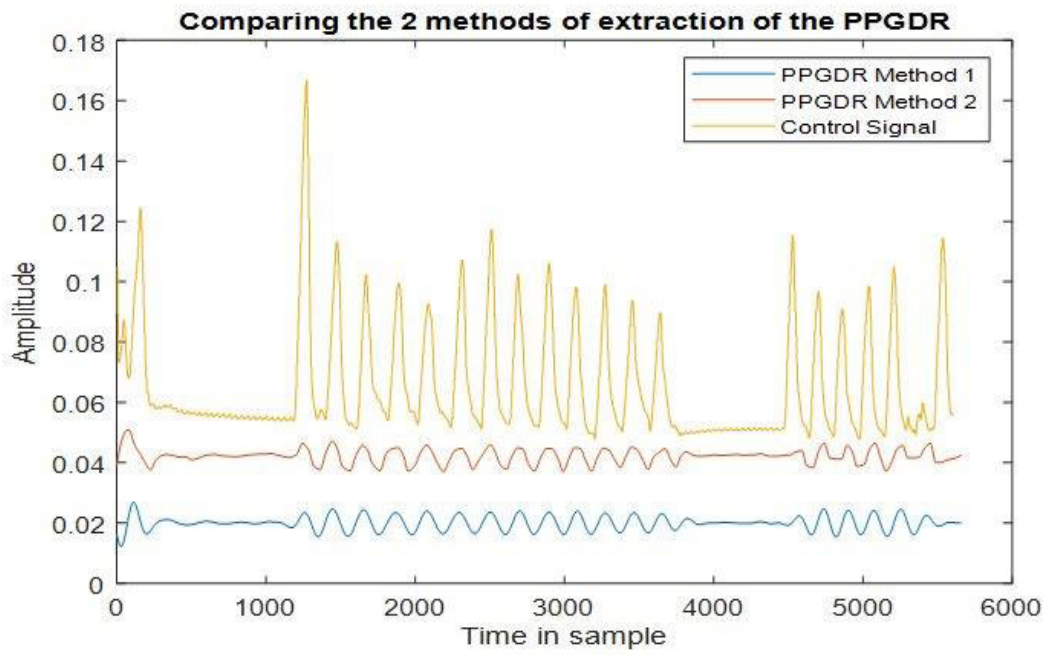


Figure 27 Comparing the 2 methods of extraction of PPGDR.

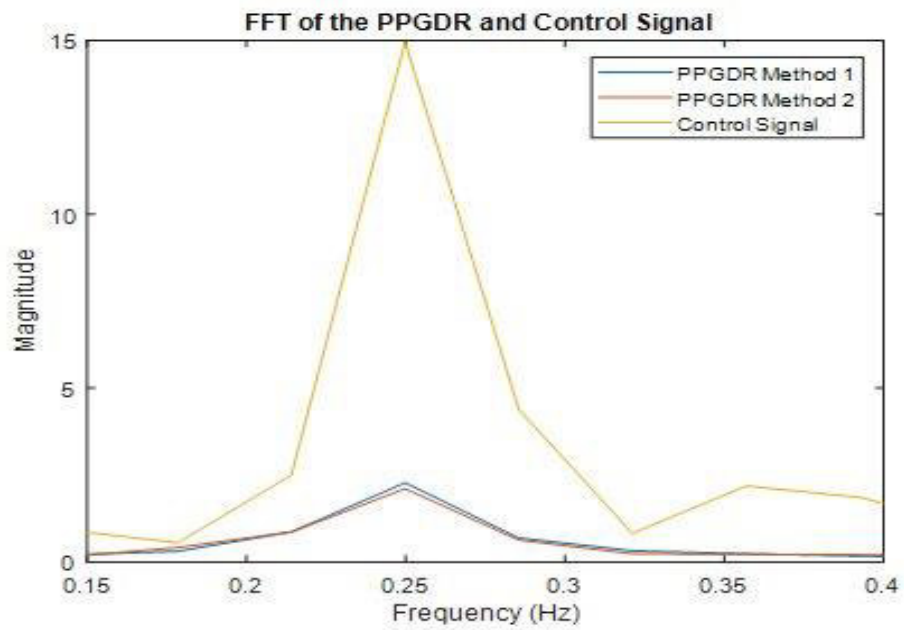


Figure 28 Fast Fourier Transform of the PPGDR methodologies compared to the Control Signal.

### 3.3 The Flowchart

In the next part of our work, we plan on incorporating a more sophisticated protocol.

Participants were positioned on a massage table to promote relaxation and mimic sleep-like conditions and reach the closest possible state to sleep since blood pressure is affected by positions.

Also, a nose clip and a mouthpiece wide enough for patients will be used to breathe through it and will be blocked when needed to simulate central/obstructive apnea. A flowchart was designed and will be used to classify the apneic events as shown in the Figure 30.

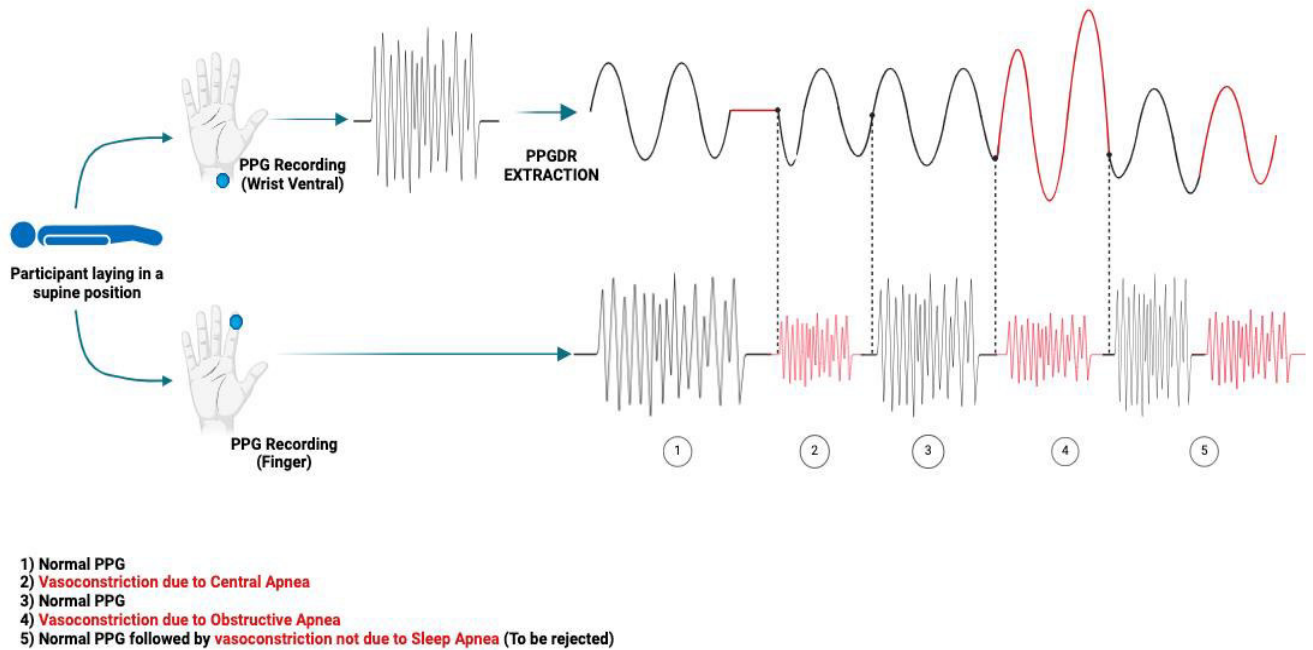


Figure 29 Strategy of Detection and Classification of Apneic Events

All these features will be used in Chapter 6 to create classifying algorithms (K-Nearest Neighbors, Support Vector Machine, logarithmic Regressions, Multilayer feed forward neural networks models etc...) to distinguish normal from apneic regardless of the type of apnea after significance test.

We are therefore hoping to have information on whether or not an apnea happened and if so, was there an effort present (OSA) or was there no effort (CSA) which is also showing in the following decision tree (Figure 31).

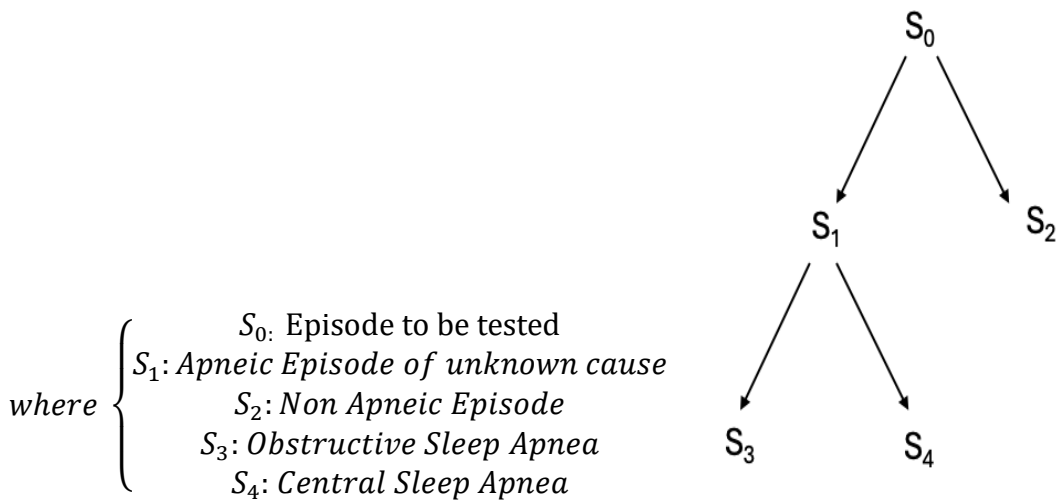


Figure 30 Decision Tree of the full system

### 3.4. Signal Alignment

During our experiment, one challenge we encountered was the use of three separate sensors, each with its own acquisition system. This meant that a manual press of three different "ON" buttons was needed to start the experiment, leading to non-synchronized signals due to variations in the timing of signal initiation and this might not solve the issue due to the buffer of each sensor. Such misalignment could negatively impact the results.

We explored multiple solutions to tackle this problem.

First, we considered manually minimizing the delay between button presses to align the signals as closely as possible. Another approach involved using an AND gate—a logic component that generates an output of "1" only when all inputs (button presses) are simultaneously "1."

However, a better option to resolve the issue in software by employing an event-based method to align and correlate the signals using the 'xcross()' Matlab function and is depicted by the following function:

Cross-correlation-based signal alignment in MATLAB

Compute the cross-correlation between the two signals

```
[cross_corr, lags] = xcorr(signal1, signal2);
```

Find the index where the cross-correlation is maximum

```
[~, maxIndex] = max(cross_corr);
```

Determine the lag (time shift) corresponding to that maximum

optimalLag = lags(maxIndex);

Shift signal2 by the optimal lag to align it with signal1

alignedSignal2 = circshift(signal2, optimalLag);

$$\sum_{m=-\infty}^{m=+\infty} f[\bar{m}]g[m + n] = (f * g) [n]$$

Where  $f[m]$  and  $g[m]$  are two signals that are being computed,  $f[\bar{m}]$  is the conjugate of  $f[m]$  and  $n$  being the displacement which is commonly said as the lag.

To find the optimal lag we would therefore shift one signal and compare the similarity of the 2 signals.

[35]used the inter-beat-interval series from EKG and PPG were extracted and aligned by maximizing their cross-correlation.

[36]another method was also used where the time delay between two PPG signals from the finger and the wrist was determined using cross-correlation, selecting three consecutive peaks that satisfy specific conditions to ensure accurate detection, with the time delay either corresponding to the pulse transit time (PTT) or the sum of the heart rate period and PTT, depending on the nature of the second peak.

One example of a significant event we thought of using for this purpose was CSA, as observed, impacts both the PPGDR signals recorded from the wrist and the control signals from the Vernier belt by flattening both signals.

The same methodology can be applied to synchronize the PPG signals from the finger and the wrist. One proposed approach is to assume that the spatial distance between the finger and the wrist is negligible, effectively considering the pulse transit time (PTT) to be zero. This allows for aligning the peaks of the PPG signals from the two locations.

Next step would be to align the 2 PPG signals based on the similarity of the pulse rate variability (PRV) or peak-to-peak intervals for the assumption that it would be the same across the 2 locations.

To achieve synchronization across multiple signals, a divide-and-conquer strategy is employed. The process involves:

1. Correlating the PPG signals from the finger and the wrist to align extract the pulse intervals into 2 arrays and correlating these 2 arrays with the PRV being common ground between the 2 signals, taking advantage of the minimal delay between these two locations.

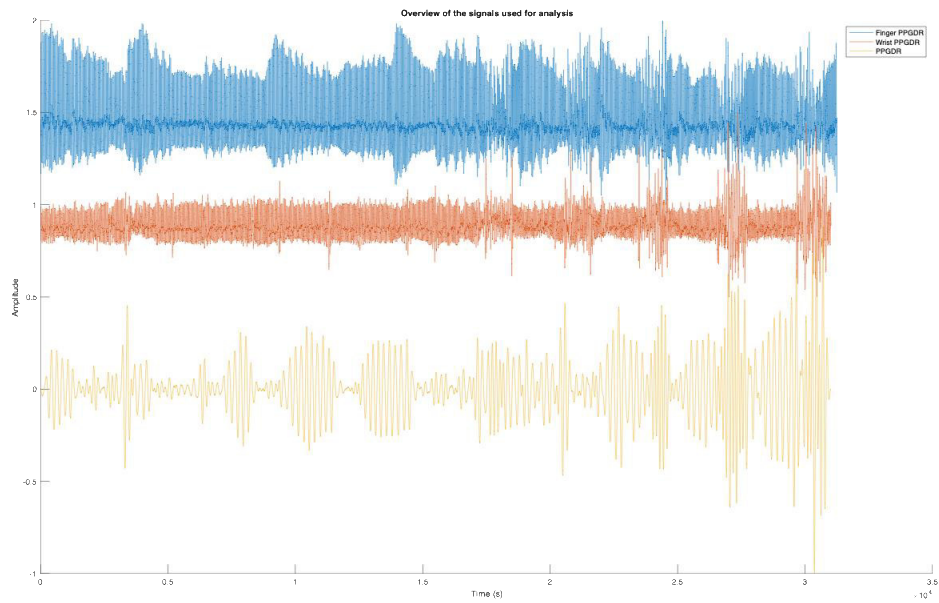


Figure 31 Wrist and Finger PPG with the extracted PPGDR

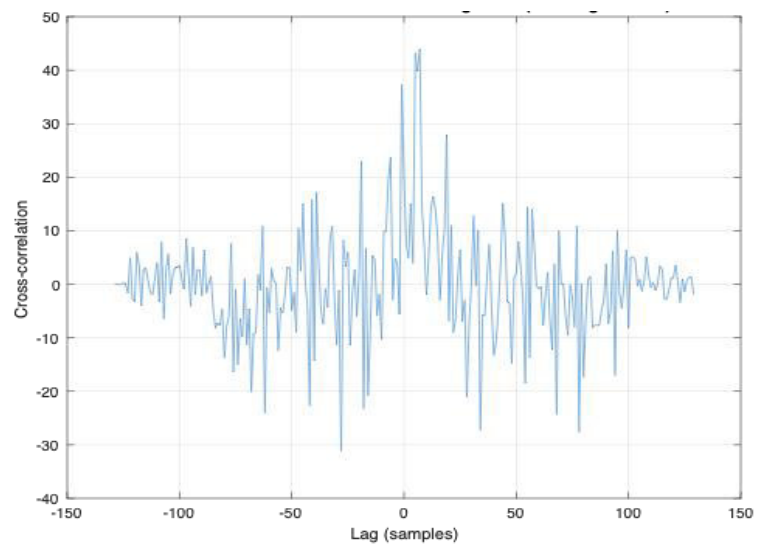


Figure 32 Cross-Correlation between Wrist and Finger PPG based on the Peak to Peak Intervals (of 7 peaks)

2. Deriving the PPGDR signal from the wrist. Correlating the PPGDR signal with the Vernier control signal to achieve full synchronization using the time delay between consecutive breaths.

In the following example, we made sure to generate a big-time delay between the Control and PPGDR signals as seen in Figure 33. In that case, we could clearly see that the PPGDR (Orange) is leading the Control signal (Blue).

After that, we would find the peaks of each of these 2 signals being the breaths

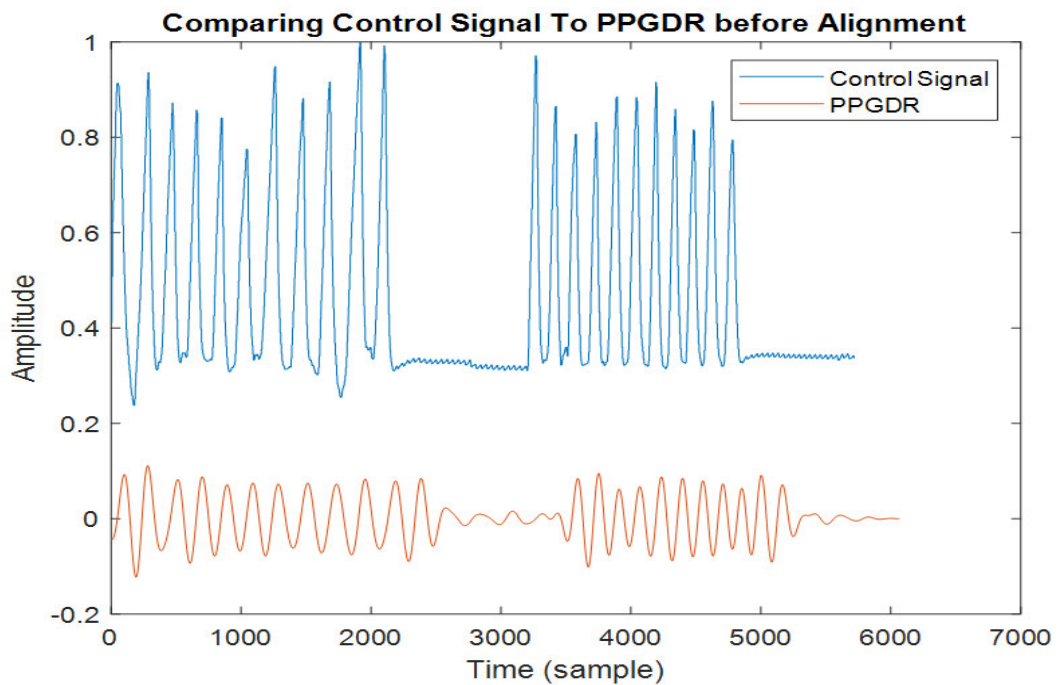


Figure 33 Comparing Control Signal to PPGDR before Alignment

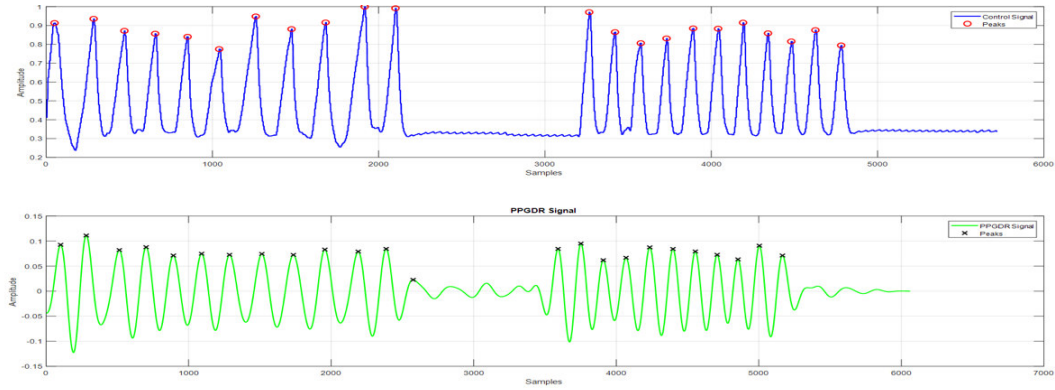


Figure 34 Detection of Peaks (Breaths) in both the PPGDR and the Control Signal

The next step would be to create 2 arrays containing the breath-to-breath intervals of each signal and then returning their cross correlation to find the following.

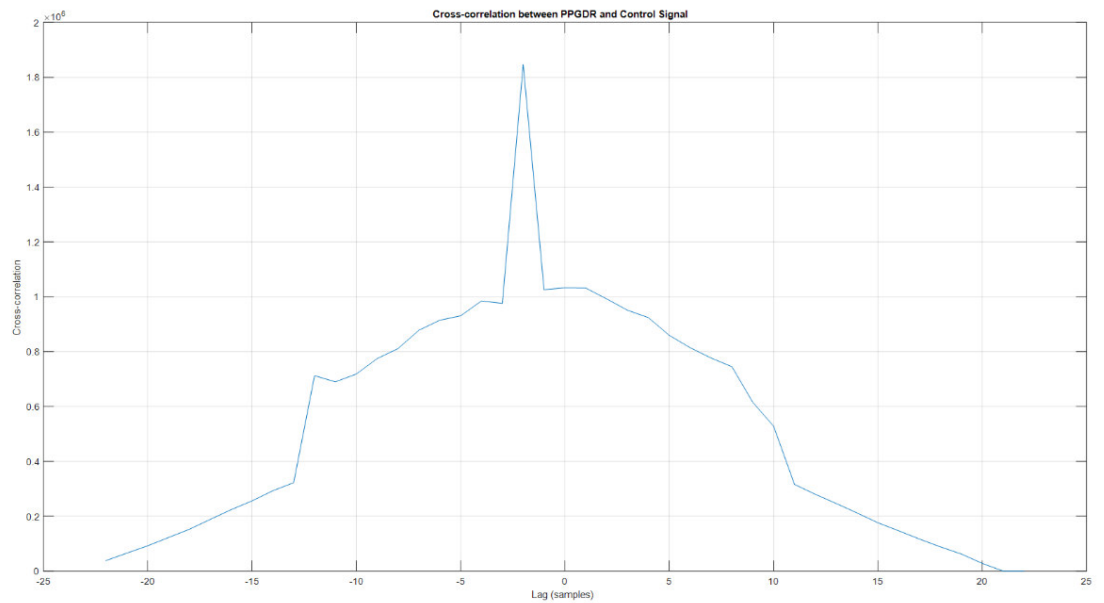


Figure 35 Cross-Correlation between the PPGDR and the Control Signal

In the Figure 33 above, we see the x axis of the plot being bounded by  $\pm 22$  being the number of breath (peaks) in the control signal.

We see a peak in the cross correlation at a  $x = -2$  meaning that the best possible correlation seems to be happening at the time where the participant took his second breath.

The PPGDR was then plotted from the location of the second breath and on and the result was found in the Figure 37 as following.

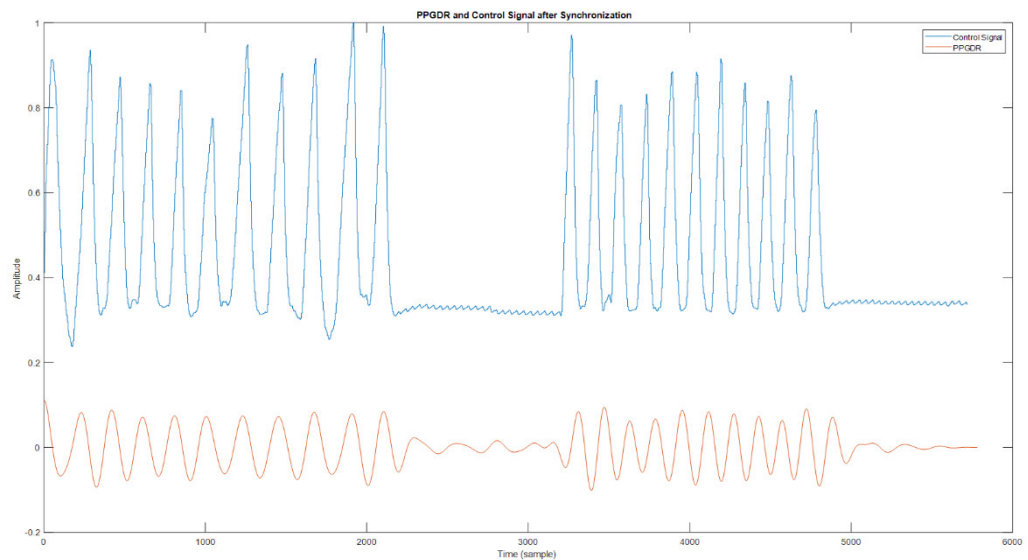


Figure 36 PPGDR and Control Signal after Alignment

We see that indeed, the CSA events and the peaks seem to correlate much more and are much better superimposed showing a higher correlation between the 2 signals. By sequentially aligning the signals in this way, we can successfully correlate all four signals (PPG from the finger, PPG from the wrist, PPGDR from the wrist, and the

control signal) despite using independent acquisition systems. This stepwise approach ensures the best possible alignment given the limitations of the setup.

### 3.5. Cases of Rejection

Not all vasoconstriction events correlate with apneic events. To better classify and understand these events [22] we used an adaptive filter based on the Root Mean Square of the signal and classified each event into 5 groups as follows:

- Group 1 involves a decrease in SaO<sub>2</sub> by at least 3% without a reduction in airflow.
- Group 2 sees airflow decrease by at least 50% for a minimum of 5 seconds without a change in SaO<sub>2</sub>.
- Group 3 combined a reduction in airflow by more than 50% with a decrease in SaO<sub>2</sub> of at least 3%.
- Group 4 includes events that do not correlate with airflow reduction or SaO<sub>2</sub> decrement,
- Group 5 encompasses events not related to apneas or SaO<sub>2</sub> decreases but involve changes in respiration.

The paper later worked only on Group 1, 2 and 3 are apneic and Group 4 and 5 are non-apneic events.

Therefore, the need for a better classification of robust method that could help determine what data corresponds to random vasoconstriction improving the model's accuracy in detecting and diagnosing sleep apnea.

This work integrates the analyses from both the finger and the wrist ventral side to make decisions about each 20-second epoch. According to AASM standards, we will identify occurrences of vasoconstrictions in the finger lasting more than 10 seconds and then evaluate these based on PPGDR output.

- If PPGDR returns a straight line, this indicates the vasoconstriction is due to central apnea. If PPGDR shows a flat signal for more than 10 seconds and finger PPG does not indicate any vasoconstriction, the conclusion will also point towards central apnea.
- If finger PPG detects vasoconstriction but normal breathing is still present, this vasoconstriction can be discarded as it may be due to random factors which is well illustrated in Figure 37 from sample 3500 to 4200.
- For obstructive apnea, vasoconstriction is considered when there is chaotic activity in the PPGDR signal. This chaos can be quantified using feature extraction, which provides a clear indication of changes in breathing effort.

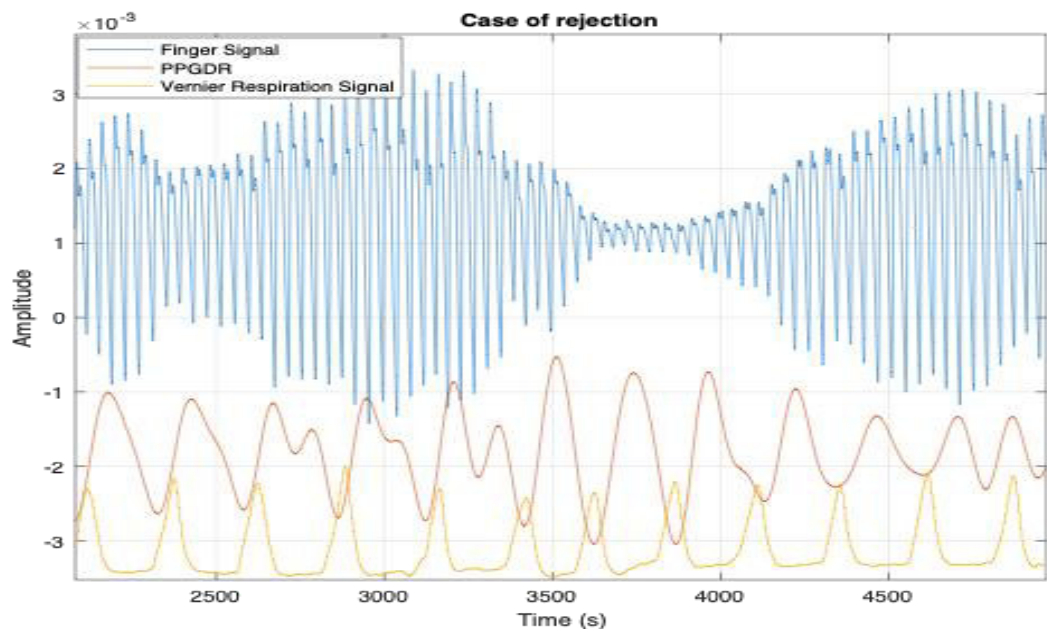


Figure 37 Example of a Case of Rejection

### **3.6. Recruitment Process**

The recruitment process started at AUB for healthy individuals willing to take part in research similarly to the one we had in previous chapters.

We once again insisted on the criteria not to simulate their cardiac/neural systems using caffeine, nicotine or any type of drugs.

A table was installed in the laboratory for them to lay comfortably in a supine position.

6 men with an average weight of  $83.33 \pm 9.71$  kg and an average age of  $23 \pm 1.9$  years old as well as 4 women with an average weight of  $66.25 \pm 16.13$  kg with an average age of 22 years old answered the call.

The finger PPG, Wrist PPG and respiration Band were attached to them and recordings started for 10 minutes for each one of the candidates where candidates were asked to simulate at least 1 apneic episode per minute either Central or Obstructive wearing a nose-clip and a mouthpiece.

#### *3.6.1 Finger PPG extraction*

After testing the PPGDR, we decided to test the features of the PPG. Previously we decided to have 2 clusters, one for apneic (vasoconstricted PPG) and one for control PPG.

We then used the features discussed in Aim 1.2 and computed a p-test to show the relevance of the 32 features.

The following table summarizes the features and computes the p-test of each of the features comparing 'Normal' to 'Apneic' signal.

Table 2 Significance Test of the Extracted Features

No.	Feature	Apneic Mean $\pm$ SD	Control Mean $\pm$ SD	Two-sided T test
1	AUC(Area Under the Curve)	3.9456 $\pm$ 0.6381	5.6092 $\pm$ 0.9269	0.0108*
2	Median	0.4853 $\pm$ 0.0545	0.5013 $\pm$ 0.0615	0.6759
3	MAD	0.1033 $\pm$ 0.0192	0.1446 $\pm$ 0.0160	0.0061*
4	Trimmed Mean 25%	0.4772 $\pm$ 0.0547	0.4828 $\pm$ 0.0579	0.8787
5	Trimmed Mean 50%	0.4790 $\pm$ 0.0564	0.4877 $\pm$ 0.0618	0.8226
6	Geometric Mean	0.4247 $\pm$ 0.0541	0.4350 $\pm$ 0.0502	0.7636
7	RMS value	0.4981 $\pm$ 0.0503	0.5153 $\pm$ 0.0501	0.6019
8	IQR	0.1674 $\pm$ 0.0545	0.2570 $\pm$ 0.0406	0.0184*
9	Mean	0.4789 $\pm$ 0.0504	0.4833 $\pm$ 0.0506	0.8951
10	STD (Standard Deviation)	0.1323 $\pm$ 0.0164	0.1757 $\pm$ 0.0171	0.0035*

11	Standard Error	0.0042±0.0005	0.0056 ± 0.0005	0.0035*
12	Teager Energy	0.0022± 0.0007	0.0035 ±0.0007	0.0134*
13	Average Low/High Frequency Energy Ratio	0.2502±0.0497	0.2677 ± 0.0502	0.5949
14	Shape Factor	0.7273±0.0347	0.7558 ± 0.0346	0.2293
15	Central Moment (10th order)	0.0000±0.0000	0.0000± 0.0000	1
16	Skewness	0.1193±0.2709	0.0042± 0.3281	0.562
17	Kurtosis	3.2557± 0.7138	2.3993± 0.3661	0.0441*
18	Time to reach peak	0.6019±0.5074	0.5389± 0.4369	0.8387
19	Amplitude	0.5348±0.1138	0.6131 ± 0.0793	0.2425
20	Mean PPI Time Differences	1.0676±0.2274	0.9751± 0.1824	0.4981
21	DK (Dispersion Coefficient)	27.7375± 3.4746	36.5372± 4.0201	0.006*

22	Xmin (Minimum Value)	0.1362 ±0.0178	0.0928± 0.0307	0.0258*
23	Xmax (Maximum Value)	0.8491 ± 0.0297	0.8864± 0.0222	0.0542
24	Mean Width	0.8384 ±0.1089	0.8524± 0.1080	0.8437
25	Activity	0.0189 ±0.0042	0.0321± 0.0059	0.0034*
26	Mobility	0.2443 ± 0.0319	0.2407± 0.0346	0.8701
27	Complexity	0.4318 ± 0.1171	0.4334± 0.1115	0.9824
28	p-value (from Sign Test)	0.0000±0	0.0000± 0	1
29	Velocity PG(VPG)	0.1166± 0.0266	0.1560± 0.0271	0.0644
30	Acceleration PG (APG)	0.0670 ± 0.0252	0.0893 ± 0.0288	0.2549
31	Mode	0.1362 ± 0.0178	0.1049 ± 0.0166	0.0311*

P-value<0.05 \*

The reduced number of significant features in our study, compared to those using actual apneic PPG signals, may stem from the physiological differences between Mueller Maneuver-induced apnea and true apnea.

Unlike real apnea, the Mueller Maneuver does not induce hypoxia or hypercapnia, leading to weaker autonomic and cardiovascular responses. Additionally, participant variability in airway anatomy and maneuver adherence further limits feature consistency.

These factors likely explain why fewer features in our study achieved statistical significance, highlighting the challenges of simulating true apnea and will be better explained in the limitation of the work.

After extracting the data from the participants, and having a better idea of the significant features, multiple machine learning algorithms will be used to classify first apneic from normal finger PPG signal, then classify the apneic finger PPG into Central and Obstructive using the PPGDR.

## CHAPTER 4

### CLASSIFICATION MODELS

This study was conducted in accordance with the ethical standards approved by the Institutional Review Board at AUB, protocol number BIO-2024-0243

#### **4.1. Distribution of the Data**

The data of the 7 participants was used to train the models whether for PPG or PPGDR and 3 others to test them. We imported the data and trained multiple algorithms which will then be tested on the data of 2 other participants leaving us with 70% of the dataset being used for training and 30% for testing.

#### **4.2. Classification at the level of the Finger (PPG)**

Data was extracted from the PPG of the participants' fingers, the dataset utilized for the significant physiological features along with corresponding labels indicating the presence or absence of apnea. To ensure data quality and improve model performance, rows containing NaN values in any feature column were excluded.

Five-fold cross-validation was employed, optimizing for  $F_1$ -score to maintain a balance between precision and recall.

#### **4.3. Classification models**

In both the classification of PPG and PPGDR we used multiple machine learning models to better classify our data.

## 4.4. Logistic Regression

Logistic regression is a linear model used for binary classification that predicts the probability of an outcome using a logistic function. It's interpretable and works well for understanding how input features influence the predicted probabilities

### 4.4.1 Hyperparameters

The model's regularization strength (C) was systematically evaluated across eight orders of logarithmic magnitude ( $10^{-4}$  to  $10^3$ ) to balance bias and variance. This ensured optimal generalization without overfitting the PPG-derived features.

#### 4.4.1.1 Algorithm Selection

Two solvers—L-BFGS (lbfgs) for efficiency and LIBLINEAR for smaller datasets—were compared. Their performance was assessed to determine the most suitable optimization approach for the apnea classification task. Five-fold cross-validation was employed, optimizing for  $F_1$ -score to maintain a balance between precision and recall.

The best hyperparameters came as follows:

```
{'C': 0.021544346900318832, 'solver': 'lbfgs'}
```

## 4.5. XG-Boost

XG-Boost is an algorithm that builds decision trees step by step to improve predictions, making it great for complex data. It handles imbalanced datasets well and efficiently finds patterns in structured data.

### 4.5.1. Hyperparameters

The maximal depth parameter controlled individual tree complexity, tested at depths 3, 5, and 7 to balance model expressiveness and overfitting risk. Simultaneously, the estimator 'n' ranged between 50 and 150 trees determined the ensemble size.

The learning rate was tested on a range of values (0.001-0.1) regulated each tree's contribution to the final prediction.

The subsample and column number by tree (0.6-1.0) introduced randomness via row/column sampling during training, improving generalization. The weight (1-3) explicitly addressed class imbalance by weighting apnea events more heavily during loss calculation

The optimal hyperparameters were as following:

```
{'colsample_bytree': 1.0, 'learning_rate': 0.2, 'max_depth': 3, 'n_estimators': 50, 'scale_pos_weight': 3, 'subsample': 1.0}
```

## 4.6. Gaussian Naive Bayes

Gaussian Naive Bayes is a classifier that assumes normally distributed features, making it well-suited for continuous data like physiological signals. Despite its naive

independence assumption, it often performs well when features roughly follow a normal distribution.

#### *4.6.1. Hyperparameters*

The variable smoothing hyperparameters which is a feature variance to prevent numerical instability when encountering near-zero-variance PPG features was the thing to optimize and came as:

```
{'var_smoothing': 1e-15}
```

### **4.7. Gradient boost**

Gradient Boosting is an ensemble learning algorithm that builds weak decision trees sequentially, with each tree correcting the errors of the previous one to improve overall predictive accuracy.

#### *4.7.1. Hyperparameters*

The number of estimators was tested on values [50, 100, 200] and then tuned to determine the optimal number of boosting stages. The maximum tree depth was varied ([2, 3, 5, 7]), to control the model's complexity and prevent overfitting.

Additionally, the learning rate was adjusted to balance convergence speed and generalization from the following test values [0.1, 0.05, 0.01, 0.001].

The tuning of the hyperparameters returned the following

## 4.8. Random Forest

A random forest is an algorithm that combines multiple decision trees' predictions to improve accuracy and prevent overfitting.

### 4.8.1 Hyperparameters

Hyperparameter tuning was done using a grid search approach to optimize the performance of the Random Forest model. Key parameters included the use of bootstrapping to determine whether trees were trained on random subsets, the criterion for measuring split quality (Gini impurity or entropy), and the maximum depth of each tree to control complexity. The model also optimized the number of features considered at each split, the minimum samples required for a split or leaf node, and the number of trees in the ensemble. Additionally, parallel processing was leveraged to speed up training, ensuring an efficient and well-generalized model.

```
param_grid_rf = {  
    {'bootstrap': False, 'criterion': 'gini', 'max_depth': 10, 'max_features': 'sqrt',  
    'min_samples_leaf': 1, 'min_samples_split': 2, 'n_estimators': 100, 'n_jobs': -1}
```

## 4.9. Evaluation Metrics

To assess model performance, accuracy, precision, recall, F1 score, and F2 score were calculated. These metrics provided a comprehensive evaluation of each algorithm's ability to distinguish between apneic and non-apneic events, with particular emphasis on recall and (F2) F $\beta$  score to prioritize sensitivity in classifying potential apneic episodes.

In our case, a F-Beta score with  $\beta=2$  was set as a scoring metric which will emphasize the recall meaning that our model is optimized to minimize false negatives since detecting the type of apnea is the most important part of the diagnosis which differs largely from Central to Obstructive apnea for example.

The comparative analysis and performance of these models is detailed in the subsequent results section :

Table 3 Performance of the Different Algorithms Used - PPG

Model	Accuracy	Precision	Recall	F1-Score	F2-Score
Random Forest	0.844	0.923	0.667	0.774	0.706
XG-Boost	0.822	0.857	0.667	0.75	0.697
Gradient Boost	0.822	0.916	0.611	0.733	0.654
Naïve Bayesian	0.733	0.687	0.611	0.647	0.625
Logistic Regression	0.711	0.667	0.555	0.606	0.574

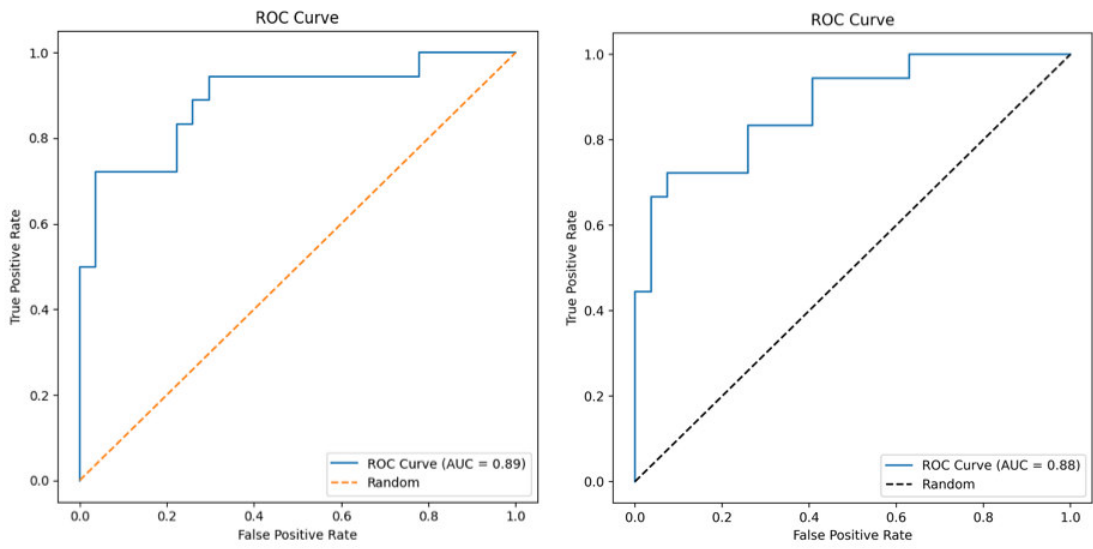


Figure 38 ROC of Gradient BOOST and Random Forest

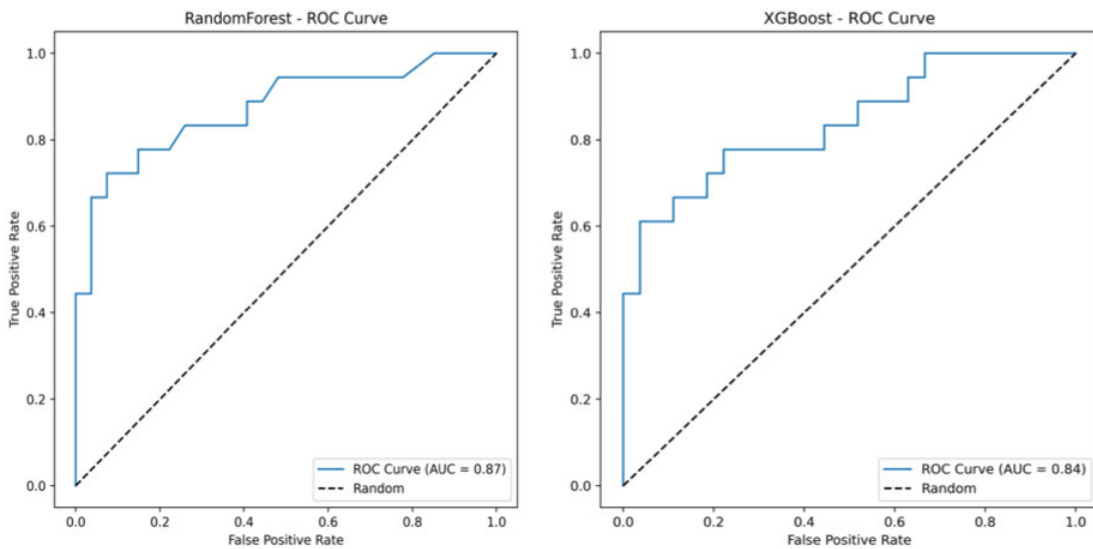


Figure 39 ROC curves of Random Forest and XG-BOOST

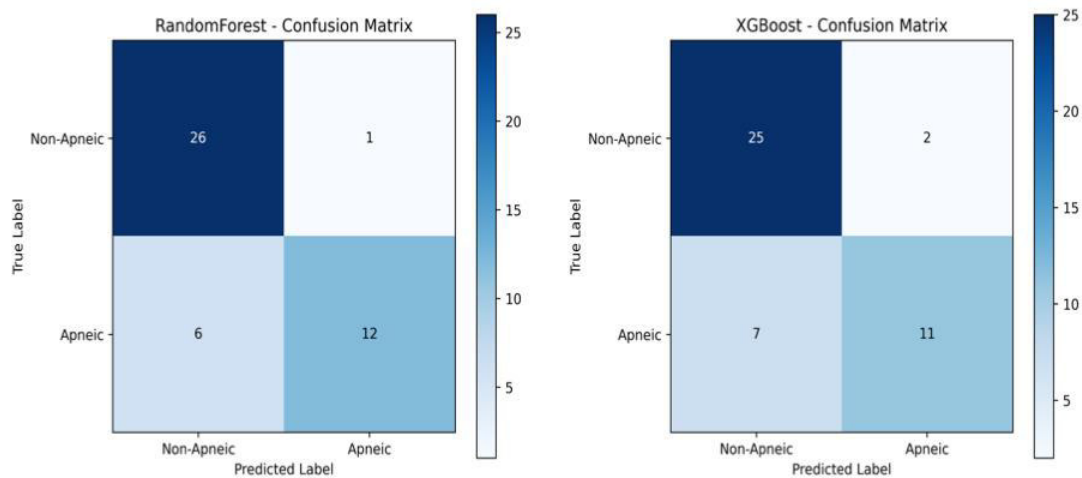


Figure 40 Confusion Matrices of (a) the Random Forest and (b) the XG-Boost models for finger PPG.

Among the tested classifiers, the **Random Forest model** exhibited the strongest overall performance, achieving an **accuracy of 84.4%**, a **precision of 92.3%**, and a **recall of 66.7%**. This indicates a high ability to correctly identify non-apneic cases (high specificity), but with a **moderate sensitivity**, reflected in a **false negative rate of 33.3%** for apneic events. The model's **F1-score of 0.774** and **F2-score of 0.706** confirm its robustness, though slightly biased toward precision over recall.

The **XG-Boost classifier** also performed well, with an **accuracy of 82.2%** and a **precision of 85.7%**, though it matched the Random Forest in recall (66.7%). Its slightly lower F1 (0.75) and F2 (0.697) scores suggest a similar, yet marginally less balanced, performance.

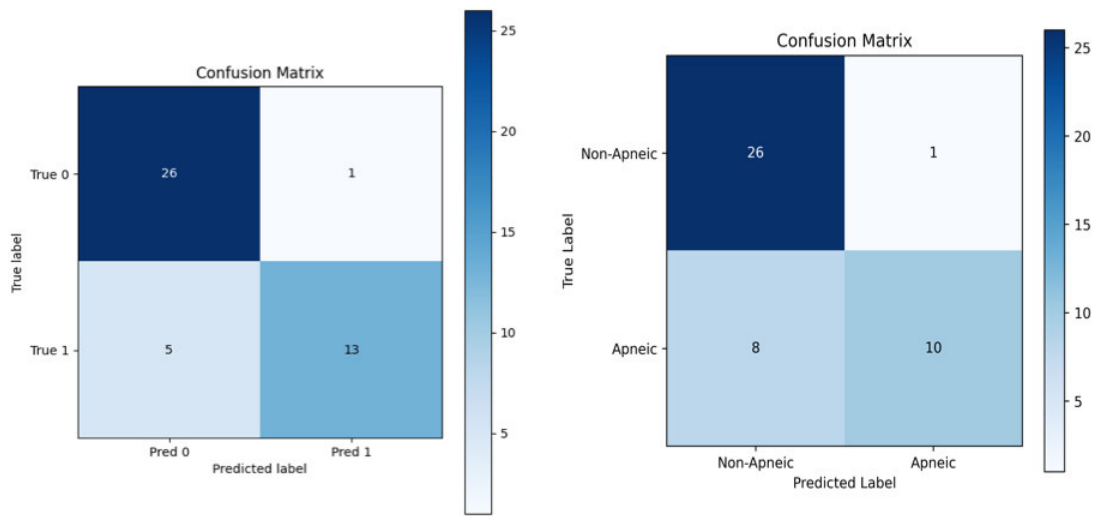


Figure 41 Confusion matrices of the Gradient Boost and the Ensemble model for finger PPG.

The Gradient Boosting model yielded comparable accuracy (82.2%) and the highest precision (91.6%), but its recall dropped to 61.1%, indicating a higher tendency to miss apneic cases. Its F1 (0.733) and F2 (0.654) scores reflect this imbalance.

In contrast, **Naïve Bayes** and **Logistic Regression** models showed noticeably lower performance across all metrics. Naïve Bayes achieved an accuracy of **73.3%**, with moderate precision (68.7%) and recall (61.1%). Logistic Regression lagged behind, with the lowest accuracy (**71.1%**), precision (**66.7%**), and recall (**55.5%**), resulting in the lowest F1 (0.606) and F2 (0.574) scores, indicating limited utility in reliably detecting apneic events.

These results suggest that ensemble-based models, particularly Random Forest and XG-Boost, offer the best trade-off between precision and recall, making them suitable for the classification of sleep apnea using PPG-derived features.

#### 4.10 Classification at the level of the Wrist (PPGDR)

For the PPGDR, several statistical features were extracted from the data to analyze respiratory patterns. These features represent various aspects of the signal, such as its central tendency, standard deviation, variability, spread, and the presence of peaks, which may correlate with respiratory events.

Cross-Validation of 5 folds was used where the model is trained on 4 of them and then tested on the 5<sup>th</sup>. This process was repeated 5 times and the performance was averaged.

Before starting with PPGDR we tested a feature permutation importance using the following equation:

$$\Delta \text{ score} = \text{score}_{\text{Original}} - \text{score}_{\text{permuted}}$$

Where:  $\left\{ \begin{array}{l} \text{score original: the model's performance metric before shuffling} \\ \text{score permuted: the model's performance after a random shuffle.} \\ \Delta \text{ score} = \text{represents the importance of that feature.} \end{array} \right.$

Given a model  $f(X)$  trained on dataset  $X$ , the importance of a feature  $j$  is:

$$I_j = E[\mathcal{M}(Y, f(X))] - E[\mathcal{M}(Y, f(X^{j\pi}))]$$

Where  $\left\{ \begin{array}{l} X^{j\pi} \text{ represents the dataset where only } j \text{ is shuffled} \\ E \text{ being the expectation taken over multiple permutations.} \\ M(Y, f(X)) \text{ is the chosen evaluation metric (e.g., } F - \text{beta score).} \end{array} \right.$

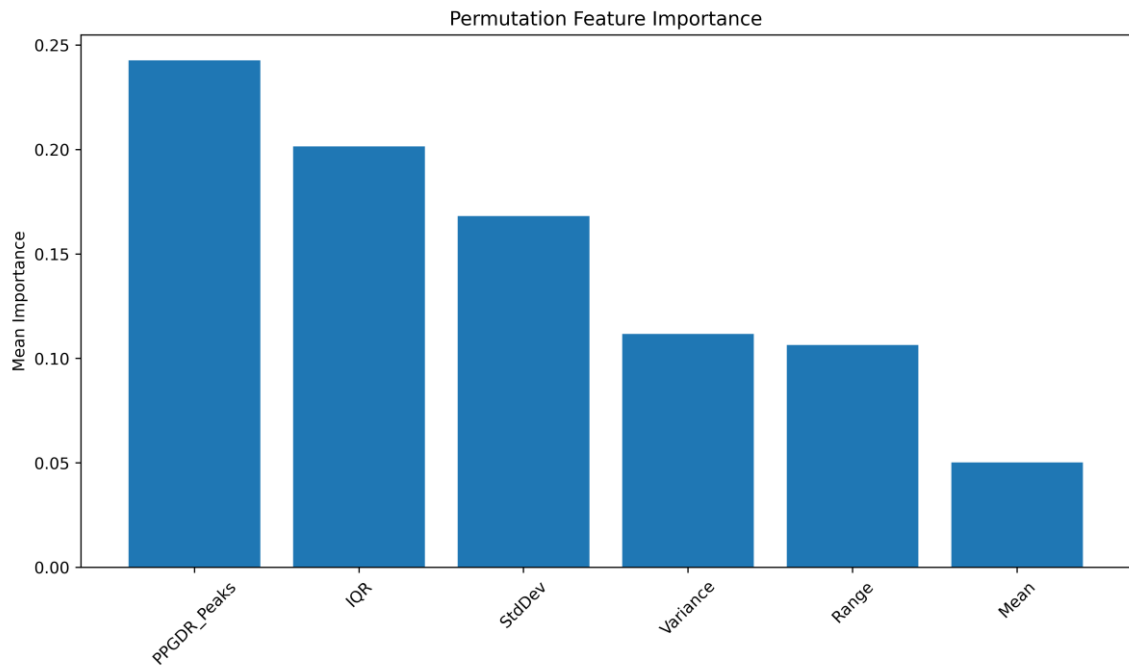


Figure 42 Permutation test of the features in PPGDR

After solving the permutations, the following graph. The most influential features for PPGDR-based classification.

The most influential feature was the number of peaks which would be minimal during CSA due to low to no breaths peaks, the number of peaks increases during OSA to higher and faster respirations especially due to the occlusion of the upper airway.

Following, the interquartile range and standard deviation, suggesting that signal variations play a significant role in distinguishing apneic states.

Variance and Range also contributed, though to a lesser extent, while **Mean** had the lowest importance, indicating it provided minimal discriminative power

For the PPGDR 3 models were chosen for the classification:

#### 4.10.1 Deep Learning using Multilayer Perceptron Neural Networks:

Multilayer Perceptron is a Deep Learning Model which is a type of Feed Forward Artificial Neural Networks (ANN) was developed with the following architecture:

-Input layer: Being the PPGDR data's features.

-The structure of hidden layers is determined by **RandomizedSearchCV**, selecting from:

Table 4 Different Hidden Layers Possibilities for Deep Learning

<b>Number of Neurons</b>	<b>Number of Hidden Layers</b>
<b>(50,)</b>	<b>1</b>
<b>(100,)</b>	<b>1</b>
<b>(50,50)</b>	<b>2</b>
<b>(100,50)</b>	<b>2</b>
<b>(100,100)</b>	<b>2</b>

- **Activation Function:** Uses **ReLU (Rectified Linear Unit)** by default, defined as:

$$f(x)=\max f(0,x)$$

To control the overfitting, we added a penalty term to the loss function alpha our model looks for the optimal alpha from {1e-4, 1e-3, 1e-2} and uses **Adam** by default, which adapts the learning rate dynamically.

Our Deep Learning model generated the following as optimal:

```
“{'mlp__hidden_layer_sizes': (50, 50), 'mlp__alpha': 0.001}”
```

This results in a 2 hidden layers architecture where each hidden layer contains 50 neurons, forming a **(50, 50)** (Figure 48) architecture with a L2 value of 0.001 preventing excessively large weight values that could lead to overfitting.

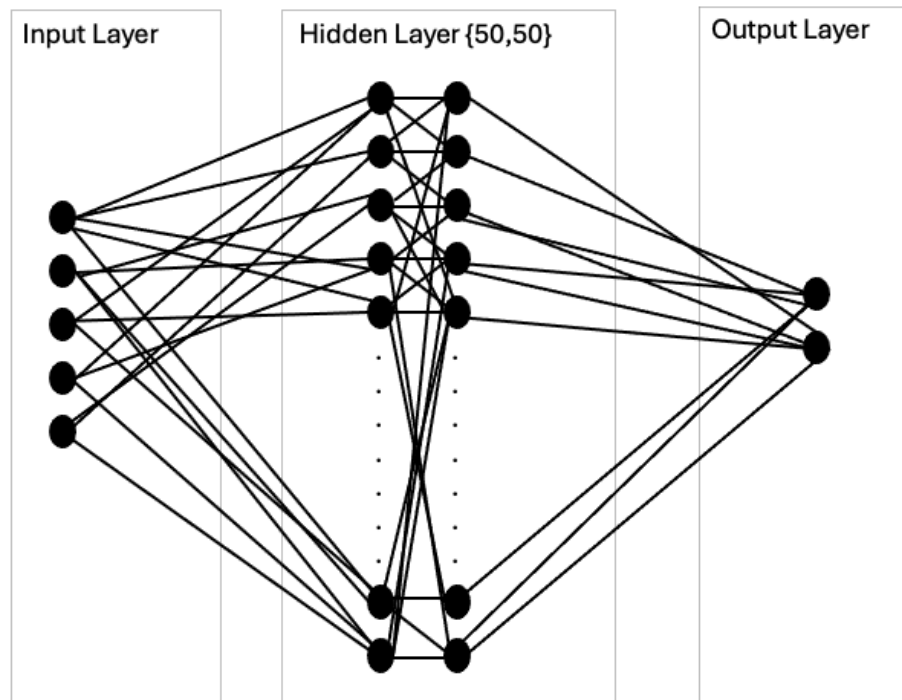


Figure 43 Optimal MLP Neural Network Model

#### 4.10.1. K-Nearest Neighbors:

K Nearest Neighbors (K-NN) is a non-parametric model that classifies data points based on their proximity to labeled training samples using a Euclidean distance by testing the neighbors of each point.

Hyperparameter Tuning was done using the function ‘RandomizedSearchCV’: The number of neighbors tested [3,5,7,9,11] as K being the number of Neighbors needed. The goal of such procedures is such that we find the best possible results without overfitting (small number K) and without underfitting (high number K).

Different weights were also tested as [‘uniform’, ‘distance’] to choose whether or not neighbors should or should not have much weight on the decision of the model.

Our model outputs the following:

```
{'knn__weights': 'distance', 'knn__n_neighbors': 5}
```

#### 4.10.2. *Naive Bayes* (**explained earlier**):

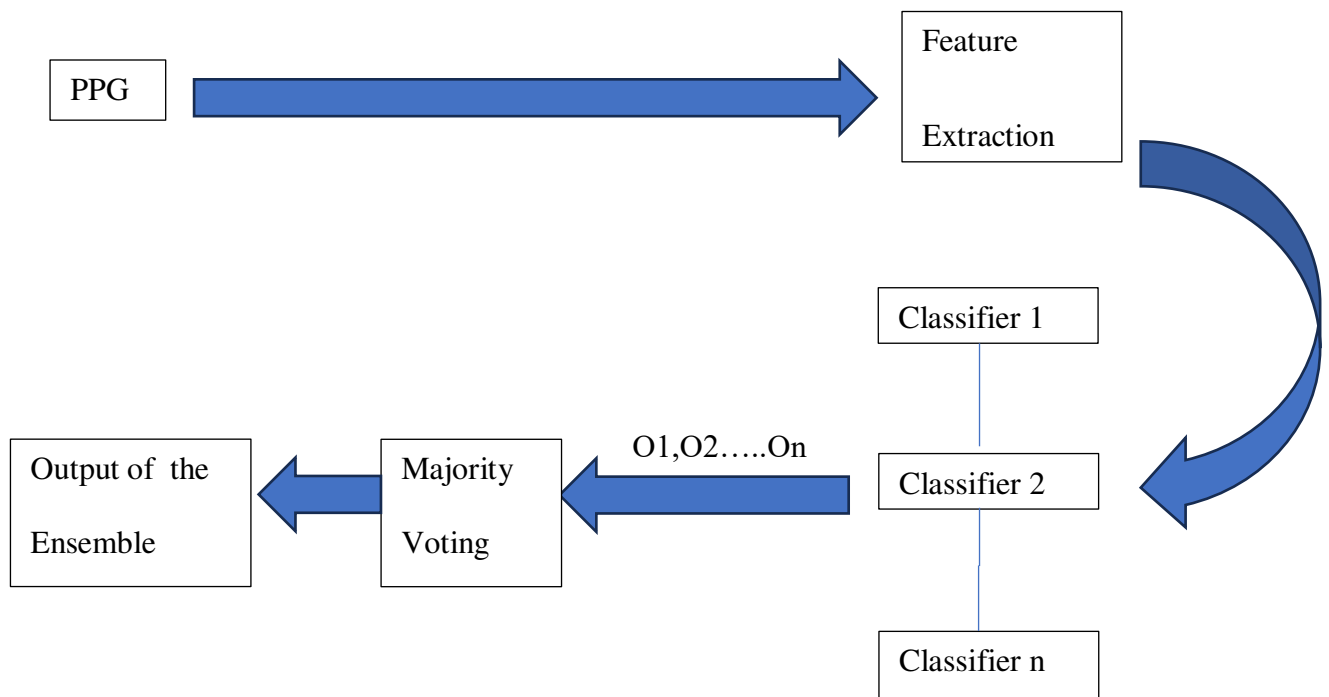
The optimization process was like the one we had before, using the “RandomizedSearchCV” function. ‘var-smoothing’ tested the log spaced values [1e-9, 1e-8, 1e-7, 1e-6] which were added to the variance to avoid the zero probability (extremely useful in small datasets).

We came to the following conclusion:

```
{'nb__var_smoothing': 1e-06}
```

#### 4.10.3. *Ensemble Method*:

Ensemble algorithms combine multiple models (in our case the 3 models explained before) to improve classification accuracy and robustness. Techniques like bagging, boosting, and stacking aggregate predictions from different models to reduce variance, bias, or improve generalization.



$O_1, O_2, \dots, O_n$  being the output of Classifier 1, 2... n.

To tune the ensemble method, we needed to figure out whether the use a hard or soft voting strategy.

- In ‘hard voting’ each of our classifiers makes a prediction and the class prediction is based on the majority vote
- In ‘soft voting’ also known as probabilistic voting, the ensemble uses the probabilities for each class from each classifier voting. In this case, the ensemble would use what is known as a ‘confidence index’ of each of the model in its predictions.

The final output of ensemble follows the following:

```
{'voting': 'hard', 'nb__var_smoothing': 1e-06, 'mlp__hidden_layer_sizes': (50, 50),
'mlp__alpha': 0.001, 'knn__weights': 'distance', 'knn__n_neighbors': 5}
```

#### 4.11. Results

The following table sums up our results:

Table 5 Performance of the Different Algorithms Used - PPGDR

Metrics	Neural Networks	KNN	Naive Bayesian	Ensemble
<b>Accuracy</b>	0.76	0.77	0.77	0.87
<b>F-2</b>	0.75	0.77	0.77	0.81
<b>Precision- Recall</b>				
Normal	0.84	0.84	0.79	0.93
CSA	0.83	0.83	0.79	0.87
OSA	0.90	0.95	0.87	0.98
<b>Area Under the Curve</b>				
Normal	0.88	0.88	0.83	0.92

CSA	0.93	0.93	0.91	0.95
OSA	0.95	0.99	0.94	0.99

We can see that individual algorithms performed similarly whereas the ensemble seemed to outperform each one of them and this is because one model may capture other aspects of the data. This diversity means that no single model is likely to fail on all instances, and their combined insights can lead to a more robust overall decision.

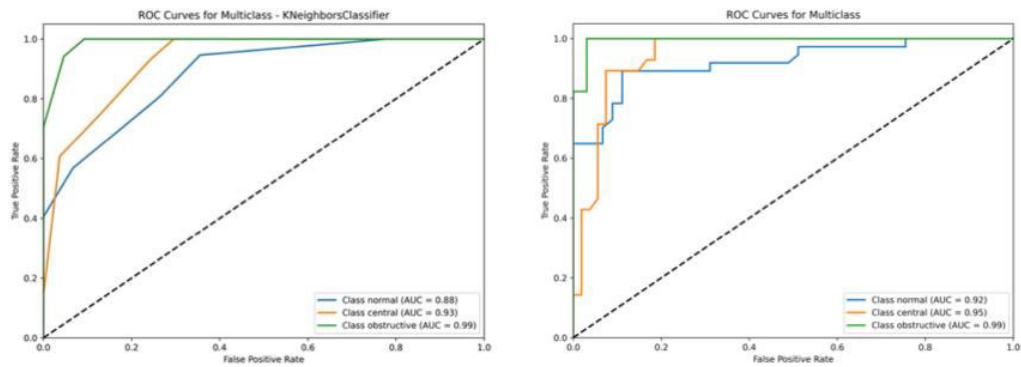


Figure 44 Area Under the Curve of K-NN and Ensemble method

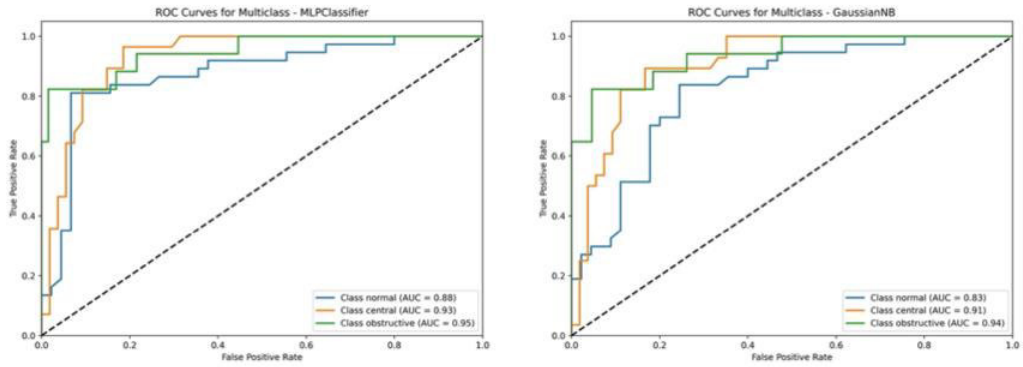


Figure 45 Area Under the Curve of the MLP and Gaussian Naïve bayesian models.

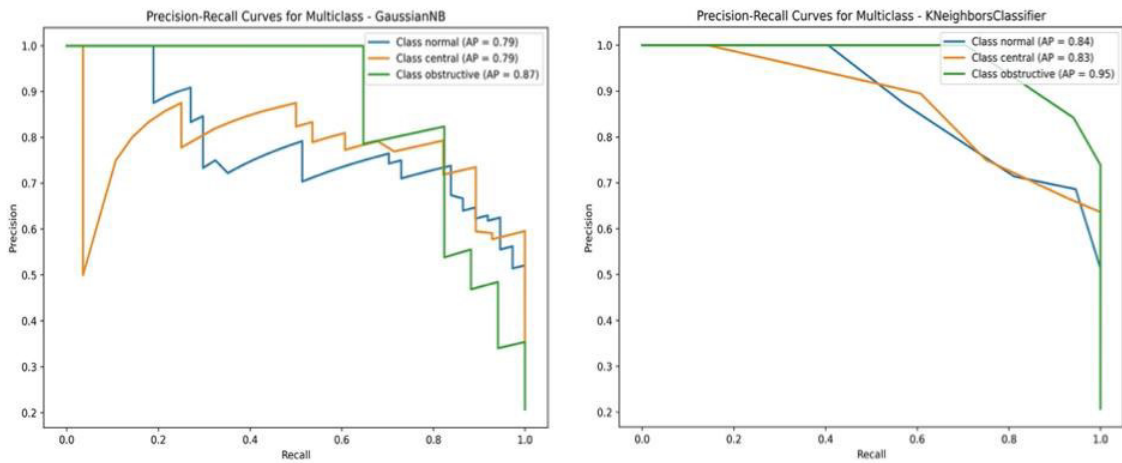


Figure 46 Precision-Recall curves for Gaussian Naive Bayesian and K-NN models

Confusion matrices confirmed the ensemble’s robustness over the rest of the models (Figure42).

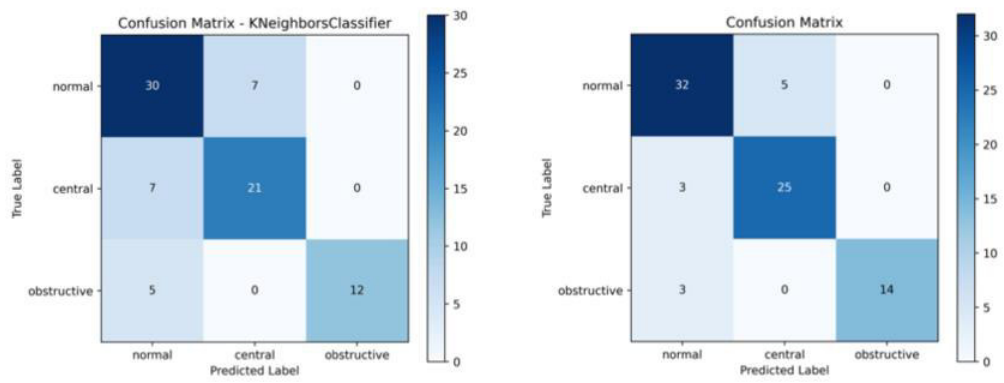


Figure 47 Confusion Matrices of K-NN and Ensemble Methods

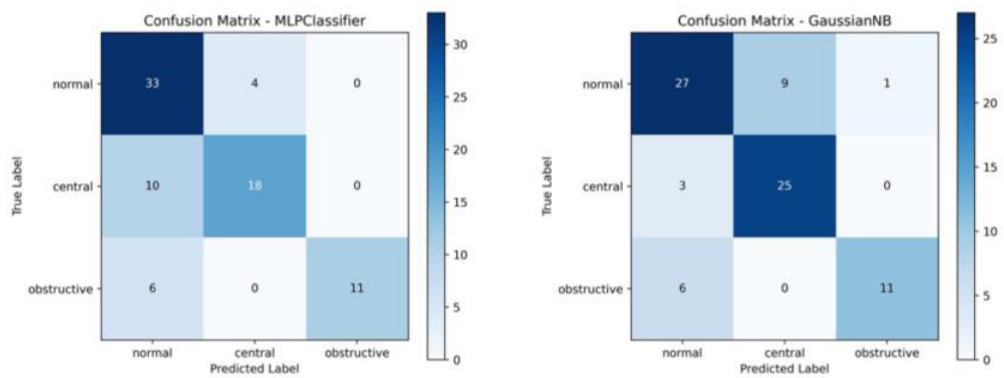


Figure 48 Confusion Matrices of the 4 Models – PPGDR.

#### *4.11.1. K-Nearest Neighbors*

Performs well in classifying normal instances but struggles with central and obstructive classes. Misclassifies some central instances as normal and obstructive, leading to moderate confusion.

#### *4.11.2. Ensemble*

Had better performance on normal, central and obstructive PPGDR classifications.

The number of misclassified obstructive and central PPGDR cases seems lower than KNN, indicating an improvement in this category.

#### *4.11.3. MLPNN*

Strong classification of normal cases, with minimal misclassification. Slightly better at distinguishing central cases compared to KNN. High confusion remains between Central and Obstructive PPGDR categories.

#### *4.11.4. Gaussian Naïve Bayes*

Struggles more with normal classifications compared to MLP and KNN. Has an overall good performance for the classification of Central PPGDR. Appears to have higher misclassification rates for Obstructive PPGDR cases.

#### 4.12. Logic Synthesis of the System

A logic table could be derived from the previous results that defines the states. Such logic-based signal interpretation frameworks are conceptually aligned with closed-loop feedback systems in neuroengineering, which emphasize adaptive decision-making based on real-time physiological input[37].

The framework is as follows:

##### 4.12.1 For PPG:

0: A state of no apnea (Control).

1: A state of general apnea.

Another variable should be used for stating PPG at time (t+1).

##### 4.12.2. For PPGDR:

00: A state of no apnea 'Normal'.

01: A state of CSA.

10: A state of OSA.

11: A state of conflicting information.

For the output:

Table 6 Logic Table of the system

State PPG(Apneic/Normal)	State PPGDR(Normal/CSA/OSA)	Final Output
0	00	00

0	01	00
0	10	00
1	00	11
1	01	01
1	10	10

By dividing the 'PPGDR state' into 2, a Most Significant Bit (MSB) and a Least Significant Bit (LSB), as well as the Final output into 3, one for CSA, one for OSA, one for 'Rejection', and a time variable for PPG for both t and t+1 we get the following table:

Table 7 Logic Table of the System taking into consideration the Delay of Vasoconstriction for CSA

PPG (t)	PPG(t+1)	MSB PPGDR(t)	LSB PPGDR(t)	OSA	CSA	Rejection (Control case)
0	0	0	0	0	0	1
0	0	0	1	0	0	1
0	0	1	0	0	0	1
0	0	1	1	0	0	1
0	1	0	0	0	0	1
0	1	0	1	0	1	0
0	1	1	0	0	0	1
0	1	1	1	0	0	1
1	0	0	0	0	0	1

1	0	0	1	0	1	0
1	0	1	0	0	1	0
1	0	1	1	0	1	0
1	1	0	0	1	0	0
1	1	0	1	0	1	0
1	1	1	0	1	0	0
1	1	1	1	0	0	1

The table could be explained by saying the following:

When ‘State of PPG’ is predicted as ‘0’ (Non-Apneic) at both present (t), the ‘MSB of PPGDR’ and ‘LSB of PPGDR’ are always 0 else the data should be neglected therefore the need of the ‘Rejection’ column and therefore a Rejection should be returned.

When the first ‘State of PPG’ is predicted as 1 (Apneic) or both the PPG signals at time ‘t’ and ‘t+1’, the system evaluates PPGDR’ bits:

If the PPGDR predicts CSA (01) or OSA (10), the system classifies the case accordingly.

Additionally, if the PPGDR state is undefined or in a contradictory state (eg. Both an ‘OSA’ and a ‘CSA ’ at the same time or an ‘OSA’/’CSA’ state without a positive ‘State of PPG’), the system will trigger a rejection to prevent inaccurate classification.

Also if a CSA happens at the level of the PPGDR followed by a apnea at the level of the PPG (t+1), the case of CSA should be returned as ‘1’.

### 4.12.3. K-mapping

Karnaugh map or K-map is an optimization method used to simplify Boolean functions and minimize logic circuits by setting up truth table values, allowing pattern identification by grouping adjacent cells representing logical '1's and deriving simplified expressions that require fewer logic gates, improving circuit efficiency and performance.

In our case, we needed to set 3 K-maps, one for each of our outputs by mapping them to our input in the following way:

- A being the input of the State of PPG at a time  $t$ .
- B being the input of State of PPG at a time  $t+1$ .
- C being the MSB of the PPGDR.
- D being the LSB of the PPGDR.

A 4-variable K-map has 16 cells, corresponding to the minterms  $m_0$  to  $m_{15}$ . The K-map is organized as follows:

Table 8 K-Map template

AB/CD	00	01	11	10
00	$m_0$	$m_1$	$m_3$	$m_2$
01	$m_4$	$m_5$	$m_7$	$m_6$
11	$m_{12}$	$m_{13}$	$m_{15}$	$m_{14}$
10	$m_8$	$m_9$	$m_{11}$	$m_{10}$



Where for:

#### 4.12.4. CSA Logic Output

Table 9 CSA Logic Output page

AB/CD	00	01	11	10
00	0	0	0	0
01	0	1	0	0
11	0	1	0	0
10	0	1	1	1

From that table, we could extract the following logic equation:

$$CSA = F(A, B, C, D) = B \cdot \bar{C} \cdot D + A \cdot \bar{B} \cdot C + A \cdot \bar{B} \cdot D$$

#### 4.12.5. OSA Logic Output

Table 10 OSA Logic Output

AB/CD	00	01	11	10
00	0	0	0	0
01	0	0	0	0
11	1	0	0	1
10	0	0	0	0

From the table, we could extract the following logic equation:

$$OSA = F(A,B,C,D) = A.B.\bar{D}$$

#### 4.12.6. REJECTION Logic Output

Table 11 REJECTION Logic Output

AB/CD	00	01	11	10
00	1	1	1	1
01	1	0	1	1
11	0	0	1	0
10	1	0	0	0

From the table, we then extract the following logic equation

$$\text{Rejection} = F(A,B,C,D) = \bar{A}.\bar{D} + \bar{A}.\bar{B} + \bar{B}.\bar{C}.\bar{D} + B.C.D$$

$$\text{Based on the following system} \left\{ \begin{array}{l} CSA = B.\bar{C}.D + A.\bar{B}.C + A.\bar{B}.D \\ OSA = A.B.\bar{D} \\ \text{Reject} = \bar{A}.\bar{D} + \bar{A}.\bar{B} + \bar{B}.\bar{C}.\bar{D} + B.C.D \end{array} \right.$$

A logic method was used to treat the output of both models to get to one logic synthesis

# CHAPTER 5

## EXPERIMENTAL RESULTS:

### 1 VERSUS 2 SYSTEMS

In this part of the work, we start by showing the performance of our architecture as a whole by combining the systems using our logic method.

Our goal would, be to verify and later on re-generalize the logic synthesized in the previous part of our work by comparing one system's output (PPGDR) to a two systems output (PPG + PPGDR) for CSA and OSA.

We decided to test our systems and study the correct outputs.

By combining the output of both systems, we aim to assess whether integrating PPG and PPGDR enhances classification performance compared to using PPGDR alone.

We therefore combined the 2 systems into 1 and returned the following results:

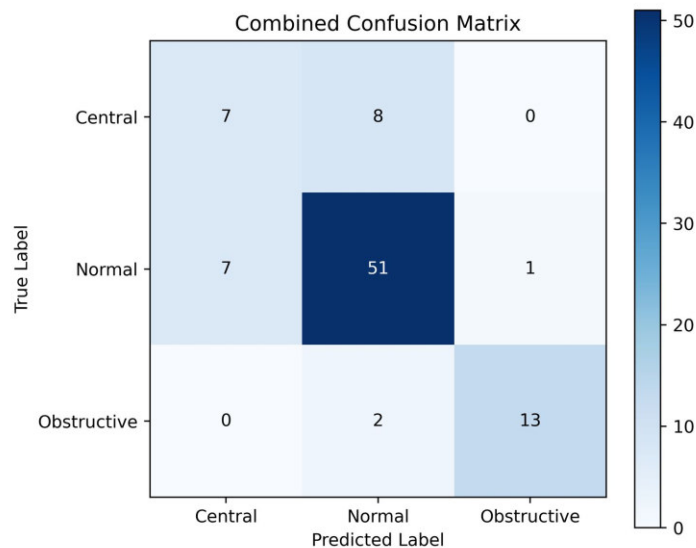


Figure 49 Confusion Matrix of the whole System on the validation set

Leading us to an accuracy of 79.78% as a whole system (Figure 54).

The model performs well in classifying Normal cases, with 51 correctly classified. CSA and OSA are sometimes misclassified as Normal but OSA classification is relatively strong, with only 2 cases being confused with Normal and none with CSA.

CSA is more frequently misclassified as Normal than OSA, supporting the hypothesis that its PPG vasoconstriction is weaker and harder to distinguish.

For us, to test the fidelity of the system to detect and classify CSA we compared the correct predictions for central apnea and found that combining the whole system would result in worse results than when only using PPGDR.

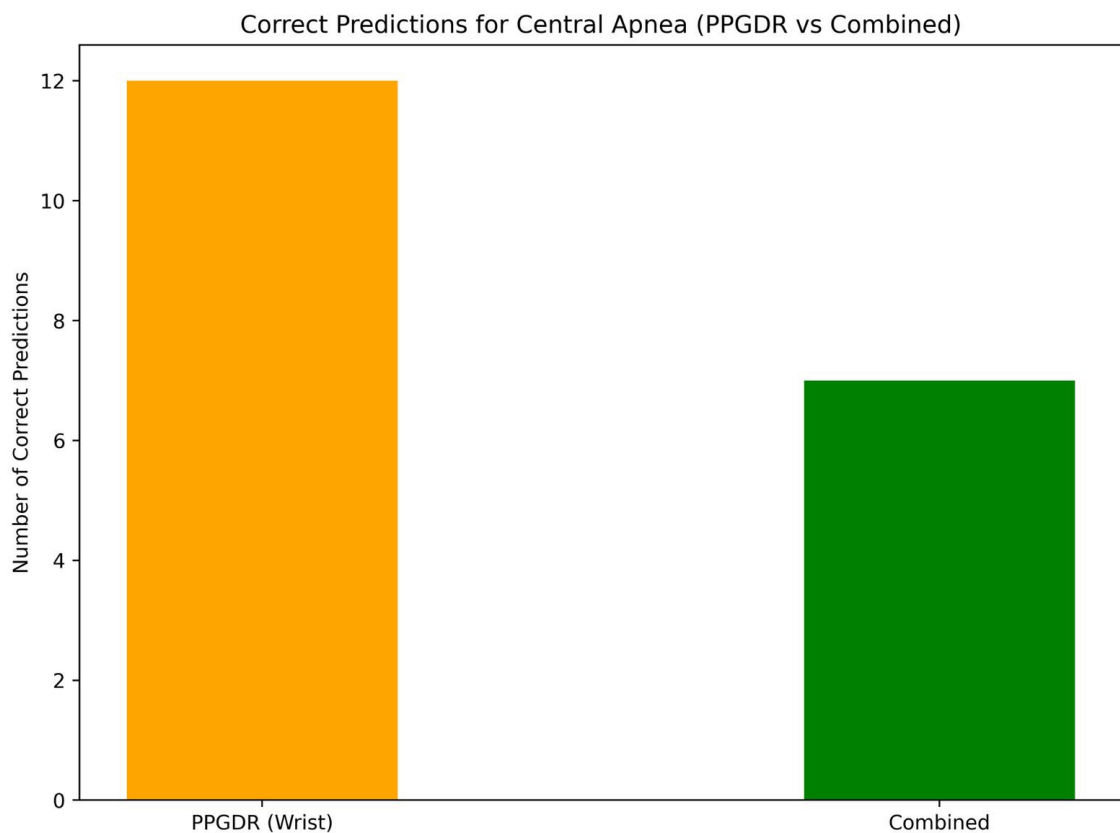


Figure 50 Correct Predictions for Central Apnea (PPGDR vs Combined)

For CSA detection, using only PPGDR resulted in higher accuracy, likely due to the weaker vasoconstriction response in the finger's PPG signal compared to OSA. This suggests that PPGDR alone is better suited for identifying CSA-specific patterns without interference from strong vasoconstrictive events. However, when combining both PPGDR and PPG, we observed improved accuracy overall. This improvement may stem from the fact that OSA generates significant vasoconstrictions, making it easier to differentiate from normal cases. Additionally, in some instances, PPGDR normal events may have been misclassified as PPGDR obstructive, further highlighting the benefits of integrating both signals for a more robust classification.

Therefore, the optimal way should be to use the response of the PPGDR when classifying CSA and the combination of PPG and PPGDR when predicting both Normal and OSA.

### 5.1. Optimized Karnaugh Map

The logic table would therefore be:

Table 12 Optimized K-Map

PPG (t)	MSB PPGDR(t)	LSB PPGDR(t)	OSA	CSA	Rejection (Control case)
0	0	0	0	0	1
0	0	1	0	1	0

0	1	0	0	0	1
0	1	1	0	0	1
1	0	0	0	0	1
1	0	1	0	1	0
1	1	0	1	0	0
1	1	1	0	0	1

For OSA:

Table 13 Optimized K-Map OSA

A/BC	00	01	11	10
0	0	0	0	0
1	0	0	0	1

For CSA:

Table 14 Optimized K-Map CSA

A/BC	00	01	11	10
0	1	0	0	0
1	0	0	1	0

For Normal:

Table 15 Optimized K-Map Rejection

A/BC	00	01	11	10
0	0	0	1	1
1	1	0	1	0

Based on the following system 
$$\begin{cases} OSA = A.B.\bar{C} \\ CSA = \bar{A}.\bar{B}.C + A.B.C \\ Normal = A.B + \bar{B}.C \end{cases}$$

To test our final results, we decided to combine our outputs to with only the PPGDR for CSA detection and the combination of PPG and PPGDR for the detection and classification of OSA.

$$Accuracy = \frac{51+12+13}{51+12+13+7+2+1+3} * 100 = 85.39\%$$

## 5.2. Main results

The work shows promising results in not only the detection but classification of sleep apnea syndrome.

We have shown how to leverage the characteristics of the wrist and finger PPG. The finger PPG has been shown to be a great indicator of vasoconstriction as a result of

apnea, whereas the wrist PPG does not vasoconstriction which led us to a high fidelity PPGDR.

We also concluded that CSA doesn't result in a vasoconstriction as strong as OSA and also, these vasoconstrictions may be delayed from the time where the apnea occurs leading to the conclusion that PPGDR is a better indicator of CSA than finger PPG and PPGDR combination.

For OSA, we have seen good results in combining both the PPG and PPGDR by localizing the vasoconstrictions (PPG) and the increase in effort (PPGDR).

## CHAPTER 6

### CONCLUSION

Most of the work published only focuses on detecting apnea events but doesn't work on classifying them into OSA and CSA without using other wearable devices which may not be very suitable for sleep.

Most of the work on PPG only focuses on detecting OSA as being the most common type of apnea, such a method isn't suited to deal with the case and may not always lead to the best prescription since OSA and CSA are treated differently.

Our work will help scientists derive more hardware for the detection of sleep apnea.

The work could also guide in the classification of sleep apnea into CSA and OSA from the comfort of one's bed eliminating the need for expensive solutions like PSG and only using wearables that are commonly popular among large populations such as smartwatches and smart rings.

#### **6.1. Significance and Future Recommendations**

Our work highlights the potential of using comfortable, wearable devices to make sleep apnea detection not only easier but also more user-friendly. By leveraging devices like rings and wristbands, we aim to move away from bulky, intrusive equipment and toward solutions that people can wear comfortably while they sleep.

In this study, we used the tip of the finger PPG signal being a gold standard in PPG and sleep studies, but we also demonstrated promising similarities between the tip of the finger and ring PPG signals.

This opens the door for future research to explore ring-based wearables as a more comfortable alternative to traditional finger sensors, which can be uncomfortable during sleep.

One of the most exciting possibilities is using these wearable technologies to not only detect sleep apnea but also classify it into central and obstructive types. This would provide doctors with detailed reports, enabling them to tailor treatments more effectively.

We would also recommend extracting SPO<sub>2</sub> signals out of PPG making it a game changer in the classification of hypopnea from apnea.

Combining a multipoint system with SPO<sub>2</sub> could be used to optimize the Apnea/Hypopnea classification.

Such advancements could be a game-changer, especially for large populations who lack access to expensive and complex polysomnography (PSG) systems. By making sleep apnea detection and classification more accessible and comfortable, we hope to improve diagnosis and treatment for millions of people worldwide.

## **6.2. Limitations of the Work**

**Healthy Participants vs. Sleep Apnea Patients:** The study involved young and healthy individuals, which may influence the physiological responses observed. Differences between these participants and those with sleep apnea could account for variations in results.

In true cases of obstructive or central sleep apnea, oxygen saturation typically decreases while carbon dioxide concentration increases. This change activates peripheral and central chemoreceptors, triggering vasoconstriction. However, if participants remain sufficiently oxygenated and do not allow carbon dioxide levels to rise significantly during a voluntary breath-hold, this trigger may be too weak to elicit a strong vasoconstrictive response.

**Individual variability also plays a role in these responses:** Factors such as age, cardiovascular health, and baseline autonomic status can influence the likelihood of measurable vasoconstriction. Younger and healthier individuals may possess more efficient compensatory mechanisms, such as effective buffering of blood gases, which can delay or minimize the onset of vasoconstriction.

**Experimental conditions further contribute to variations in results:** Differences in the duration and depth of simulated apnea, as well as the level of participant motivation and adherence, can significantly affect physiological responses. Even small discrepancies in the experimental setup may lead to substantial differences in outcomes, particularly when the levels of hypoxia or hypercapnia are relatively mild.

**The state of wakefulness versus sleep:** Is an important factor to consider. Cardiovascular responses to apnea that are commonly documented in sleeping individuals may not fully translate to wakeful conditions. Autonomic regulation during sleep differs from that during wakefulness, which may diminish or alter the effects of simulated apneas in a laboratory setting compared to clinical sleep studies.

The Müller maneuver (MM), commonly used to simulate obstructive sleep apnea (OSA) in awake individuals, has limitations in replicating true OSA pathophysiology. Unlike actual sleep-state apnea, MM lacks the effects of hypoxia and sympathetic activation, which are critical in triggering vasoconstrictive and autonomic responses. While MM is useful for identifying structural airway collapse at the velum (V-test) and tongue (T-test), it is less effective in capturing dynamic obstructions such as oropharyngeal collapse (O-test) and epiglottic instability (E-test). This is due to the absence of sustained hypoxia and the gag reflex, both of which play a role in unmasking these patterns. In contrast, drug-induced sleep endoscopy (DISE) closely mimics airway dynamics during sleep and reveals multi-level airway collapse with high concordance across V/O/E/T-tests. Older adults, who often experience amplified vasoconstriction due to vascular remodeling, are particularly underserved by MM, as it does not replicate the chronic hypoxia-driven autonomic responses seen in true OSA. Although DISE may slightly blunt sympathetic activity due to sedation, it remains the gold standard for assessing OSA. These differences highlight the need for improved awake simulations that incorporate cyclical hypoxia to better align with clinical findings and more accurately assess airway behavior.

**Small Sample Size:** The population size was too small to draw robust conclusions. Large-scale studies typically involve hundreds or thousands of participants to ensure statistical significance and reliability.

**Equipment Limitations and Signal Acquisition Challenges:** The study relied on individual sensors rather than an integrated acquisition system due to budget

constraints. This required manual correlation of signals in MATLAB, which could introduce errors in signal alignment and interpretation.

**Lack of Real PSG Data:** Unlike typical sleep apnea studies, which use Polysomnography (PSG) to monitor apneic patients during real sleep, this study relied on simulated CSA. PSG provides comprehensive data, including EEG, EOG, EMG, and respiratory signals, which are critical for accurate analysis. In standard PSG studies, PPG signals are collected alongside other physiological data, allowing for a more robust analysis of oxygen desaturation and respiratory events. The absence of real PSG data in this study limits the depth and accuracy of the findings.

### **6.3. Detection of Sleep Apnea Using SPO<sub>2</sub> Signal**

Wearable devices commonly use SpO<sub>2</sub> sensors to measure blood oxygen levels, playing a significant role in detecting sleep apnea. During apneic events, when airflow to the lungs is restricted or paused, blood oxygen levels typically drop. This is followed by a re-saturation period, during which oxygen levels return to normal. For instance, as shown in Figure 24, any drop in SpO<sub>2</sub> below 96% can be considered indicative of an apneic event [32].

A general standard would be to say that a  $\geq 3\%$  drop in SpO<sub>2</sub> lasting  $\geq 10$  seconds is commonly used to define a hypopnea event whereas a  $\geq 4\%$  drop in SpO<sub>2</sub> would be associated with an apnea.

SpO<sub>2</sub> is closely related to PPG as it was indeed shown that SpO<sub>2</sub> could be derived from PPG signals by analyzing the ratio of light absorption at red (~660 nm) and infrared (~880 nm) wavelengths. The AC and DC components of the PPG signal at the 2 wavelengths are extracted to calculate the ratio of ratios (R) using the following ratio 'R' where

(Figure 39 Figure 40) which is then mapped to SpO<sub>2</sub> using an empirical calibration curve

To derive a simple equation as  $SpO_2 = a.R + b$  using as simple device such as an SpO<sub>2</sub> sensor bought from pharmacy to deduce the values of a and b.

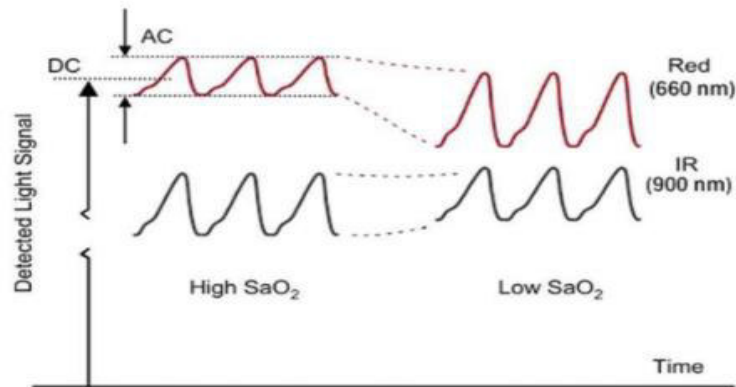


Figure 51 The AC and DC components of PPG at different wavelengths

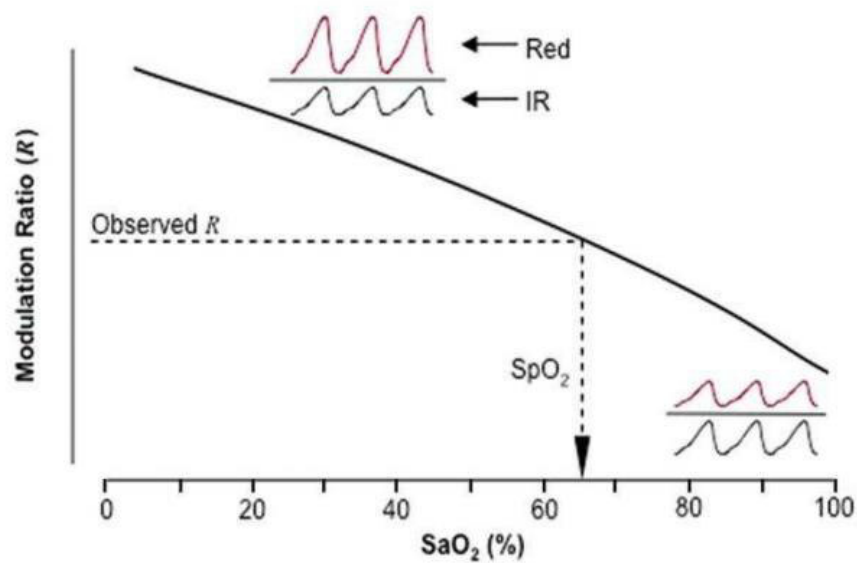


Figure 52 The usage of different PPG wavelength to extract SPO2 extracted from [29]

[38] found an equation of  $\% \text{SpO}_2 = 110 - 25 \times R$  by comparing the values to an  $\text{SpO}_2$  sensor.

To deepen our understanding of  $\text{SpO}_2$  signal and its role in sleep apnea detection, we analyzed publicly available data. We downloaded Excel files from a dataset involving children undergoing sleep studies, which include their Apnea-Hypopnea Index (AHI). This dataset is accessible at [Peter Charlton's PPG Datasets](#).

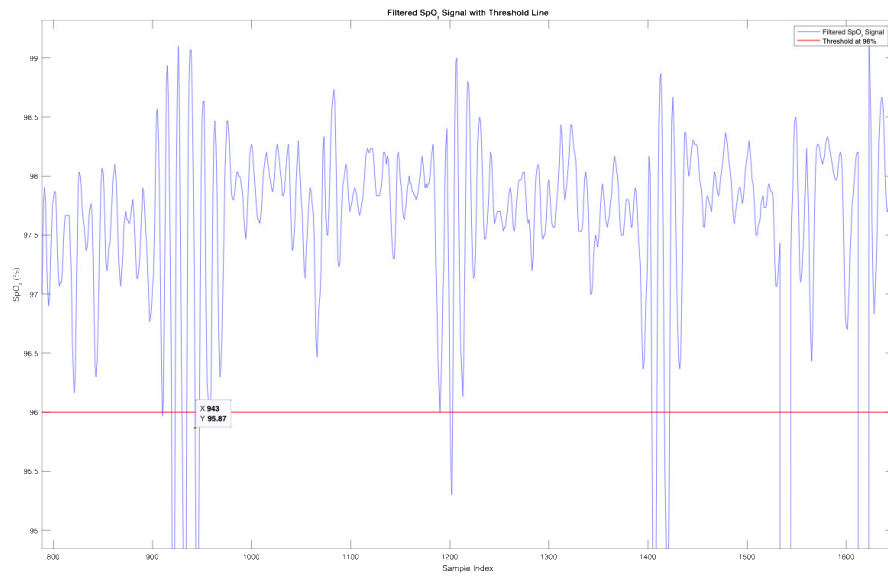


Figure 53 Filtered SPO2 signal with Apneic Threshold

To investigate whether we could reliably detect apneic events, we began by cleaning the SpO<sub>2</sub> signal. First, we removed any values above 100% or below 50%, replacing these outliers with NaN (Not a Number) values. To reconstruct the signal, we applied linear interpolation, smoothing over the missing segments. This step ensured the signal was continuous and ready for further analysis [39].

To refine the data, we up-sampled the signal from its original frequency of 1 Hz to 100 Hz using the `repelem()` function in combination with the `rat()` function. Up-sampling provided a higher resolution of the signal, allowing us to capture finer details. We then analyzed the signal by looping over it to identify periods where oxygen saturation dropped below 96%. We defined a critical duration for these events: a drop under the threshold was due to an interruption of breathing for at least 10 seconds was marked as an apneic event in red on the processed signal (as shown in Figure 42). The rationale for using around 10-second threshold could be due to the physiological

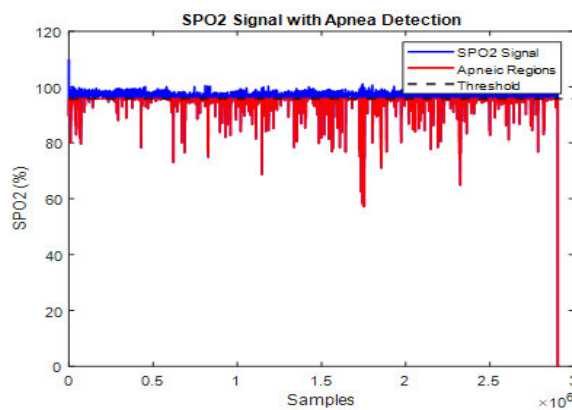
process—when the air stops reaching the lungs, the blood oxygen level drops almost immediately and takes about 10 seconds to reach the sub-threshold level.

To ensure accurate counting of apneic events, we set the duration of an "episode" to 1 minute especially because we are using a full night of sleep (8 hours on average) which is much bigger than the amount of time of the simulated study.

This decision was guided by practical considerations:

- If the episode duration were too short, a single prolonged apnea could mistakenly be counted as multiple events.
- Conversely, if the episode duration were too long, multiple apneas occurring within that timeframe might be inaccurately grouped as a single event.

By setting a balanced duration, we aimed to align our analysis with real-world apnea patterns, ensuring precise quantification of AHI.



Total apneic minutes: 68  
Total non-apneic minutes: 417  
Conversion  
Total apneic hours :1 hour .  
Total non-apneic minutes: 7 hours.  
The recordings lasted 8.08 hours.  
A whole minute is considered apneic if at least 10 seconds  
of that 1 minute is placed under the threshold of 90%

Figure 54 Filtered Apneic Spo2 Signal Highlighted in Red

For subject 3, we seemed to have found the following results: 68 apneic episodes and 417 non apneic episodes. Which resulted in an AHI of 3 similar to what was provided to us in the document given on the AHI of each patient.

Unfortunately, we could not go further with the analysis of the Apneic PPG in the dataset due to high movement corruption of the signal.

# APPENDIX 1

## 1. AUC (Area Under the Curve):

- Formula:  $AUC = \int_{t=1}^n (signal - interpolated\ minima) dt$

During apneic events, deoxygenation leads to vasoconstriction which will be reflected in the area under the curve of the PPG pulse.

It is commonly known that sleep apnea impact on stroke volume, causing changes in both the systolic (the heart's contraction phase or loading phase) and diastolic (the heart's relaxation phase or filling phase) phases of the heartbeat. Therefore, investigating both phases is crucial for a comprehensive understanding of how sleep apnea affects the cardiac cycle.

## 2. Median:

- Formula:

$$\begin{cases} X\left(\frac{n+1}{2}\right) & (n \text{ even}) \\ \frac{X\left(\frac{n}{2}\right) + X\left(\frac{n}{2} + 1\right)}{2} & (n \text{ odd}) \end{cases}$$

The median is a valuable feature because it provides a reliable measure of central tendency, is less sensitive to outliers

## 3. MAD (Median Absolute Deviation):

- Formula:  $MAD = \text{median}(|\text{signal} - \text{median}(\text{signal})|)$

Mean Absolute Deviation is the average distance between each data point in a dataset and the mean of this dataset. It gives us an idea about the variability in a dataset.

#### **4. Trimmed Mean 25%:**

Formula: Trimmed Mean 25% =  $\text{mean}(\text{signal}, \text{trimmed } 25\%)$

The trimmed mean studies the mean of the signal while taking 25/50% of the points as being outliers on the tails of the signal that can affect the arithmetic mean. In the case of PPG the outliers could be outliers could sometimes be generated by the movement of the hand of the patient.

#### **5.. Trimmed Mean 50%:**

- Formula: Trimmed Mean 50% =  $\text{mean}(\text{signal}, \text{trimmed } 50\%)$

#### **6 . Geometric Mean:**

Formula: Geometric Mean =  $(\prod |\text{signal}(i)|)^{(1/n)}$  or 'geomean(signal)'

During normal breathing, the PPG signal might have a consistent amplitude and shape, leading to a stable geometric mean over time. However, during an apnea event, the amplitude and shape of the PPG waveform can change significantly due to interruptions in breathing.

The geometric mean is an important feature for detecting changes in the shape of biosignals like PPG for sleep apnea because it effectively captures multiplicative changes, reduces the impact of extreme values.

## 7. RMS (Root Mean Square):

- Formula: 
$$\text{RMS} = \sqrt{\frac{1}{T_2 - T_1} \int_{T_1}^{T_2} |f(t)|^2 dt}$$

The Root Mean Square is used to evaluate the amplitude of the signal and signal energy in the time domain. (1) developed an adaptive filter to study the drop in amplitude of the PPG pulse based the root mean square of the PPG signal.

## 8. IQR (Interquartile Range):

- Formula:  $\text{IQR} = Q_3 - Q_1$ , where  $Q_3$  is the third quartile and  $Q_1$  is the first quartile

The interquartile range in descriptive statistics provides information about the distribution of the middle half of your sample. Any distribution arranged from low to high can be divided into four equal portions using quartiles.

The IQR provides a measure of variability, is resilient to outliers, and helps in identifying anomalous periods such as apneic events.

## 9. Mean:

- Formula:  $\text{Mean} = \text{Mean} = \frac{1}{n} \sum_1^n (\text{signal}(n))$

During abnormalities, the mean difference of the signal should decrease due to vasoconstriction resulting in the decrease in signal amplitude mean.

## 10. STD (Standard Deviation):

Formula: 
$$\text{STD} = \sqrt{\frac{1}{n-1} \sum_{i=0}^n (\text{signal}(i) - \mu)}$$

$\mu$  = mean of the signal

N = Total number of data points

Standard Deviation is a measure of how far the signal fluctuates around the mean of the signal. A signal returned by vasoconstricted blood vessels would usually return a smaller standard deviation since the amplitude of the signal returned is much smaller than a non-apneic PPG signal.

### 11. (Standard Error):

- Formula: 
$$\text{StdErr} = \frac{\sqrt{\frac{1}{n-1} \sum_{i=0}^n (\text{signal}(i) - \mu)^2}}{\sqrt{n}}$$

Standard Error is used to estimate the accuracy and consistency of a sample.

### 12. Teager Energy:

- Formula: 
$$\text{Teager Energy} = \Psi(x[n]) = x[n]^2 - x[n-1] \cdot x[n+1]$$

Teager Energy can be particularly useful in analyzing photoplethysmography (PPG) signals due to its ability to capture instantaneous energy changes and detect events such as pulse peaks and variations. The instant change of energy in the signal during apneic and normal signals varies due to the smaller fluctuations happening during apneic events.

### **13. Average Low Frequency (0.05-0.15 Hz) over High Frequency (0.16-0.4 Hz) Energy Ratio**

In addition to statistical and mathematical features, the study also deals with study of energies in the frequency domain.

The PPG signal contains 2 main categories of frequencies:

- The low Frequency, which ranges from 0.05 to 0.15 Hz.
- The high Frequency, which ranges from 0.15 up to 0.4 Hz.

During apnea, activation of the parasympathetic nervous system typically leads to an increase in HF energy.

Meanwhile, LF power may decrease or remain relatively stable, representing the balance between sympathetic and parasympathetic influences.

The ratio between HF and LF is defined as the sympatho-vagal balance.

### **14. Shape Factor:**

- Formula: Shape Factor  $\frac{RMS(signal(i))}{\frac{1}{N} \sum_{i=1}^N |signal(i)|}$

Shape factor is a ratio of the Root Mean Square of the signal over the absolute value of the mean of the signal. This ratio is independent of the size of the sample. A shape factor equal to one usually represents an ideal case or maximum symmetry (like a cube).

### **15. Central Moment (10th order):**

- Formula: Central Moment 10 = moment(signal, 10)

### **16. Skewness:**

- Formula: Skewness = 
$$\frac{\frac{1}{N} \sum_{i=1}^N (\text{signal}(i) - \overline{\text{signal}})^3}{\left(\frac{1}{N} \sum_{i=1}^N (\text{signal}(i) - \overline{\text{signal}})^2\right)^{\frac{3}{2}}}$$

Skewness factor gives a clear picture of the asymmetry of the distribution of the data. A right Skewed result would return a positive value whereas a left skewed dataset would result in a negative value.

### **17. Kurtosis:**

- Formula: Kurtosis = 
$$\frac{\frac{1}{N} \sum_{i=1}^N (\text{signal}(i) - \overline{\text{signal}})^4}{\left(\frac{1}{N} \sum_{i=1}^N (\text{signal}(i) - \overline{\text{signal}})^2\right)^2}$$

Kurtosis factor shows how much of the data resides in the tails. A high Kurtosis factor would usually show us a spiked signal. A small kurtosis factor would show a flat signal.

### **18. Mean Tp (Mean Time Interval between Minima and Maxima):**

- Description: Mean of the time intervals between successive minima and maxima.

Time to rise reflects the vascular response and can tell about disrupted autonomic control.

### **19. Mean Amplitude:**

- Description: Mean of the amplitude differences between maxima and their preceding minima.

Reduced amplitude during apneic episodes may indicate decreased cardiac output and peripheral vasoconstriction during vasoconstriction

### **20. Mean Time Differences:**

- Description: Mean of the time differences between successive maxima.

Peak to Peak intervals reflect the commonly known “Beat per minute (BPM)” and could change due to Bradycardia, as sleep apnea is sometimes characterized by slower heart rates.

### **21. DK (Dispersion Coefficient):**

- Formula: 
$$DK = \frac{\sqrt{\frac{1}{n-1} \sum_{i=0}^n (\text{signal}(i) - \mu)^2}}{\left| \frac{1}{n} \sum_{i=1}^n (\text{signal}(n)) \right|}$$

Degree of variation is a ratio between the standard deviation and the mean of the signal it shows how the signal varies compared to the average value in a percentage.

### **22. Xmin (Minimum Value):**

- Formula:  $X_{\min} = \min(\text{signal})$

### **23. Xmax (Maximum Value):**

- Formula:  $X_{\max} = \max(\text{signal})$

### **24. Mean Width (Mean Time Width between Minima):**

- Description: Mean of the time differences between successive minima.

The width of the PPG which indicates the duration of the heartbeat which could be altered easier by the weak filling or contraction of the heart.

**25. Activity:**

- Activity =  $\sigma^2 = \frac{1}{N} \sum_{i=1}^N (\text{signal}(i) - \mu)^2$

**26. Mobility:**

- Formula: Mobility =  $\sqrt{\frac{\text{Var}(\text{signal}')}{\text{Var}(\text{signal})}}$  *signal'* being the derivative of signal

**27. Complexity:**

- Formula: Complexity =  $\frac{\text{Mobility}(\text{signal}')}{\text{Mobility}(\text{signal})}$  *signal'* being the derivative of signal

One method for displaying a signal's statistical characteristics in the time domain is the Hjorth parameter, which has three different types of parameters (Activity, Mobility, and Complexity)[40]. The variance of the time function, or the activity parameter, can be used to determine the power spectrum's surface in the frequency domain. In other words, if there are many or few high frequency components in the signal, the value of Activity yields a large or small value. The square root of the ratio between the variances of the signal's first derivative and its own is the definition of the mobility parameter. This metric

is a power spectrum fraction of standard deviation. The complexity parameter shows how a signal's form resembles that of a pure sine wave.

### **28. p-value / h-value (from Sign Test):**

Description: Statistical p-value from the sign test of the signal.

- Description: Hypothesis test result (1 if null hypothesis is rejected, 0 otherwise) from the sign test of the signal.

### **29. Mode :**

- Description: Representation of the most frequent amplitude value. Helping identify baseline shifts between normal and apneic conditions.

### **30.31. VPG and APG:**

Velocity and Acceleration studying the velocity and acceleration of the PPG by differentiating the signal once for the velocity (VPG) and twice for the acceleration (APG). The decrease of the mean of the amplitude shows how the blood decelerates during apnea.

Suboh et al. [41] Used the 1<sup>st</sup>, 2<sup>nd</sup>, 3<sup>rd</sup> and 4<sup>th</sup> derivative to detect points on the PPG such as the systolic and diastolic peak.

### **32. Distance to reach Diastolic Peak (Td):**

The systolic is easily detected as it is the highest point reached by the PPG.

However, the diastolic peak is much harder to locate as they are far below the systolic peak and are commonly found to be only present in the finger's PPG.

Age and other factors which affect the elasticity of the blood vessels will reduce the shape of the diastolic peak as previously discussed.

McDuff, et al [33] concluded that the systolic peaks are usually represented by the biggest minima within the second-order derivative, and the diastolic peaks/inflections are usually represented by the minima that follow these.

## REFERENCES

- [1] K. Abu, M. L. Khraiche, and J. Amatoury, "Obstructive sleep apnea diagnosis and beyond using portable monitors," (in eng), *Sleep Med*, vol. 113, pp. 260-274, Jan 2024, doi: 10.1016/j.sleep.2023.11.034.
- [2] A. A. o. S. Medicine, "Sleep-related breathing disorders in adults: recommendations for syndrome definition and measurement techniques in clinical research. The Report of an American Academy of Sleep Medicine Task Force," *Sleep*, vol. 22, pp. 667-689, 1999.
- [3] C. V. Senaratna *et al.*, "Prevalence of obstructive sleep apnea in the general population: a systematic review," *Sleep medicine reviews*, vol. 34, pp. 70-81, 2017.
- [4] Y. Li, N. Lin, J. Ye, Q. Chang, D. Han, and A. Sperry, "Upper airway fat tissue distribution in subjects with obstructive sleep apnea and its effect on retropalatal mechanical loads," *Respiratory care*, vol. 57, no. 7, pp. 1098-1105, 2012.
- [5] J. Rahme, S. Saleh, T. Al-Sadek, J. Amatoury, and M. Khraiche, "Comparative Analysis of Photoplethysmogram (PPG) Waveform Characteristics Across Various Body Sites Under Normal and Apneic Conditions," *Annu Int Conf IEEE Eng Med Biol Soc*, vol. 2024, pp. 1-4, Jul 2024, doi: 10.1109/EMBC53108.2024.10781801.
- [6] S. P. Patil, H. Schneider, J. J. Marx, E. Gladmon, A. R. Schwartz, and P. L. Smith, "Neuromechanical control of upper airway patency during sleep," *Journal of applied physiology*, vol. 102, no. 2, pp. 547-556, 2007.
- [7] D. J. Eckert, A. S. Jordan, P. Merchia, and A. Malhotra, "Central sleep apnea: pathophysiology and treatment," *Chest*, vol. 131, no. 2, pp. 595-607, 2007.
- [8] K. Abu, M. L. Khraiche, and J. Amatoury, "Obstructive sleep apnea diagnosis and beyond using portable monitors," *Sleep Medicine*, 2023.
- [9] M.-M. Serghani, C. Heiser, A. R. Schwartz, and J. Amatoury, "Exploring Hypoglossal Nerve Stimulation Therapy for Obstructive Sleep Apnea: A Comprehensive Review of Clinical and Physiological Upper Airway Outcomes," *Sleep Medicine Reviews*, p. 101947, 2024.
- [10] "Standard Guide for Accelerated Aging of Sterile Medical Device Packages," *ASTM International Designation*, vol. F 1980- 02.
- [11] C. Lombardi, S. Caravita, and G. Parati, "Central sleep apnea during continuous positive airway pressure therapy in obstructive sleep apnea patients: from the compliance to adaptation, maladaptation and reflexes," *Journal of Thoracic Disease*, vol. 9, no. 11, p. 4152, 2017.
- [12] N. A. Collop *et al.*, "Clinical guidelines for the use of unattended portable monitors in the diagnosis of obstructive sleep apnea in adult patients," *Journal of Clinical Sleep Medicine-JCSM*, vol. 3, no. 7, pp. 737-747, 2007.
- [13] H. Najjar, F. Khoury, S. Saleh, and M. Khraiche, "Optimizing Wrist-Based Bioimpedance: The Role of Electrode Type, Positioning and Signal Frequency in Health Monitoring," in *2023 IEEE 4th International Multidisciplinary Conference on Engineering Technology (IMCET)*, 12-14 Dec. 2023 2023, pp. 209-213, doi: 10.1109/IMCET59736.2023.10368229.
- [14] M. L. Khraiche and R. El Hassan, "Advances in three-dimensional nanostructures for intracellular recordings from electrogenic cells," *Journal of Science: Advanced Materials and Devices*, vol. 5, no. 3, pp. 279-294, 2020.
- [15] A. Khandoker, C. Karmakar, T. Penzel, M. Glos, and M. Palaniswami, "Investigating relative respiratory effort signals during mixed sleep apnea using photoplethysmogram," *Annals of biomedical engineering*, vol. 41, pp. 2229-2236, 2013.

- [16] T. Sadek, J. Ahmad, F. Khoury, H. Badawe, and M. Khraiche, "Detecting Cardiovascular Disease From PPG Signals using Machine Learning," in *2023 IEEE 4th International Multidisciplinary Conference on Engineering Technology (IMCET)*, 2023: IEEE, pp. 203-208.
- [17] S. Ha, M. L. Khraiche, G. A. Silva, and G. Cauwenberghs, "Direct inductive stimulation for energy-efficient wireless neural interfaces," *Annu Int Conf IEEE Eng Med Biol Soc*, vol. 2012, pp. 883-6, 2012, doi: 10.1109/EMBC.2012.6346073.
- [18] C. Park and B. Lee, "Real-time estimation of respiratory rate from a photoplethysmogram using an adaptive lattice notch filter," *Biomedical engineering online*, vol. 13, pp. 1-17, 2014.
- [19] P. S. Addison, "Respiratory effort from the photoplethysmogram," *Medical engineering & physics*, vol. 41, pp. 9-18, 2017.
- [20] Z. Habli, F. Kobeissy, and M. L. Khraiche, "Advances in point-of-care platforms for traumatic brain injury: recent developments in diagnostics," *Rev Neurosci*, vol. 33, no. 3, pp. 327-345, Apr 26 2022, doi: 10.1515/revneuro-2021-0103.
- [21] F. Massie, S. Vits, A. Khachatryan, B. Van Pee, J. Verbraecken, and J. Bergmann, "Central sleep apnea detection by means of finger photoplethysmography," *IEEE Journal of Translational Engineering in Health and Medicine*, vol. 11, pp. 126-136, 2023.
- [22] E. Gil, R. Bailón, J. M. Vergara, and P. Laguna, "PTT variability for discrimination of sleep apnea related decreases in the amplitude fluctuations of PPG signal in children," *IEEE Transactions on Biomedical Engineering*, vol. 57, no. 5, pp. 1079-1088, 2010.
- [23] J. Lázaro *et al.*, "Pulse photoplethysmography derived respiration for obstructive sleep apnea detection," in *2017 computing in cardiology (CinC)*, 2017: IEEE, pp. 1-4.
- [24] M. K. Uçar, M. R. Bozkurt, C. Bilgin, and K. Polat, "Automatic sleep staging in obstructive sleep apnea patients using photoplethysmography, heart rate variability signal and machine learning techniques," *Neural Computing and Applications*, vol. 29, pp. 1-16, 2018.
- [25] V. Hartmann, H. Liu, F. Chen, W. Hong, S. Hughes, and D. Zheng, "Toward accurate extraction of respiratory frequency from the photoplethysmogram: Effect of measurement site," *Frontiers in physiology*, vol. 10, p. 732, 2019.
- [26] D. Jarchi, D. Salvi, L. Tarassenko, and D. A. Clifton, "Validation of instantaneous respiratory rate using reflectance PPG from different body positions," *Sensors*, vol. 18, no. 11, p. 3705, 2018.
- [27] A. H. Khandoker, C. K. Karmakar, T. Penzel, M. Glos, and M. Palaniswami, "Investigating Relative Respiratory Effort Signals During Mixed Sleep Apnea Using Photoplethysmogram," *Annals of Biomedical Engineering*, vol. 41, no. 10, pp. 2229-2236, 2013/10/01 2013, doi: 10.1007/s10439-013-0827-1.
- [28] M. L. Khraiche, J. Rogul, and J. Muthuswamy, "Design and Development of Microscale Thickness Shear Mode (TSM) Resonators for Sensing Neuronal Adhesion," *Front Neurosci*, vol. 13, p. 518, 2019, doi: 10.3389/fnins.2019.00518.
- [29] A.-C. Stöwhas *et al.*, "The Effect of Simulated Obstructive Apnea and Hypopnea on Aortic Diameter and BP," *Chest*, vol. 140, no. 3, pp. 675-680, 2011/09/01/ 2011, doi: <https://doi.org/10.1378/chest.10-2799>.
- [30] G. Camen *et al.*, "The effects of simulated obstructive apnea and hypopnea on arrhythmic potential in healthy subjects," *European journal of applied physiology*, vol. 113, no. 2, pp. 489-496, 2013.

- [31] J. Lázaro *et al.*, "Pulse photoplethysmography derived respiration for obstructive sleep apnea detection," in *2017 Computing in Cardiology (CinC)*, 24-27 Sept. 2017, pp. 1-4, doi: 10.22489/CinC.2017.273-229.
- [32] E. Jothi, A. Jude, and J. D., "An automatic screening approach for obstructive sleep apnea from photoplethysmograph using machine learning techniques," *TELKOMNIKA (Telecommunication Computing Electronics and Control)*, vol. 19, p. 1260, 08/01 2021, doi: 10.12928/telkomnika.v19i4.19371.
- [33] M. L. Khraiche, Y. Lo, D. Wang, G. Cauwenberghs, W. Freeman, and G. A. Silva, "Ultra-high photosensitivity silicon nanophotonics for retinal prosthesis: electrical characteristics," *Annu Int Conf IEEE Eng Med Biol Soc*, vol. 2011, pp. 2933-6, 2011, doi: 10.1109/IEMBS.2011.6090807.
- [34] T. Iqbal, A. Elahi, S. Ganly, W. Wijns, and A. Shahzad, "Photoplethysmography-based respiratory rate estimation algorithm for health monitoring applications," *Journal of medical and biological engineering*, vol. 42, no. 2, pp. 242-252, 2022.
- [35] G. Regalia *et al.*, "Sleep assessment by means of a wrist actigraphy-based algorithm: agreement with polysomnography in an ambulatory study on older adults," *Chronobiol Int*, vol. 38, no. 3, pp. 400-414, Mar 2021, doi: 10.1080/07420528.2020.1835942.
- [36] R. Lazazzera, Y. Belhaj, and G. Carrault, "A New Wearable Device for Blood Pressure Estimation Using Photoplethysmogram," *Sensors (Basel)*, vol. 19, no. 11, Jun 4 2019, doi: 10.3390/s19112557.
- [37] Z. Chou *et al.*, "Bidirectional neural interface: Closed-loop feedback control for hybrid neural systems," *Annu Int Conf IEEE Eng Med Biol Soc*, vol. 2015, pp. 3949-52, 2015, doi: 10.1109/EMBC.2015.7319258.
- [38] S.-S. Oak and P. Aroul, "How to design peripheral oxygen saturation (SpO<sub>2</sub>) and optical heart rate monitoring (OHRM) systems using the AFE4403," *Texas Instruments*, 2015.
- [39] A. Garde, P. Dehkordi, W. Karlen, D. Wensley, J. M. Ansermino, and G. A. Dumont, "Development of a screening tool for sleep disordered breathing in children using the phone Oximeter," *PLoS One*, vol. 9, no. 11, p. e112959, 2014, doi: 10.1371/journal.pone.0112959.
- [40] S.-H. Oh, Y.-R. Lee, and H.-N. Kim, "A Novel EEG Feature Extraction Method Using Hjorth Parameter," *International Journal of Electronics and Electrical Engineering*, vol. 2, pp. 106-110, 01/01 2014, doi: 10.12720/ijeee.2.2.106-110.
- [41] M. Z. Suboh, R. Jaafar, N. A. Nayan, N. H. Harun, and M. S. F. Mohamad, "Analysis on Four Derivative Waveforms of Photoplethysmogram (PPG) for Fiducial Point Detection," (in eng), *Front Public Health*, vol. 10, p. 920946, 2022, doi: 10.3389/fpubh.2022.920946.